Lipase-specific foldase-aided folding of Lipase A from *Pseudomonas aeruginosa*

Inaugural-Dissertation

zur Erlangung des Doktorgrades
der Mathematisch-Naturwissenschaftlichen Fakultät
der Heinrich-Heine-Universität Düsseldorf

vorgelegt von

Peter Dollinger

aus Leverkusen

Düsseldorf, August 2018

Aus dem Institut für Molekulare Enzymtechnologie
der Heinrich-Heine-Universität Düsseldorf

Gedruckt mit der Genehmigung der
Mathematisch-Naturwissenschaftlichen Fakultät der
Heinrich-Heine-Universität Düsseldorf

Referent: Herr Prof. Dr. Karl-Erich Jaeger
Korreferent: Herr Prof. Dr. Claus A.M. Seidel

Tag der mündlichen Prüfung: 28.11.2018

Nothing in Biology Makes Sense
Except in the Light of Evolution

(Theodosius Dobzhansky, 1973)

Acknowledgments

I would like to express my appreciation and gratitude to my doctoral advisor Prof. Dr. Karl-Erich Jaeger for giving me the opportunity to research this very exciting topic and for providing all opportunities and support needed to conduct my research. I want to thank him for all his support, the interesting discussions and the connections with other working groups.

I would also like to thank Prof. Dr. Claus A.M. Seidel for agreeing to act as a second referee and for the successful collaboration and his contribution to the FRET dynamic measurements.

Furthermore, I am very thankful to Dr. Filip Kovačić for supervising my thesis and mentoring me in my doctoral studies. I truly enjoyed the inspiring discussions and the ideas and criticism that helped to advance my research. I want to thank him very much for his constant support.

Next, I would like to thank every collaboration partner who has contributed to my research and helped me with my experiments. I want to thank Dr. Jakub Kubiak for his smFRET measurements, which helped to characterize the structure and dynamics of foldase. I thank Neha Verma and Prof. Dr. Holger Gohlke for providing their insights into the behavior of foldase by molecular dynamic simulations. I also would like to thank Dr. Aldino Viegas and Dr. Manuel Etzkorn for the structure determination of foldase by NMR. In addition, I would like to thank Dr. Renu Batra-Safferling and Dr. Joachim Granzin for the introduction to protein crystallization, the opportunity to conduct crystallization experiments and the data acquisition. I also would like to thank Dr. Bernd König for conducting ITC measurements with me.

Herewith, my thanks go to all my colleagues and the employees of the Institute of Molecular Enzyme Technology for the enjoyable working environment, and I want to thank everybody who contributed ideas and know-how that helped me to accomplish my research and my thesis.

Moreover, I would like to thank the graduate school “iGRASPseed” and the *Deutsche Forschungsgemeinschaft* (DFG) for financial support. I thank all members and supervisors for their friendly support, their helpful suggestions and their ideas during retreats and workshops.

Most importantly, I want to thank my family, my girlfriend and my close friends for their constant support throughout the years at university and during my doctoral studies.

Thank you all so much!

Table of contents

List of tables

List of figures

Abbreviations

Amp^r	ampicillin resistance
ANS	8-anilinonaphthalene-1-sulfonic acid
approx.	approximately
APS	ammonium persulfate
ATP	adenosine triphosphate
AV	accessible volume
BC	before Christ
BG	*Burkholderia glumae*
BisTRIS	2-[bis(2-hydroxyethyl)amino]-2-(hydroxymethyl)propane-1,3-diol
Cam^r	chloramphenicol resistance
CD	circular dichroism
DNA	deoxyribonucleic acid
DMSO	dimethyl sulfoxide
dNTP	deoxy nucleoside triphosphate
DSF	differential scanning fluorimetry
DSS	4,4-dimethyl-4-silapentanesulfonic acid
DTT	dithiothreitol
EC	enzyme class
ECL	enhanced chemiluminescence
EDTA	ethylenediaminetetraacetic acid
EHD	elongated helix domain
ESI-MS	electrospray ionization mass spectrometry
et al.	*et alii* (lat.): and others
FRET	fluorescence resonance energy transfer
HIC	hydrophobic interaction chromatography
IEC	ion-exchange chromatography
IPTG	isopropyl β-D-1-thiogalactopyranoside
IMAC	immobilized metal ion affinity chromatography
Kan^r	kanamycin resistance
Kat	Katal = substrate cleavage rates mol/s
kDa	kilo Dalton, 1 kDa = 1,000 g/mol
LB	lysogeny broth
MD	mini domain
MFD	multiparameter fluorescence detection
NMR	nuclear magnetic resonance
$OD_{580\ nm}$	optical density at 580 nm
PA	*Pseudomonas aeruginosa*
PAGE	polyacrylamide gel electrophoresis
PCR	polymerase chain reaction
PDB	Protein Data Bank
PEG	polyethylene glycol
***p*NPP**	*para*-nitrophenyl palmitate
ppm	*part per million*
PTFE	polytetrafluoroethylene (Teflon)
PVDF	polyvinylidene difluoride
rcf	relative centrifugal force
RMSD	root-mean-square deviation
RNA	ribonucleic acid
SEC	size exclusion chromatography
SDS	sodium dodecyl sulfate
SLIC	sequence and ligation independent cloning
SPR	surface plasmon resonance
SRP	signal recognition particle
TBST	TRIS buffered saline with Tween®20
TCEP	tris(2-carboxyethyl)phosphine
TEMED	tetramethylethylenediamine
Tet^r	tetracycline resistance
TRIS	tris(hydroxymethyl) aminomethane
UV	ultra violet

1. Introduction

Biocatalytic processes for brewing and manufacturing food were used long before it was possible to put this knowledge into writing. Evidence of fermented beverages made in Jiahu (Henan province, China) dates back to the 7th millennium BC,[1] when symbols were still used only as signs rather than as a writing system.[2]

Compared to this period of 9000 years, it was only recently that we started to understand how these processes work. With the research of Louis Pasteur starting in the 1850s, it was recognized that fermentation is caused by metabolic processes of microorganisms.[3] In 1877, Wilhelm Kühne coined the term “enzymes” (from Greek: “in yeast”) and defined them as nonliving substances that are able to catalyze reactions.[4] It took a further 50 years before James B. Sumner was able to indisputably characterize enzymes as protein entities by crystallizing urease in its pure form in 1926.[5] All these findings have opened the doors for modern biocatalysis, which currently uses specific enzymatic activities for defined reactions.

The increasing number of available enzymes and knowledge about their functioning is still driving the growth of the field of biocatalysis.

1.1. The use of bacterial lipases in biocatalysis

Lipases occur ubiquitously in every domain of life: plants, fungi, microorganisms, and animals from humans to insects.[6] Because they share similarities but also exhibit many individual traits, it is challenging to describe this enzyme family consistently. Therefore, the focus will be on bacterial lipases, whose characteristics and their diversity make them one of the most commonly used enzyme classes in industry.[7]

Bacterial lipases belong to the enzyme class EC 3.1.1.3 and catalyze the hydrolysis of ester bonds of long-chain acylglycerols. Their catalytic mechanism is based on a catalytic triad consisting of a nucleophilic, a basic and an acidic residue (Figure 1.1). The molecular reaction mechanism consists of two consecutive nucleophilic substitutions. The first substitution is initialized by the attack of the nucleophilic residue at the carbonyl group of the substrate cleavage site, resulting in a covalently linked acyl enzyme intermediate that is cleaved by a second nucleophilic substitution with an external nucleophile. The basic residue enhances the reactivity of the nucleophilic residue by increasing its electron density due to partial deprotonation. Furthermore, it neutralizes the substitution reaction by taking up excessive

protons. The resulting charge at the basic amino acid is stabilized by the negatively charged carboxylate of the acidic residue. This mechanism of action was first postulated by Blow *et al.* (1968)[8] and termed a charge relay system because the electron density of the negatively charged acidic amino acid is distributed to the nucleophile, enhancing its reactivity.

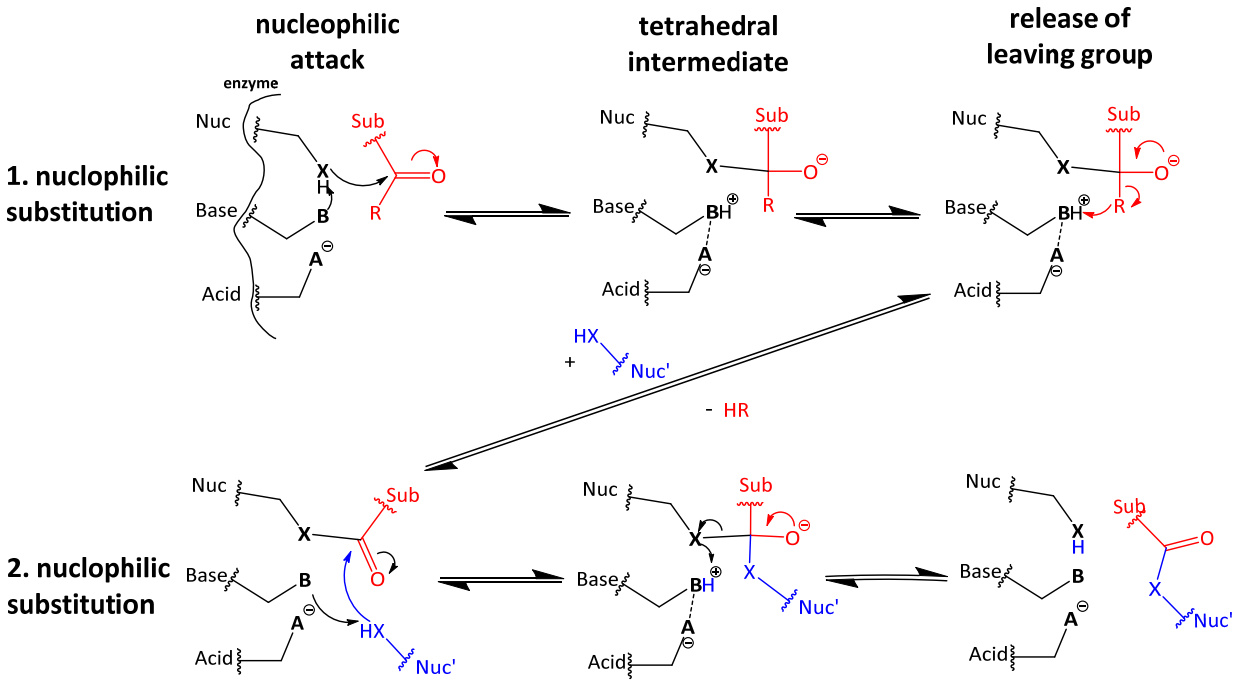

Figure 1.1: Molecular mechanism of the catalytic triad in hydrolases.
The amino acid residues that form the catalytic triad in hydrolases are shown schematically. The reactive groups of the nucleophile (Nuc), the base and the acid are generalized as X, B and A, respectively. The substrate is shown in red, with R as a variable leaving group. The second nucleophilic substitution is initiated by an external nucleophile (Nuc') shown in blue.

This mechanism is found in several hydrolytic enzyme classes, such as proteases, esterases, β-lactamases, asparaginases and thioesterases.[9,10] Because these hydrolytic enzymes share the same catalytic mechanism but often have no structural similarity, this mechanism seems to have developed independently multiple times during evolution as a result of missing reactive nucleophilic functional groups among the proteinogenic amino acids.[10] The most commonly occurring catalytic triad in hydrolases in general and lipolytic enzymes in particular consists of Ser, Asp and His.[10] This universal reaction mechanism makes lipases reactive against all types of esters and amides and increases their applicability in industry.[7,11–13] Their substrate specificity seems to depend not on the active site but rather on the form of the substrate binding pocket. In addition to the steric and charge characteristics of the substrate binding pocket, which selects by substrate accessibility, a so-called oxyanion hole provides catalytic efficiency by stabilizing the negatively charged carbonyl group during the formation

of the tetrahedral intermediate and thus selects for substrates that fit in the right orientation for the active serine and the oxyanion hole (Figure 1.2).[14–16]

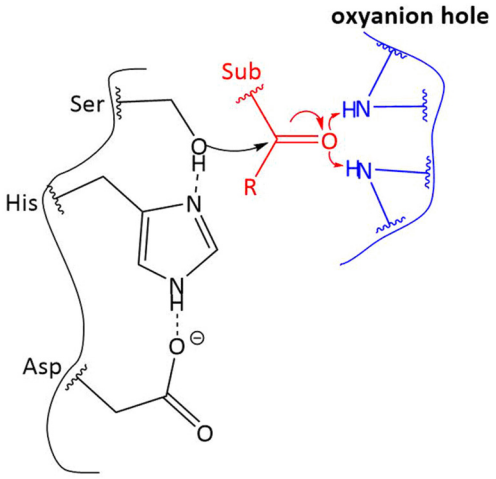

Figure 1.2: Ser Asp His catalytic triad in lipases and the role of the oxyanion hole.
In black, the charge relay system of the catalytic triad Ser His Asp initiates a nucleophilic attack on a substrate (red) at its carbonyl group. The electrophilicity of the carbon atom is further increased by electron density displacement by the oxyanion hole (blue).

Because the nucleophilic substitution follows an S_N2 mechanism, which allows the stereospecific and enantioselective cleavage of substrates, lipases are often found or successfully engineered to be enantioselective.[11,17–20] The hydrolysis of the acyl enzyme intermediate is dependent on the presence of a water molecule near the active site for the second nucleophilic substitution. Under water exclusion, other nucleophilic molecules can serve as reactants, resulting in transferase reactions. For this reason, this charge relay system is found not only in hydrolytic enzymes but also in the enzyme class of transferases.[21,22] Moreover, for that reason, lipases are able to perform ester synthesis and transesterification in nonaqueous media.[11,23–25]

The diversity of lipase-producing microorganisms and the fact that lipases are often secreted enzymes, evolved to withstand various harsh conditions found outside the cell, make them a versatile biocatalytic toolbox with a wide range of useful characteristics. Many lipases have been found to be extraordinarily stable in organic solvents or nonaqueous media and to be stable and active at high and low temperatures and at high salt concentrations. Therefore, they are used in the laundry detergent, paper, food, leather, polyester, biodiesel and pharmaceutical industries.[13,26–29]

1.2. LipA from *Pseudomonas aeruginosa*

Lipases produced by bacteria of the *Pseudomonas* genus have attracted substantial attention for industrial applications.[11,30–32] The well-studied lipase LipA from *Pseudomonas aeruginosa* was the first lipase of subfamily I.1 whose structure was solved[33] and was therefore often used as model lipase of this subfamily. It shows extraordinary catalytic reactivity[34] and high stability in organic solvents and nonaqueous media.[23] It was possible to demonstrate its use for the production of biodiesel[23] and other industrially relevant esterification and transesterification reactions.[23,35] Furthermore, LipA was successfully engineered for altered substrate specificity and enantioselectivity.[17,36]

1.2.1. Structure of LipA from *Pseudomonas aeruginosa*

The structure of LipA from *P. aeruginosa* was solved by Nardini *et al.* in 2000.[33] It shows LipA in its open conformation, inhibited by a phosphonate substrate analog. LipA exhibits an α/β hydrolase fold[37] (Figure 1.3), a structure that is highly conserved among hydrolases.[14] It consists mainly of 5 parallel β-strands forming the core sheet surrounded by connecting α-helices. The structural elements of LipA were named in consistency with those of the slightly different canonical α/β hydrolase fold (Figure 1.3 B). Its catalytic triad is formed by S82, D229 and H251, which are located on the loops following β5, α8 and β8', respectively. The substrate binding pocket is formed mostly by α4, α5, α6 and α8, among which α5 functions as a lid that covers the active site and opens in the presence of substrates. The oxyanion hole is formed by the backbone amides of M16 and H83 located on the loops following β3 and β5 directly next to the active site serine, respectively.

LipA incorporates a calcium ion inside its structure, which is coordinated octahedrally by the side chain carboxy groups of D209 and D253, the backbone carbonyl groups of Q257 and L261 and two water molecules close to the active site. This metal binding pocket is highly conserved among bacterial lipases and is needed for their lipolytic activity. Because of its distance to the active serine of 15 Å, it is most likely not involved in the catalytic mechanism but is thought to be important in retaining the structure of the active site by coordinating H251 of the catalytic triad at the proper position.[33] Directly next to the metal binding site is found a highly conserved cis-peptide conformation of the backbone amide between Q257-V258, which

might be necessary for calcium binding.[38] Two cysteines (C183 and C235) form a disulfide bridge, which is not necessary for activity but increases the stability of LipA.[39]

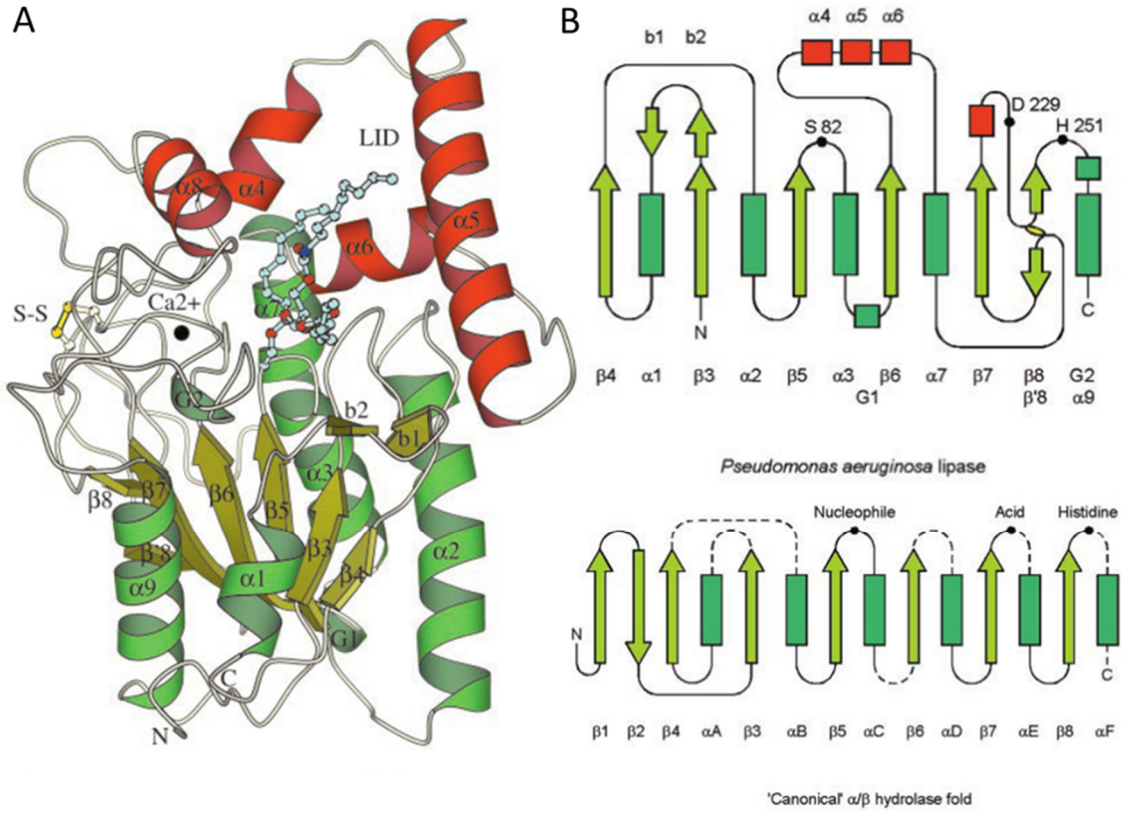

Figure 1.3: The structure of LipA from *P. aeruginosa.*
A) Schematic representation of the structure of *P. aeruginosa* LipA. α-Helices, β-strands, and coils are represented by helical ribbons, arrows, and ropes, respectively. α-Helices belonging to the cap domain involved in substrate binding are shown in red. The phosphonate inhibitor covalently bound to the nucleophile Ser82, the calcium ion, and the disulfide bridge are shown in ball and stick representation in cyan, black, and yellow, respectively. B) Secondary structure topology diagram of LipA. The catalytic triad residues (Ser82, Asp229 and His251) and the position of the disulfide bridge are indicated, and a comparison with the canonical α/β hydrolase fold is given. α-Helices and β-strands are represented by rectangles and arrows, respectively. G1 and G2 are 3_{10} helices and are represented by squares. Locations where insertions in the canonical fold may occur are indicated by dashed lines. The figure and adapted description is reprinted with permission from Nardini *et al.* (2000).[33]

1.2.2. Secretion of LipA in Pseudomonas aeruginosa

LipA is a secreted enzyme that is exported in two steps through the type II secretion system into the extracellular space (Figure 1.4). The first step is translocation across the cytoplasmic membrane into the periplasm by the Sec pathway, and the second is export through the Xcp complex into the extracellular space.[40] The Sec pathway is the major transport pathway for extracytoplasmic proteins.[41] Secretory proteins are directed by an N-terminal signal sequence to the Sec pathway.[42] This signal sequence has a conserved structure consisting of

20-25 amino acids with a positively charged N-terminus, a central hydrophobic core and a polar C-terminal domain.[43,44]

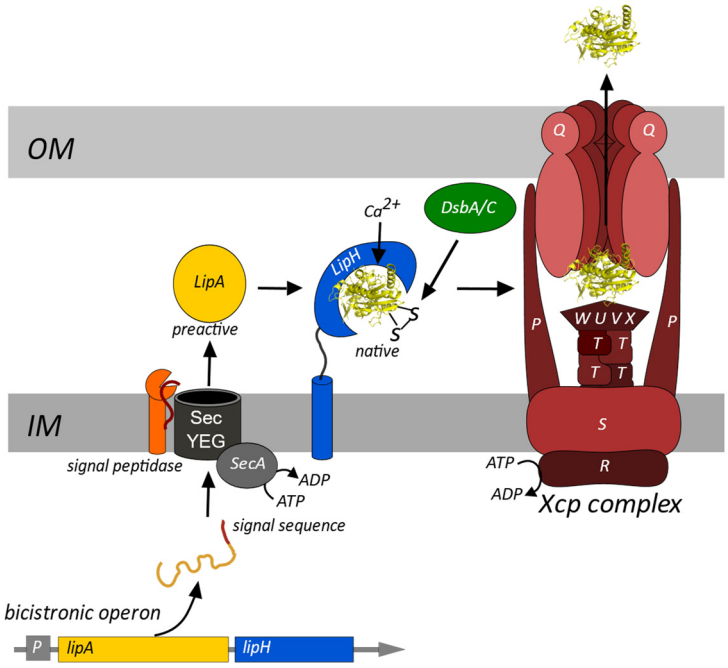

Figure 1.4: Secretion pathway of LipA in *P. aeruginosa*.
LipA (yellow) is transcribed and translated from a bicistronic operon with its lipase-specific foldase LipH (blue) and directed by an N-terminal signal sequence to the Sec pathway after synthesis. Driven by ATP hydrolysis, SecA pushes the unfolded LipA peptide chain through the SecYEG channel. After transport across the inner membrane (IM), LipA starts to fold into its preactive state and is further matured by the cleavage of its signal sequence, the binding of a calcium ion, the formation of a disulfide bridge (S-S) and activation by its lipase-specific foldase. Afterwards, it is transported across the outer membrane (OM) by the Xcp complex and released into the extracellular space. The graphic is based on the description of Rosenau *et al.* (2004)[45] and Douzi *et al*. (2011 and 2012).[40,46]

The translocation can be co- or posttranslational. For cotranslational translocation, the signal recognition particle (SRP) binds to the nascent chain and directs the ribosome to the Sec-channel. This so-called SRP pathway is mostly used for integral membrane proteins.[47,48] The posttranslational translocation can be triggered by the signal sequence recognition by the cytoplasmic chaperone SecB, which binds the nascent protein chain, preventing its folding, and later passes the preprotein to SecA at the Sec-channel.[49,50] The signal sequence of the translated protein can also be directly recognized by cytoplasmic SecA and passed to the Sec channel.[51]

SecA is an ATP-driven translocase that drives the transport of the protein across the inner membrane by transporting the peptide chain via ATP hydrolysis through the protein conducting channel, which is formed by a heterotrimeric protein complex (SecYEG).[52] First, the loop of the signal sequence and the N-terminus of the mature enzyme are inserted into the protein conducting channel, resulting in cytoplasmic orientation of the signal sequence

and periplasmic exposure of the loop.[53] The signal sequence is released through a lateral gate of SecY into the membrane, forming a transmembrane helix anchor for the translocating protein,[54] which is further propelled by SecA through the protein conducting channel in 20-30 amino acid steps.[53,55,56] During translocation, the preprotein starts to fold into its native structure, and the signal sequence is cleaved by a signal peptidase during or shortly after translocation.[53] For its native state, LipA needs to incorporate a calcium ion inside its metal binding center, and the formation of its disulfide bridge is supported by disulfide oxidoreductases DsbA and DsbC.[57] Furthermore, to reach its active conformation, LipA is dependent on the help of a steric chaperone, LipH. LipH binds to LipA during or after translocation and induces a conformational change that leads to the native stable structure of LipA.[45] After LipA has reached its native conformation, it is transported by the Xcp complex into the extracellular space. The Xcp complex is conserved in most Gram-negative bacteria and was first found in *Klebsiella* species.[58] Generally, 12 proteins are involved in its formation. In *P. aeruginosa,* they are called XcpA and XcpP to XcpZ.[59] XcpQ is the only outer membrane component and forms a dodecameric pore (secretin) with a diameter of approximately 55 Å that is responsible for the final release of secretory proteins into the extracellular space.[60] XcpP is anchored in the inner membrane and interacts with secretin to form a channel that spans the entire periplasmic space. Inside this channel, XcpT, XcpU, XcpV, XcpW and XcpX form a pseudo pilus, which consists of a quaternary complex (XcpU - XcpX) as the pilus tip and helical polymerized XcpT as the piston.[61] The polymerization of XcpT and therefore the elongation of the pseudo pilus is driven by XcpR under ATP hydrolysis to transport secretory proteins inside the secretin channel out of the cell.[62] In addition to the Xcp complex, *P. aeruginosa* exhibits another set of genes encoding a similar export machinery called Hcx. Each of these export machineries secretes a specific set of substrates.[63] How these two secretion machineries recognize their substrates is not known. Because of the lack of a defined signal sequence, it is highly likely that the secretory proteins are recognized by structural motifs that direct the proteins into the secretin channel by specific interactions with components of the export machinery.[40]

1.3. Protein folding

Protein folding is a spontaneous, highly cooperative process that allows proteins to fold into their native state within microseconds to minutes.[64] It is driven by hydrophobic interactions, the formation of hydrogen bonds, van der Waals forces and sometimes covalent bonds. In addition to these intrinsic forces, protein folding is highly influenced by the surroundings, which can compete with intramolecular interactions or favor folding via entropic forces.

Folding occurs on different timescales with fast formation of secondary structure elements such as α-helices and β-strands via short range contacts and slow formation of tertiary structure elements from the established secondary structure elements via long-range contacts. The two processes also influence each other and are not strictly separable.[65]

The process of cooperative protein folding is often represented as a folding funnel, in which the conformational freedom of the protein chain is described by the width of the funnel, and the decrease in free energy during the folding process is represented by the depth of the funnel (Figure 1.5).

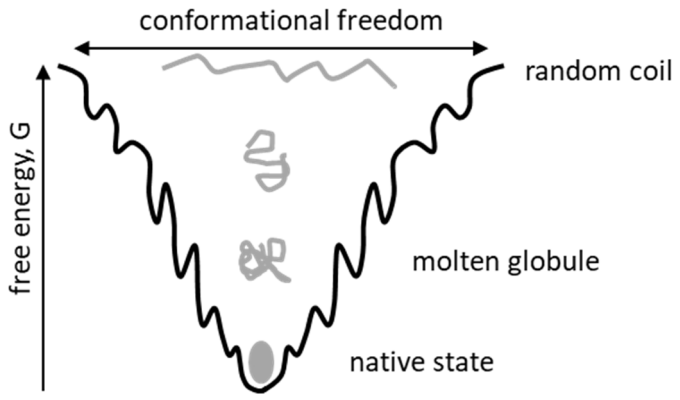

Figure 1.5: Schematic representation of protein folding energy landscape as folding funnel.
During the folding process, the protein chain (shown in gray) undergoes conformational changes from unfolded random coil to molten globular states to the final native state. The conformational freedom is narrowed and the Gibbs free energy decreased with every new intramolecular contact on the path to the native state.[66]

The protein “falls down” the funnel during folding, decreasing its conformational space and its free energy during the formation of native contacts until it folds into its native conformation at the bottom of the funnel. The roughness of the funnel walls represents local energetic minima with small energetic barriers that must be overcome by partial conformational changes to progress along the folding pathway to the native state. This representation describes the folding pathway for proteins that find their native state at the global energetic minimum and whose folding is strictly thermodynamically controlled. The folding funnel representation is mainly based on the “thermodynamic hypothesis of protein folding“, postulated by Christian Anfinsen, after he observed the reversible refolding of ribonuclease A.[67] This hypothesis states that the three-dimensional structure of a native

protein, under normal physiological conditions, is the one in which the Gibbs free energy of the whole system is the lowest and that all information needed for folding into the native state is given by the amino acid sequence, which was designed by the selection pressure for its specific physiological conditions during evolution.[68]

This theory is valid for many small proteins, but most larger proteins are not able to refold into their native structure after complete denaturation.[69] Normally, folding starts immediately during the translational process at the ribosome. This cotranslational protein folding gives the polypeptide chain a defined starting point for folding and excludes many pathways that would lead to other non-native energetic minima. Therefore, thermodynamically driven protein folding does not have to lead to the global energetic minimum but to accessible local energetic minima, which are protected by energetic barriers that, under near-physiological conditions, prevent the drift off into energetically lower misfolded states.[70]

1.3.1. Chaperones

The folding process of proteins is highly influenced by their surroundings. Polar or nonpolar interactions with solvent and other neighboring molecules can compete with the intrinsic forces that drive protein folding, leading to side pathways and misfolded nonfunctional conformations. Several stress factors, such as pH, heat, salt strength or chemicals, can also influence the energetic landscape of folded proteins and may provide pathways to new energetic minima into which the protein can fall and misfold.[71] Upon removal of the stress factors, misfolding might be reversible or irreversible.[72]

Because misfolded proteins can be dangerous for the cell, nature has developed a strict housekeeping system that helps proteins to refold into their native conformation or degrades them to avoid further cell damage caused by false activity or protein aggregation. Molecular chaperones are an important part of this housekeeping system. They form a highly inhomogeneous class of proteins that are involved in protein folding at several stages.[73] Some chaperons are involved in the assembly of nascent protein chains to accomplish fast and effective folding. Peptidylprolyl isomerases and disulfide bridge isomerases help to accelerate specific slow folding steps.[74] Some prevent fast folding by holding proteins in unfolded states, for example, for protein trafficking, as described above for SecB.[49] Stress response chaperones, such as heat shock proteins, help to refold proteins into their native conformation

after they have misfolded as stress response and are also involved in protein unfolding for proteolytic degradation.[72]

Molecular chaperones support protein folding without high substrate specificity and do not add additional steric information to the folded proteins during their support. In contrast, nature has developed another class of chaperones that act highly specifically on one substrate and are necessary for their substrate proteins to reach the native conformation because they provide additional steric information that is not encoded in the mature amino acid sequence of the protein.[75] These so-called steric chaperones help their target proteins overcome energetic barriers on their folding pathway to their native state. The best studied examples of steric chaperones are the prodomains of the secreted protease subtilisin from *Bacillus amyloliquefacies* and of the α-lytic protease from *Lysobacter enzymogenes*.[74] These prodomains are produced as N-terminal extensions of the proteases and act as intramolecular steric chaperones.

Proteases need to fold into a tightly packed conformation to exclude flexible parts as contact points for proteolytic degradation and to enable longevity under harsh environmental conditions.[76] This tight packaging of structural elements is accompanied by a loss of structural entropy, which destabilizes the folded state. The native states of these proteases are marginally thermodynamically stable or occupy even higher energetic states than the preactive state into which these proteases fold in the absence of their prodomains.[77] Their native states are able to exist because they are protected by a large energetic barrier derived by highly cooperative folding that protects them from unfolding. Steric chaperones help to overcome this energetic barrier by stabilizing the transition intermediate and lowering the energetic barriers. In the case of proteases, the prodomains are autocatalytically cleaved off after activation but stay bound to act as protease inhibitors to prevent proteolytic activity inside the cell before secretion until they are proteolytically degraded by the mature protease.[74]

1.3.2. Lipase-specific foldases

Lipase-specific foldases (Lifs) form another class of steric chaperones that are necessary for the folding and secretion of microbial lipases.[78] The dependency of the correct folding of lipases on these classes of steric chaperones was first discovered for the *Burkholderia cepacia* lipase in 1991.[79] Today, many other lipases have been found to be dependent on such a

chaperone.[45] Such chaperones are always encoded in bicistronic operons downstream of the lipase genes and, in contrast to most other steric chaperons, act intermolecularly as separate protein entities and not as prodomains, which are later cleaved off. Based on their sequence similarities, the class of Lifs were divided into four distinct families (Table 1.1).[45]

Table 1.1: Classification of Lifs from Gram-negative bacteria based on amino acid homology.

Family no.	Origin of Lif	Identity [%]	Size Residues [kDa]	Amino acid composition [%] hydrophobic LIFVM	charged KRED	Acc. number
I	*P. aeruginosa* PAO1	100	340 (37.6)	25.0	26.2	CAA44998
	P. aeruginosa TE3285	100	340 (37.7)	24.7	26.2	Q01725
	P. pseudoalcaligenes	55	344 (37.9)	25.3	24.4	CAA02276
	P. mendocina	51	335 (37.3)	26.9	25.1	AAM14702
	P. wisconsinensis	30	352 (39.6)	24.1	25.6	O05938
II	*B. glumae* PG1	100	353 (36.8)	19.0	21.8	Q05490
	*P. spec.*KWI-56	57	344 (36.5)	19.5	21.8	P25276
	P. fragi	56	344 (36.3)	20.1	22.7	E04514
	B. cepacia	56	344 (36.4)	18.9	22.7	B39133
	X. fastidosa Temicula 1	46	353 (40.0)	29.7	26.1	NP 778696
	X. fastidosa 9a5c	46	350 (39.7)	30.6	26.0	NP 298472
	R. metallidurans	29	351 (38.6)	19.9	24.8	ZP 00025702
III	*A. calcoaceticus* BD413	100	343 (39.0)	25.4	21.6	Q43961
	A. calcoaceticus (RAG1)	32	346 (38.6)	28.3	21.4	Q9X2S4
IV	*V. cholerae* ElTor	100	284 (32.6)	24.3	21.8	NP 232621
	V. vulnificus CMCP6	41	280 (31.8)	27.5	28.2	NP 761197
	P. spec. KFCC10818	33	279 (33.3)	30.1	26.5	AAD22079

Table is reproduced with permission from Rosenau *et al.* (2004).[45]

The Lifs of *P. aeruginosa* PA01, *Burkholderia glumae* PG1, *Acinetobacter calcoaceticus* BD413 and *Vibrio cholerae* ElTor represent families I - IV, respectively.

Members of the different families share low sequence identities: only 8 amino acids are highly conserved among all known Lifs. Sequence-based structure prediction reveals that all Lifs possess similar structural folds, consisting of 70 % α-helices and 30 % random coils.[45,74,80] In 2006, Pauwels *et al.*[81] solved the structure of the *Burkholderia glumae* lipase-specific foldase (LipB). The structure shows the folding domain of LipB in the complex with its lipase (LipA) (Figure 1.6). The folding domain consists of 11 α-helices, which can be divided into 3 small domains (called mini domain 1, elongated helix domain and mini domain 2). These 3 domains engulf the globular structure of LipA, with the mini domains positioned on opposite sides of LipA, resulting in a very large contact interface of approximately 5,400 $Å^2$. The interactions of LipA and LipB are mainly nonpolar with only 20 intermolecular hydrogen bonds.[81]

The folding domain is connected by a flexible alanine- and proline-rich linker to a highly conserved transmembrane helix, which anchors them in the cytoplasmic membrane.[78,82]

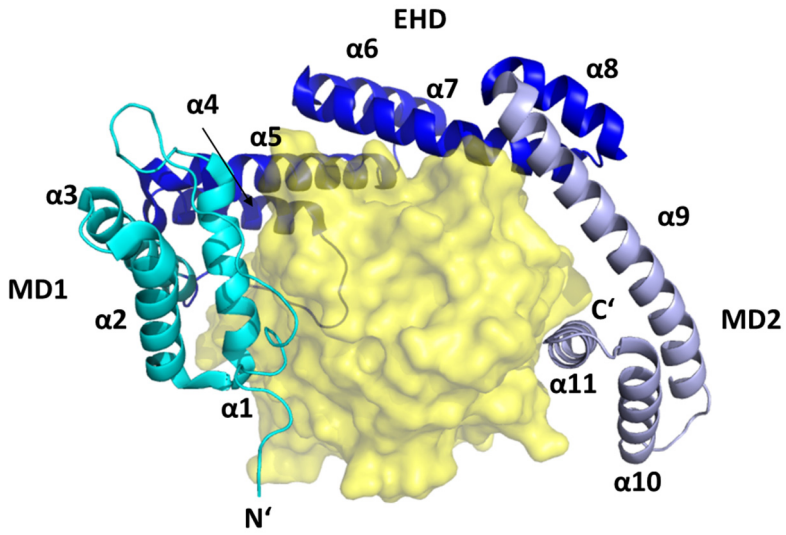

Figure 1.6: Structure of the LipB in the complex with LipA from *Burkholderia glumae.* Lipase-specific foldase structure of *B. glumae* PG1 solved by Pauwels *et al.*[81] (PDB entry: 2ES4) in complex with LipA. The folding domain of LipB consists of 11 α-helices divided into 3 domains. Mini domain 1 (MD1), elongated helix domain (EDH) and mini domain 2 (MD2) are colored cyan, dark blue and light blue, respectively. LipA is shown in yellow as a transparent surface representation.

In vitro refolding experiments with lipases and truncated Lifs showed that only the folding domain is needed for lipase activation.[83–85] *In vivo*, the flexible linker and the N-terminal transmembrane helix seems to play a crucial role during the secretion process of lipases by retaining Lif in the inner membrane during the secretion of LipA or positioning the folding domain for interactions with the secretion machinery, which is important for the secretion of lipases.[86–89]

Cells produce lipase-specific foldases at much lower levels than their lipases; thus, it was assumed that foldases function as multiturnover catalysts for lipase activation.[90,91] Interestingly, the *in vitro* refolding of lipases with foldases showed 1:1 complex formation without observed lipase release and multiple lipase activations.[45,74,81,83,85,88,92,93]

1.4. Aim of this thesis

Lipases are an important class of enzymes for biotechnology, but the accessibility of many lipases for biotechnological applications is hindered by challenges in their expression. The establishment of cultivation procedures for the homologous production of target enzymes in uncultivated strains can be cost- and time-intensive. The yields of secreted enzymes are often low, and strains must be genetically engineered to increase enzyme production to an appropriate level. Often, heterologous production in well-studied model organisms is also difficult due to the complex mechanism of secretion and, in the case of some secreted lipases, the requirement for lipase-specific foldases.

Several attempts to obtain active lipases by heterologous expression with coexpressed lipase-specific foldases resulted in the production of inactive insoluble protein aggregates (inclusion bodies). The solubilization of these inclusion bodies by denaturation and renaturation in the presence of lipase-specific foldases yields active lipases, but often with low total enzymatic activity.

This thesis aims to extend the understanding of the mechanism of action of foldases and the refolding of lipases *in vitro* using the lipase-foldase system (LipA and LipH) of *Pseudomonas aeruginosa* PA01 as a model system.

By structural investigations of LipH and comparison with the known structure of LipB from *Burkholderia glumae,* we tried to identify the essential characteristics of lipase-specific foldases for their refolding. Biophysical and biochemical characterization and comparison of the preactive state and native state of LipA should provide new insights into the changes occurring during the lipase-specific foldase-mediated folding reaction of LipA *in vitro*. Both approaches should help to extend the existing knowledge of the underlying mechanism and to answer open questions, such as what the differences between the *in vitro* and *in vivo* processes are and why foldases act as single-turnover catalysts *in vitro*, whereas they are as multiturnover catalysts *in vivo.*

2. Materials and methods

2.1. Used materials and instruments

All commercially available chemicals and instruments were purchased from distributors given in Table 2.1.

Table 2.1: List of distributors.

Analytik Jena AG	Jena	Germany
BANDELIN electronic GmbH & Co. KG	Berlin	Germany
BioBudget Technologies GmbH	Krefeld	Germany
Biometra GmbH	Götttingen	Germany
Biotix Inc.	San Diego	California, USA
Bio-Rad Laboratories GmbH — Deutschland	Munich	Germany
Brand GmbH + Co. KG	Wertheim	Germany
Bruker Corporation	Billerica	Massachusetts, USA
Capp ApS	Odense	Denmark
Carl Roth GmbH + Co. KG	Karlsruhe	Germany
Eppendorf AG	Hamburg	Germany
Eurofins Genomics GmbH	Ebersberg	Germany
GE Healthcare Europe GmbH	Freiburg	Germany
GFL Gesellschaft für Labortechnik mbH	Burgwedel	Germany
Hampton Research	Aliso Viejo	California, USA
Intas Science Imaging Instruments GmbH	Göttingen	Germany
JASCO Germany GmbH	Groß-Umstadt	Germany
Integrated DNA Technologies	Coralville	Iowa, USA
Merck KGaA	Darmstadt	Germany
Molecular Devices LCC	Sunnyvale	California, USA
NanoTemper Technologies GmbH	Munich	Germany
New England Biolabs GmbH	Frankfurt/Main	Germany
Olympus Corporation	Tokyo	Japan
Perkin Elmer Las GmbH	Rodgau	Germany
PicoQuant GmbH	Berlin	Germany
QIAGEN GmbH	Hilden	Germany
Raytest Isotopenmessgeräte GmbH	Straubenhardt	Germany
Rigaku Europe SE	Ettlingen	Germany
Sarstedt AG & Co.	Nümbrecht	Germany
Sartorius AG	Göttingen	Germany
Tecan	Männedorf	Schweiz
Thermo Fisher Scientific GmbH	Dreieich	Germany
VWR International GmbH	Langenfeld	Germany

Basic chemicals were generally provided by Carl Roth or Sigma Aldrich (Merck). For advanced chemicals or instruments, distributors are entitled directly within the method. All used commercially available enzymes were purchased from Thermo Fisher Scientific, if not stated otherwise. All buffers were prepared with DIN ISO 3696:1991-06 conform ultra-pure water (further stated as pure water), that was derived from Milli-Q® integral water purification system (Merck).

To avoid adsorption of hydrophobic proteins to plastic ware, following low-binding materials were used:

- 1000 µl pipette tips xTIP® low retention (Biotix),
- 200 µl and 10 µl pipette tips ultra-low retention tips (Brand),
- protein low-binding Eppendorf tubes (Eppendorf),
- Plate+™ glass coated microtiter and deep well plates (Greiner) (plates were recycled by washing with pure water and 100 % ethanol directly after experiments and dried at 40 °C),
- low binding *Expell* PCR tubes and 96 well PCR plates (Capp)

2.2. Used bacterial strains, oligonucleotides and plasmids

Table 2.2: List of used bacterial strains and their genotype.

Strain	Genotype	Reference
E. coli DH5α	F– Φ80*lac*ZΔM15 Δ(*lac*ZYA-*arg*F) U169 *rec*A1 *end*A1 *hsd*R17 (rK–, mK+) *pho*A *sup*E44 λ– *thi*-1 *gyr*A96 *rel*A1	Hanahan (1983)[94]
E. coli BL21 (DE3)	*E. coli* B dcm ompT hsdS($r_B^-m_B^-$) gal, λDE3	Studier *et al*.(1986)[95]
E. coli B834 (DE3)	F- ompT hsdSB(rB- mB-) gal, dcm, met, λDE3	Wood *et al*. (1966)[96]
P. aeruginosa PAO1	wild type	Holloway *et al.* (1979)[97]
P. aeruginosa PABST7.1	Δ(¾lipA ⅓lipH) miniD-180 (tetA tetR lacIq PlacUV5-T7gene1)	Jaeger *et al.* (1997)[98]

Table 2.3: List of used oligonucleotides.

P#	Name	Sequence	Features
1	seq_lipAH_mid_FW	GACAACTACCGGATGAACCAC	sequencing primer; binding: *lipA* bases 810-831 downstream
2	seq_LipAH_mid_RV	AACGCCAGTGGAATCAGCAG	sequencing primer; binding: *lipH* bases 15-35 upstream
3	NdeI_LipH_FW	cttaa**CATATG**AAGAAAATCCTC CTGCTGATTCC	cloning primer; binding: *lipH* downstream; feature: NdeI cutting site 5' end
4	BamHI_LipH_RV	cttaa**GGATCC**TCAGCGCTGCTC GGCCTGG	cloning primer; binding: *lipH* upstream; feature: BamHI cutting site 5' end
5	LipH_dLinkVD_FW	**GGCCATCACCATCACCATCAC**C TGCCAACCTCCTTCAGGG	mutational primer; binding: *lipH* bases 195-214 downstream, overlap to LipH_dLinkVD_RV; feature: insert Gly(2)-His_6, ΔVD
6	LipH_dLinkVD_RV	CAG**GTGATGGTGATGGTGATG GCC**CATGGTATATCTCC	mutational primer; binding: pEHTHis19-startcodon, overlap to LipH_dLinkVD_FW; feature: insert Gly(2)-His_6, ΔVD
7	LipH_E268C_FW	GTCAGCAACTGGTGGGCGCC**T** **GC**GCCACCACCCGCCTGGAGC	mutational primer; binding: *lipH* bases 804-823 upstream, overlap to LipH_E268_RV; feature E268C
8	LipH_E268_RV	GGCGCCCACCAGTTGCTGACG C	mutational primer; binding: *lipH* bases 804-823
9	LipH_backbone_FW	TGACCGGCACGGAAACGC	mutational primer; binding: *lipH*-Stop codon-pEHTHis19 downstream
10	LipH_MD1_RV	TTTCCGTGCCGGTCACAGTTCC TTCTTGTAGTCGATG	mutational primer; binding: *lipH* bases 416-438, overlap to LipH_backbone_FW; feature: ΔEHD-MD2
11	EHDMD2_FW	GGC **CATCACCATCACCATCAC** GAAGACCAGCAGGAAAGCGTG C	mutational primer; binding: *lipH* bases 675-697 downstream, overlap to EHDMD2_RV; feature insert Gly(2)-His_6, ΔMD1-α6EHD
12	EHDMD2_RV	TTCGTGATGGTGATGG TGATGGCCCAT GGTATATCTCC	mutational primer; binding: pEHTHis19-Met-Gly(2)-His_6-LipH-E226 upstream
13	LipA_S82_FW	CACGGCGGGCCGACCATCCGC TACG	mutational primer; binding: *lipA* bases 324-349 downstream
14	LipA_S82A_RV	CGGATGGTCGGCCCGCCGTG**G** **GC**GTGGCCGATCAGGTTGACC	mutational primer; binding: *lipA* bases 302-321 upstream, overlap to LipA_S82_FW; feature: LipA S82A
15	LipH_Y99A_FW	ACATCCGCAACCTGTTCGAC**GC** **C**TTCCTCAGCGCCGTCGGCG	mutational primer; binding: *lipH* bases 297-316 downstream, overlap to LipH_Y99_RV; feature: LipH Y99A
16	LipH_Y99_RV	GTCGAACAGGTTGCGGATGTC GC	mutational primer; binding: *lipH* bases 271-294 upstream

small letters: non-sense bases; bold letters: introduced features; grey letters: complementary overlapping sequences

Table 2.4: List of used plasmids.

Name	Genotype	Reference
pBBR1MCS2	Kan^r rep mob Kan^r lacZα P_{lac} P_{T7}	Kovach *et al.* (1995)[99]
pET-19b (+)	ColE1 Amp^r $lacI^q$ P_{T7}	Novagen (Merck)
pET-22b (+)	ColE1 Amp^r $lacI^q$ P_{T7}	Novagen (Merck)
pBBR1MCS/PA *lipAH*	pBBRPA-lipA with *lipH* from pBBRPA lipH (NdeI/BamHI), $P_{T7,}$ Cam^r	Janosch (2002)[100]
pBBR2/PA *lipAH*	pBBR1MCS/PA *lipAH*, exchanged resistance cassette, Kan^r from pBBR1MCS2 (XhoI/ SfiI)	this work
pBBR2lipAHff	pBBR2/PA *lipAH* with reinserted wild type *lipH* gene PAO1with P#:3+4	this work
pLipA-SS	pET22b (NdeI, BamHI, 916 bp; *lipA Δ1-78 bp* coding for signal sequence, Ser1Met, under P_{T7} control), Amp^r	Hausmann *et al.* (2008)[101]
pEHTHis19	pET19b (NdeI, BamHI, 985 bp; lipH Δ1-60bp coding for TMD, substitution 84 bp His_{10}-tag and soluble linker, under P_{T7} control), Amp^r	Hausmann *et al.* (2008)[101]
pEHTHis19 LipH Q137C	pEHTHis19; mut. LipH Q137C	Keijer (2012)[102]
pEHTHis19 LipH A215C	pEHTHis19; mut. LipH A215C	Keijer (2012)[102]
pEHTHis19 LipH E268C	derived from pEHTHis19; mut. LipH E268C, P#:7+8	this work
pEHTHis19 LipH R296C	pEHTHis19; mut. LipH R296C	Keijer (2012)[102]
pEHTHis19 LipH Q137C/A215C	pEHTHis19; mut. LipH Q137C/A215C	Keijer (2012)[102]
pEHTHis19 LipH Q137C/E268C	derived from pEHTHis19 LipH Q137C; E268C, P#:7+8	this work
pEHTHis19 LipH Q137C/R296C	pEHTHis19; mut. LipH Q137C/R296C	Keijer (2012)[102]
pEHTHis19 LipH A215C/E268C	derived from pEHTHis19 LipH A215C; E268C, P#:7+8	this work
pEHTHis19 LipH A215C/R296C	pEHTHis19; mut. LipH A215C/R296C	Keijer (2012)[102]
pEHTHis19 LipH E268C/R296C	derived from pEHTHis19 LipH R296C; E268C, P#:7+8	this work
pETLipH ΔVD	pET19b, MGH_6-LipH(ΔTMD-VD), derived from pEHTHis19 with P#:5+6	this work
pETLipH MD1	pET19b, MGH_6-LipH (MD1), derived from pETLipH ΔVD with P#:9+10	this work
pETLipH EHDMD2	pET19b, MGH_6-LipH (EHD(α7,8)-MD2), derived from pETLipH ΔVD with P#:11+12	this work
pLipA-SS S82A	derived from pLipA-SS, mut. LipA S82A, P#:13+14	this work
pETLipH Y99A	derived from pEHTHis19; mut. LipH Y99A, P#:15+16	this work
pETLipH MD1 Y99A	derived from pETLipH MD1; mut. Y99A P#:15+16	this work

All provided plasmids were sequences before use. Detailed sequential organizations are given in Appendix 8.2. "P#" is indicating the primer numbers used for genetic changes (Table 2.3).

2.3. DNA handling and manipulation

Manipulations of vectors, like insertion, deletion or mutation of DNA sequences, were performed by a so-called Sequence and Ligation Independent Cloning (SLIC) method, which is independent from restriction sites. Instead, it uses complementary DNA sequences that are introduced into the desired gene fragment by PCR and enzymatically digested to yield single stranded DNA overhangs. The affinity of these single stranded DNA overhangs is high enough that DNA pieces stay annealed during transformation, without the need of covalent ligation.

For insertion of large DNA sequences into a vector, insert and backbone were amplified by PCRs in two separate reactions followed by annealing. For the introduction of mutations, small insertions or the deletion of sequences, the whole vector was amplified by PCR using mutagenic primers that carried the mutation, insertion or deletion site.

Remaining primers and dNTPs were always removed by fast silica-based DNA purification procedure after PCR. If site-products were observed, desired PCR products were isolated by preparative gel electrophoresis and gel extraction. *E. coli* DH5α cells were transformed with the SLIC reaction mixture and streaked out on LB-agar plates. If possible, single colonies were tested for the manipulated gene by colony-PCR and restriction, before plasmids were isolated and sequenced.

For vectors, which sequences of interest were not completely known, the classic restriction and ligation method was used. The detailed procedures are described in the following chapters.

2.3.1. Primer design for SLIC

Primer pairs for SLIC were generally designed as it is shown in Figure 2.1. The primers consisted of annealing parts for template amplification during PCR (shown in black), an overhang which is complementary to the other primer (shown in gray) and in between the site of interest (shown in red), in which a mutation, an insertion or a deletion can be introduced.

The annealing parts were designed according to the recommendations of Phusion polymerase distributor. Generally, a sequence length of 18-24 nucleobases was chosen depending on its melting temperature, which was calculated by the online tool “Tm calculator” from New England Biolabs[103]. High GC-content of *P. aeruginosa* DNA, can cause melting temperatures of primers above 72 °C. In this case, annealing temperatures in PCRs were set to 66 °C. To increase the affinity of the reverse primer to the template DNA compared to the

complementary overhang, the annealing part of the reverse primer was chosen 3-5 nucleobases longer than the overhang.

Figure 2.1: Design of primer pairs for SLIC.

Final primer sequences were further validated with the online tool "Oligoanalyzer 3.1" from Integrated DNA Technologies[104,105] to exclude strong secondary structures or dimer formation. Oligonucleotides were purchased from Eurofins in standard quality (0.01 µmol scale, salt free, unpurified).

2.3.2. Polymerase chain reaction

Amplification of DNA fragments was done by polymerase chain reaction using the Phusion High-Fidelity DNA Polymerase according to manufacturer's recommendation. 50 µl PCR reaction mixture, which contained 1 x concentrated GC buffer, approximately 1 ng DNA template, 200 µM of each dNTP, 500 nM of each primer, 1.5 % (v/v) DMSO, and 1 U Phusion DNA polymerase, was incubated in Biometra TAdvanced (Biometra) thermal cycler with the following thermal program:

1.	Initial denaturation:	1 min at 98 °C
2.	Denaturation:	10 s at 98 °C
3.	Annealing:	10 s at 66 °C
4.	Elongation:	30 s/1 kb of template length at 72 °C
5.	Repetition of step 2 - 4 for 35 times	
6.	Final elongation:	10 min at 72 °C

If the desired product could not be obtained, the annealing temperature, annealing time or DMSO concentration was modified. After successful PCR reaction, template DNA was digested with 10 U DpnI at 37 °C overnight.

2.3.3. Agarose gel electrophoresis of nucleic acids

Agarose gel electrophoresis was used to analyze DNA samples or to isolate larger amounts of DNA fragments following the protocol described by Sambrook *et al.*[106]. Depending on the

expected size of DNA fragments, agarose gels were casted from 0.8 - 2 % (w/v) of molten agarose in 0.5 x TBE buffer (44.5 mM TRIS, 44.5 mM boric acid, 1 mM EDTA, pH 8) into an appropriate gel chamber. 0.5 % (v/v) ethidium bromide was added to the still molten agarose. DNA samples and standard size marker (Gene Ruler 1 kb DNA ladder, Thermo Fisher Scientific) were mixed with DNA sample buffer (Thermo Fisher Scientific) before loading into gel pockets. The electrophoresis was performed in Mini-Sub® Cell GT aperture (Bio-Rad) in 0.5 x TBE buffer at 135 mA for 35 min. Ethidium bromide stained DNA was visualized under UV light using the Gel iX Imager (Intas Science Imaging Instruments).

2.3.4. Isolation and purification of DNA

Plasmidic DNA preparations were done by the method of alkaline lysis and silica-membrane based DNA adsorption. Therefore, the innuPREP Plasmid Mini Kit (Analytik Jena) was used according to manufacturer's recommendations. For the extraction of DNA fragments from agarose gel or for the fast purification of PCR products the innuPREP DOUBLEpure Kit (Analytik Jena) was used according to manufacturer's recommendations. Genomic DNA was isolated using the DNeasy Blood & Tissue Kit (Qiagen) following the procedure for isolation of genomic DNA from Gram-negative bacteria after manufacturer's recommendation.

2.3.5. Determination of DNA concentration

DNA concentrations were determined by measuring the absorbance at 260 nm with NanoDrop 2000c (Thermo Fisher Scientific) using 2 µl samples.

2.3.6. Sequence and ligation independent cloning

Ligation independent cloning was first described by Aslanidis *et al.* (1990)[107]. It uses *in vitro* homologous recombination with complement single stranded DNA overhangs, which have been produced by the exonuclease activity of T4-DNA polymerase in absence of dNTPs. The lengths of these overhangs had been controlled by the absence of one nucleobase in the complement sequence and the addition of this specific dNTP to the reaction mixture. This procedure has been further simplified and improved[108,109] to a really fast and reliable bench top protocol described by Jeong *et al.* (2012)[110]. Here, the exonuclease activity of T4-DNA polymerase is not controlled by the absence of one nucleobase anymore, but simply by

reaction time and temperature, making this cloning procedure a completely sequence independent method.

20 nucleobases, that were introduced by PCR primers, were used as complement DNA overhangs and were digested to single stranded overhangs in the following reaction. Approximately 100 ng of amplified vector and 40 ng of insert(s) were mixed with 1 µg BSA and 1 µl of NEB Buffer 2 (New England Biolabs) in a 10 µl reaction at room temperature. 1.5 U of T4-DNA polymerase was added and incubated for 2.5 min at room temperature followed by 10 min on ice. Afterwards, 1-2 µl of the reaction mixture was used for transformation of *E. coli* DH5α (see chapter 2.4.5).

2.3.7. Colony PCR

Colony PCR was used to determine whether a colony carried the desired plasmidic DNA or not. Therefore, a PCR reaction mixture was prepared like described in chapter 2.3.2 without template DNA. A colony from solid agar plates or cell mass from pelleted cultures were picked with a sterile toothpick and added to the PCR mixture by dipping and carefully swirling. The remaining cells at the toothpick were used to inoculate a new culture for further experiments. The PCR was incubated in the same thermal program that is described in chapter 2.3.2 with initial denaturation lasting for 5 min.

2.3.8. Sequence determination

DNA sequencing reactions were performed by Eurofins. To exclude sequencing errors, forward and reverse sequencing reactions of the desired gene were performed and aligned with the sequence of interest.

2.3.9. Restriction and ligation

DNA restrictions were performed with restriction enzymes according to manufacturer's recommendations. The restricted DNA fragments were purified by preparative gel electrophoresis and gel extraction and were ligated by T4-DNA ligase according to manufacturer's recommendations.

2.4. Cultivation and preparation of bacterial cells

2.4.1. Used media

Media and solutions were sterilized by autoclaving at 121 °C, 200 kPa for 20 min.

LB medium:
10 g/l tryptone, 5 g/l yeast extract, 10 g/l NaCl, pH 7 (as premixed powder from Roth).

LB agar medium:
LB medium supplemented with 1.5 % (w/v) agar

M9 medium:
Modified after Sambrook *et al.*[106]

10 %	Solution I:	40 g/l glucose
1 %	Solution II:	20 g/l $MgSO_4 \times 7\ H_2O$
1 %	Solution III:	2 g/l $CaCl_2 \times 2\ H_2O$
10 %	Solution IV	70 g/l Na_2HPO_4 x 2 H_2O; 30 g/l KH_2PO_4; 5 g/l NaCl
0,1 %	Solution V:	1.6 g/l $MnSO_4$; 2.8 g/l H_3BO_3; 0.02 g/l $CuCl_2$; 0.24 g/l $ZnSO_4$, 0.8 g/l Na_2MoO_4
0.12%	Solution VI:	5 g/l $FeSO_4$; 0.16 % (v/v) HCl
10%	Solution VII:	10 g/l NH_4Cl

Solution I-IV were separately autoclaved and solution V-VII were sterile filtrated (0.2 µM pore size, cellulose acetate membrane, VWR). M9 Medium was prepared by mixing solution I-VII in the above given ratios. The remaining volume was filled up with autoclaved pure water. For ^{15}N and/or ^{13}C enriched M9 medium, the needed amount of solution I and/or VII was freshly prepared with sterile filtrated $^{15}NH_4Cl$ and ^{13}C-glucose.

2.4.2. Cultivation and storage of cells

Liquid cultures were cultivated in Erlenmeyer flasks with a volume 10 times greater than the culture volume. All cultures were incubated at 37°C under shaking at 165 rpm on a rotational incubation shaker (3033, GFL). For cultivation on solid media, heated (60 °C) liquid LB agar was poured into Petri dishes. To gain colonies, grown from single cells, diluted cultures were streaked out on solid media using a Drigalski spatula. The Petri dishes were incubated upside down at appropriate temperature overnight. To retain the genetic stability of strains, the culture media were supplemented with respective antibiotic at the concentrations given in Table 2.5. Overnight cultures were inoculated with cells from one colony or from cryo-stocks and cultivated for 16 h. For long-term storage, fresh *E. coli* and *P. aeruginosa* overnight cultures were supplemented with 30 % (v/v) sterile glycerol or 7 % (v/v) DMSO respectively and stored at -80 °C.

Table 2.5: Used antibiotics and concentrations.

Resistance	Antibiotic	Concentration [µg/ml]	
		E. coli	*P. aeruginosa*
Amp^r	Ampicillin	100	--
Kan^r	Kanamycin	50	400
Tet^r	Tetracycline	10	100

2.4.3. Production of electrocompetent *E. coli* cells

Electrocompetent *E. coli* cells were produced according to a modified protocol from Sambrook *et al.*[106]. 250 ml LB-medium was inoculated to an $OD_{580\,nm}$ of 0.1 with *E. coli* cells from a fresh overnight culture and cultivated until an $OD_{580\,nm}$ of 0.4-0.6 was reached. The culture was incubated on ice for 30 min before cells were harvested by centrifugation (4,000 rcf, 4 °C, 15 min). After cell harvesting, cells were always kept cold and all solutions were cooled on ice prior using. The cell pellet was washed three times by suspension (carefully swirling, not pipetting) and centrifugation. The first two times, cells were washed with sterilized pure water and the third time with the sterile solution of 10 % (v/v) glycerol. After washing, the pellet was suspended in 2 ml of 10 % (v/v) glycerol and aliquoted into 50 µl fractions. Electro competent cells were directly transformed with DNA or snap-frozen in liquid nitrogen and stored at -80 °C.

2.4.4. Production of electro competent *P. aeruginosa*

Electro competent *P. aeruginosa* cells were produced after a modified protocol from Choi *et al. (2005)*[111]. Cells of 0.5 ml fresh overnight culture, per electro competent aliquot, were harvested by centrifugation (16,000 rcf, RT, 2 min). The cells were washed twice by suspension and centrifugation with 1 ml of sterile pure water containing 300 mM sucrose. Afterwards, the pellet was suspended in 100 µl of 300 mM sucrose as final volume for electroporation. Depending on the needs, this protocol can be scaled up. Remaining aliquots of electro competent cells can be snap-frozen in liquid nitrogen and stored at -80 °C if glycerol (10 % (v/v)) was added to the buffer in the last suspension step.

2.4.5. Transformation by electroporation

For transformation by electroporation, the frozen electro competent cells (see chapter 2.4.3 and 2.4.4) were thawed on ice. 10 pg to 25 ng of plasmid DNA in a volume of 1 - 4 µl were added to the cells and mixed by pipetting. The suspension was transferred into a pre-chilled and dry electroporation cuvette (2 mm gap width, BioBudget). After applying an electric

impulse of 2500 V/cm with a length of 4 to 5.4 ms using the MicroPulser electroporation devise (BioRad), the cell suspension was taken up with 1 ml LB-media without antibiotics and incubated at 37 °C under slight agitation for an appropriate amount of time (for Amp^r: 1 h, Kan^r: 2 h and Tet^r: 3 h). After incubation, the cells can be spread on agar plates or transferred to liquid-medium containing an appropriate amount of antibiotics.

2.4.6. Expression of *lipA* and *lipH* in *E. coli*

LipA, *lipH* and their variants were expressed in *E. coli* BL21 (DE3) using the T7-expression system with the plasmids pLipA-SS and pEHTHis19 or their derivatives. Therefore, a main culture was inoculated with a fresh overnight culture in LB or M9 media to an OD_{580nm} of 0.1 and cultivated until it reached an OD_{580nm} of 0.5-0.7. The gene expression was induced by addition of 1 mM IPTG. After further cultivation for 2 h, the cells were harvested by centrifugation (10,000 rcf, 4 °C, 30 min) and stored at -20 °C.

2.4.7. Labeling of LipA and LipH with selenomethionine in *E. coli.*

To solve the phase problem in X-ray crystallography by multiwavelength anomalous diffraction phasing[112], LipA and LipH were labeled with selenomethionine. Therefore, *lipA* (on pLipA-SS) and *lipH* (on pEHTHis19) were expressed in the methionine auxotrophic *E. coli* strain B834(DE3) following a modified expression procedure of EMBL[113]. Transformed *E. coli* B834(DE3) cells were cultured in M9 media supplemented with 50 µg/ml (335 µM) methionine. An expression culture was inoculated from a fresh overnight culture to an OD_{580nm} of 0.1 and cultivated to an OD_{580nm} of 1. Cells were separated from culture medium by centrifugation (5,000 rcf, 4 °C, 5 min) and suspended in fresh M9 medium without methionine. Remaining methionine was consumed during starvation for 3 h at 37 °C with slight agitation before 50 µg/ml (255 µM) selenomethionine was added to the culture. It was further cultivated for 30 min before the expression was induced by the addition of 1 mM IPTG. Cells were harvested 2 h after induction by centrifugation (10,000 rcf, 4 °C, 30 min) and stored at -20 °C until purification of labeled proteins.

2.4.8. Expression of *lipA* in *P. aeruginosa*

Native LipA was derived from *P. aeruginosa* PABST7.1 strain, which was transformed with the plasmid pBBR2lipAHff. For overexpression, 200 ml LB medium in a 5 l Erlenmeyer flask was

inoculated with a fresh overnight culture to an OD_{580nm} of 0.4 and grown at 37 °C under shaking at 150 rpm for 40 h. Cells were removed by centrifugation (10,000 rcf, 4 °C, 30 min) and the supernatant containing LipA was further processed as it is described in chapter 2.5.7.

2.5. Protein purification and preparation

2.5.1. Cell disruption

For preparative scale, cells were disrupted by French Press Cell Disruptor with 40,000 psi standard French pressure cell (Thermo Fisher Scientific) in 5 cycles at 500 psi at high range (551 bar). For analytic purposes, samples were disrupted by sonication using the Bandelin Sonoplus UW 2070 with MS 73 sonotrode. An amplitude of 40 % was applied for 3 x 5 min with 0.5 s pulses. Samples were kept on ice during sonication.

2.5.2. Purification of $LipH_{\Delta TMD}$ variants by IMAC

$LipH_{\Delta TMD}$ and their variants were expressed as described in chapter 2.4.6. The cell pellet was suspended in IMAC buffer A (50 mM TRIS, 10 mM imidazole, pH 8) and cells were disrupted by French Press (see chapter 2.5.1). The cell debris were removed by centrifugation (40,000 rcf, 4 °C, 30 min). The IMAC purification of LipH and its variants were done by gravity flow. Therefore, a gravity flow column was filled with 5 ml Ni^{2+}-NTA Superflow Resin (Qiagen) per liter culture volume and equilibrated with 5 column volumes IMAC buffer A. The supernatant was applied in batch binding mode with 5 min incubation on ice and occasionally inverting. The resin was washed with 20-50 column volumes of IMAC buffer A in continuous flow with 2 batch washing steps in between until no protein was detectable anymore in the washing fractions tested with Bradford reagent (see chapter 2.5.8). The protein was eluted with IMAC buffer B (50 mM TRIS, 500 mM imidazole, pH 8) also in a combination of continuous flow and batch mode until no protein was detectable in the elution fractions anymore. The elution fractions were combined and concentrated to < 2.5 ml by ultrafiltration (see chapter 0). Imidazole was removed, and buffer was exchanged to 10 mM TG buffer (5 mM TRIS, 5 mM glycine) by applying the elution phase to a desalting column (see chapter 0). Purified LipH was stored at -20 °C without any additives.

2.5.3. Concentrating of protein samples and buffer exchange

Proteins were concentrated by ultrafiltration at 4,000 rcf at 4 °C. Vivaspin® 20 (Sartorius) filtration devices were used for crude samples. If renatured LipA was present or if a high recovery rate was desired, Amicon® Ultra (Merck) filtration units were used. For full length

LipA and LipH proteins, a cutoff size of 10 kDa and for single LipH domains a cutoff size of 5 kDa was chosen. If high concentration and a buffer exchange were needed in one step, the sample buffer was washed out during ultrafiltration to a theoretical concentration below 0.1 %.

Alternatively, buffers of samples were exchanged by desalting columns using the PD columns of different sizes from GE healthcare following the manufacturers gravity protocol.

2.5.4. Labeling of LipH for FRET measurements

For FRET measurements, LipH was labeled with maleimide functionalized $Alexa_{488}$ and $Alexa_{647}$ dyes (Thermo Fisher Scientific) by a thiol-Michael addition[114,115]. Amino acid residues that should be labeled were substituted by cysteines by SLIC (see chapter 2.3) and the double cysteine variants of LipH were purified as it is described in chapter 2.5.2. The labeling reactions were done successively and labeled protein was purified after each labeling step. Therefore, 100 nmol of purified protein were taken up in 1 ml label buffer (50 mM TRIS, pH 8 at 4 °C) (final concentration: 100 µM). 5 mM TCEP was added from 500 mM stock solution that was adjusted to pH 7.5 and the sample was incubated for 10 min at room temperature. 80 nmol $Alexa_{488}$ (dissolved in DMSO) was added and the sample was incubated for 3 h at room temperature in the dark with slight agitation. Single $Alexa_{488}$ labeled LipH molecules were separated from unlabeled or double labeled by ion exchange chromatography using a 1 ml ResourceQ column (GE Healthcare) on an Äkta explorer system (GE Healthcare). Therefore, the column was equilibrated with IEC buffer A (50 mM BisTRIS, pH 6.3 at RT) before sample application. It was washed with 10 ml IEC buffer A with 1 ml/min, before LipH was eluted in a linear NaCl gradient [IEC buffer B (50 mM BisTRIS, 500 mM NaCl, pH 6.3 at RT), 100 % in 180 min]. Elution phase was collected in 2 ml fractions. During elution, the absorption at 280 nm, 488 nm and 647 nm was recorded. The elution profile varies slightly depending on the charge of the substituted amino acids. Because of the additional negative charge, that is introduced by the Alexa dyes, the unlabeled LipH fractions elutes first, followed by single labeled, double labeled and free dye. The fractions containing single $Alexa_{488}$ labeled LipH were combined and the remaining salts were washed out with labeling buffer during concentration by ultrafiltration (see chapter 0). The concentration of LipH and the labeling efficiency was determined by absorption at 280 nm and 488 nm (NanoDrop 2000c, Thermo Fisher Scientific) using the formula of equations (I) and (II). The $Alexa_{647}$ labeling reaction was

performed similar to the first labeling step using 5 times molar excess of $Alexa_{647}$. After reduction with TCEP, labeling and purification, the fractions with $Alexa_{488}$ and $Alexa_{647}$ labeled LipH were combined washed with label buffer and concentrated to 100 µl by ultrafiltration. 20 % (v/v) glycerol was added for storage at -20 °C.

$$c_{Prot} = \frac{A_{280nm} - \mathrm{corrF}_{488} * A_{488nm} - \mathrm{corrF}_{647} * A_{647nm}}{\varepsilon_{Prot} * l} \quad \text{(I)}$$

$$c_{Dye} = \frac{A_{wavelenght\ dye}}{\varepsilon_{Dye} * l} \quad \text{(II)}$$

ε_{Prot} = 19,940 M^{-1} cm^{-1}
corrF_{488} = 0.11 [a]
corrF_{647} = 0.02 [a]
l = Light path lengths
$\varepsilon_{Alexa488}$ = 71,000 M^{-1} cm^{-1} [b]
$\varepsilon_{Alexa647}$ = 265,000 M^{-1} cm^{-1} [b]
[a] correction factors are given by ratio of absorption at 280 nm and 488 nm and 647 nm respectively. Values were given by the distributor.
[b] excitation coefficients are batch specific and should be validated for each aliquot with given lot number and the certificate of analysis, found on the internet site of Thermo Fisher Scientific.

2.5.5. Purification of LipA inclusion bodies

The inclusion bodies of LipA were purified after a modified protocol of Hausmann[92]. The cell pellet containing LipA as inclusion bodies (see chapter 2.4.6) was suspended in 30 ml IB-buffer (50 mM TRIS, 5 mM EDTA, freshly added 1 mM TCEP, pH 7) and disrupted by French press (see chapter 2.5.1). To avoid degradation, samples and buffers were kept cold. The inclusion bodies were isolated by centrifugation (15,000 rcf, 4 °C, 30 min) and washed 3 times by thorough suspension and centrifugation (4,000 rcf, 4 °C, 15 min). Twice with IB-buffer and the third time with plain 50 mM TRIS buffer. The purified inclusion bodies were suspended in a small amount of water to dissolve large chunks. Afterwards 8 M urea (0.5 ml/100 ml culture volume) was added and it was incubated for 1 h at 37°C (or until all inclusion bodies have been dissolved). Remaining cell debris were removed by centrifugation (21,000 rcf, 4°C, 10 min) and denatured LipA inclusion bodies were stored at -20 °C.

2.5.6. Renaturation and refolding of LipA inclusion bodies

Chemically denatured LipA inclusion bodies (see chapter 2.5.5) were renatured by fast dilution of the denaturant. Therefore, frozen LipA urea stock was thawed and centrifuged (21,000 rcf,

4 °C, 10 min) to remove aggregates that can serve as nuclei for protein aggregation. Afterwards, LipA was diluted at least 100 times into ice cold 10 mM TG (5 mM TRIS, 5 mM glycine) buffer (normally to a final concentration between 1 and 10 µM). To ensure a fast drop of urea concentration, the dilution step was done by fast pipetting and short vortexing. Afterwards, diluted LipA was incubated at 60 °C for 1 h to increase the overall activity of renatured LipA sample after refolding by LipH. The refolding by foldase was performed by adding LipH (if not otherwise stated in an equimolar concentration) and incubation at 4 °C, overnight.

2.5.7. Purification of LipA from supernatant of *P. aeruginosa*

Native LipA was purified from supernatant of *P. aeruginosa* PABST7.1 carrying pBBR2LipAHff (see chapter 2.4.8), by hydrophobic interaction chromatography. Therefore, 200 ml supernatant was sterile filtrated by 0.2 µm Filtropour BT25 (Sarstedt) under vacuum pressure and dialyzed (with standard dialysis membrane tubes) twice against 5 l TG buffer (5 mM TRIS, 5 mM glycine, pH 9) at 4 °C (1st: 4 h, 2nd: overnight). NaCl was carefully added from a 6 M stock solution to a final concentration of 3 M. A 25 ml octyl sepharose 4 fast flow (GE Healthcare) column was equilibrated with HIC buffer A (5 mM TRIS, 5 mM glycine, pH 9, 3 M NaCl) using an Äkta explorer system (GE Healthcare). The crude supernatant was loaded onto the column with 2 ml/min flowrate. First, the column was washed with HIC buffer A with 3 ml/min flowrate until A_{280nm} signal reach its initial value. Afterwards, it was washed with 95 % HIC buffer B (5 mM TRIS, 5 mM glycine, pH9) until A_{280nm} reached base level. LipA is eluted with HIC buffer C (5 mM TRIS, 5 mM glycine, pH9, 80 % (v/v) ethylene glycol). LipA can be stored at -20 °C in HIC buffer C.

2.5.8. Determination of protein concentration

Protein concentrations were primarily determined by the method of Bradford[116] modified by measuring the absorption ratio at wavelengths 595 nm and at 450 nm to consider the absorbance of free Coomassie dye as it is described from Zor *et al.* (1996)[117]. The Pierce™ Coomassie Plus Bradford Assay Reagent (Thermo Fisher Scientific) was used according to their protocol for the microtiter plate assay. Bovine serum albumin in a concentration range from 31.25 µg/ml to 2 mg/ml was used as standard. The samples were diluted to expected concentration of 0.1 mg to 2 mg. 5 µl of the standards and diluted samples were pipetted into

a microtiter plate and mixed with 250 µl of Bradford reagent (at room temperature). Absorption at 595 nm and 450 nm was measured after 10 min incubation at room temperature. The ratios of 595 nm/450 nm were calculated, and the blank value was subtracted from all standards and samples. The values of samples were divided by the dilution factor and the slope of the standard regression line to yield the sample protein concentration in mg/ml. The molar concentration of the protein of interest was calculated using the molecular weight of the protein. Alternatively, the concentration of the protein of interest was determined by absorption at 280 nm using the specific extinction coefficient and Lambert-Beer law by using the NanoDrop 2000c (Thermo Fisher Scientific). The used extinction coefficient and the specific molecular weight for each variant were calculated as described in chapter 2.7.3 and are given in Table 2.6.

Table 2.6: List of extinction coefficients and molecular weights.

Protein variant	Extinction coefficient at 280 nm [M^{-1} cm^{-1}]	Molecular weight [g/mol]
LipA ΔSS	27515	30180
LipA ΔSS S82A	27515	30164
LipH ΔTMD	19940	38332
LipH ΔTMD Q137C	19940	38297
LipH ΔTMD A215C	19940	38354
LipH ΔTMD E268C	19940	38296
LipH ΔTMD R296C	19940	38269
LipH ΔTMD Q137C/A215C	19940	38329
LipH ΔTMD Q137C/E268C	19940	38270
LipH ΔTMD Q137C/R296C	19940	38244
LipH ΔTMD A215C/E268C	19940	38328
LipH ΔTMD A215C/R296C	19940	38300
LipH ΔTMD E268C/R296C	19940	38243
LipH ΔTMD Y99A	18450	38229
LipH ΔTMD-VD	14440	32132
LipH MD1	5960	10094
LipH MD1 Y99A	4470	10002
LipH EHD(α7,8)-MD2	6990	14120

2.5.9. SDS-polyacrylamide gel electrophoresis (SDS-PAGE)

Protein samples were analyzed by discontinuous SDS-PAGE using the protocol of Sambrook *et al.*[106] and the Mini PROTEAN® PAGE system from Bio-Rad. 0.75 mm discontinuous gels were casted with following recipe with 12 % or 16% separation and 5 % stacking gels. 70 % (v/v) ethanol was used to overlay freshly poured separation gels to ensure polymerization and a plane interface between separation and stacking gel. Samples were supplemented with 1x SDS sample buffer (50 mM TRIS pH 6.8, 2 % (w/v) SDS, 5 % (v/v) glycerol, 0.015 % (w/v) bromophenol blue, for reducing conditions: 200 mM 2-mercaptoethanol) and boiled for

10 min at 99 °C. Prestained Protein Ladder (Thermo Fisher Scientific) was used as molecular weight standard. Electrophoresis was carried out in 1 x SDS running buffer (25 mM TRIS, 250 mM glycine, 3.5 mM sodium dodecyl sulfate) at 100 V for 15 min and 35-45 min at 200 V using the Electrophoresis Power Supply EPS 601 (GE Healthcare). Protein bands were fixated and stained following the protocol of Neuhoff *et al.*, (1988)[118] using Coomassie Brilliant Blue R-250 solution (10 % (w/v) ammonium sulfate, 0.12 % (w/v) Coomassie Brilliant Blue R-250, 1.2 % (v/v) phosphoric acid, 20 % (v/v) methanol) overnight with slight agitation.

Table 2.7: Recipe for two discontinuous SDS-PAGE gels.

	Separation gel			Stacking gel
In ml	**12%**	**16%**	**In ml**	**5%**
Water	3.3	2.1	Water	3.4
30% acrylamide [a]	4.0	5.3	30% acrylamide [a]	0.83
1.5 M TRIS (pH 8.8)	2.5	2.5	1 M TRIS pH 6.8	0.63
10 % (w/v) SDS	0.1	0.1	10 % (w/v) SDS	0.05
10 % (w/v) APS	0.1	0.1	10 % (w/v) APS	0.05
TEMED	0.01	0.01	TEMED	0.01
Total	10	10	Total	5

[a] mix of 29% (w/v) acrylamide and 1 % (w/v) *N,N'*-methylene-bisacrylamide

2.5.10. Western blot and immunological detection of proteins

For specific identification of proteins on SDS PAGE (see chapter 2.5.9), proteins were transferred from SDS PAGE to a polyvinylidene difluoride (PVDF) membrane[119–121] and visualized by enhanced chemiluminescent (ECL) reaction of immunologically attached horseradish peroxidase[122–124]. The transfer was done with the Mini Trans-Blot Electrophoretic Transfer Cell (BioRad) in Dunn Carbonate buffer (10 mM $NaHCO_3$, 3 mM Na_2CO_3, pH 9.9 and 20 % (v/v) methanol)[125] with PVDF membranes which were activated for 5 min in methanol and equilibrated for 2 min in pure water. After transfer for 15 min at 150 mA and 30 min at 300 mA, the PVDF membrane was blocked with 5 % (w/v) skim milk in TRIS buffered saline with Tween®20 (TBST) (25 mM TRIS, 150 mM NaCl, 1 mM $MgCl_2$, pH 6.8, 0.2 % (v/v) Tween®20) for 1 h at 37 °C under slight shaking.

LipA and LipH were probed by primary polyclonal rabbit antibodies, specific against LipA (dilution 1:50,000) or LipH (dilution 1:200,000) (both from Microbial Biology, Ruhr University Bochum, Germany), and binding of secondary goat anti-rabbit antibody, that was conjugated to horseradish peroxidase (BioRad, dilution 1:5,000). The antibody binding steps were performed in TBST for 1 h at room temperature under mild agitation. After each binding step, the membrane was washed 3 times with TBST for 15 minutes to remove unbound antibodies. Finally, proteins of interest were detected by measuring the chemiluminescence at 428 nm

developed as result of luminol degradation by the attached HRP. Chemiluminescence was recorded using the Stella 3200 Imaging System (Raytest). ECL solution[126] was freshly prepared by adding 100 µl p-hydroxy coumarate solution (6.7 µM in DMSO, stored at room temperature) and 0.3 µl 30 % (v/v) H_2O_2 (stored at 4 °C) to 1 ml luminol solution (1.4 µM in 100 mM TRIS pH 8.6, stored at 4 °C).

2.6. Protein characterization

2.6.1. Determination of lipolytic activity

Para-nitrophenyl palmitate (*p*NPP) was used as substrate to determine lipolytic activities. Cleavage of the ester bond causes release of *para*-nitrophenolate that can be quantified spectrometrically by the absorption at 410 nm. Activity assays were performed in microtiter plates in a total volume of 200 µl. 2 to 100 µl samples were provided and substrate emulsion was added simultaneously to all samples using a multichannel pipette (Eppendorf Xplorer® plus). To prepare the substrate emulsion, 40 mM *p*NPP was dissolved in isopropanol at 37 °C and added rapidly to the assay buffer if not otherwise mentioned in 10 mM TG (5 mM TRIS, 5 mM glycine, pH 9, 1 mM $CaCl_2$) to a final concentration during the activity assay of 1 mM. The increase of absorption at 410 nm was recorded every 15 s with 3 s shaking in between for 10 min at room temperature using the Spectramax 250 plate reader (Molecular Devices). The activities were quantified from the initial rates, given by the slope of the linear increase of A_{410nm}. The catalytic activities can be calculated from ΔA_{410nm}/min values with given equation (III).

$$catalytic\ activity = \frac{\Delta A_{410nm}/\min * V_{Assay}}{\varepsilon * l} \qquad \text{(III)}$$

V_{Assay} = Volume of activity assay
l = Light path lengths
ε = Extinction coefficient

With given extinction coefficient of 15500 M^{-1} cm^{-1} (see Appendix 8.4) under used assay conditions and a light path length of 0.605 cm for an assay volume of 200 µl, the catalytic activity of ΔA_{410nm}/min of 1 can be calculated as 0.356 nkat. With known enzyme amount or concentration, the specific activity can be calculated from volumetric catalytic activity.

2.6.2. Protein stability determination by activity

Thermal protein stability was determined by the remaining activity after heat treatment. Therefore, protein samples were incubated at different temperatures for 1 h using the gradient function of the PCR cylcer TAdvanced (Biometra) and 96 well PCR plates [either low binding (Expell, Capp) or non-low binding (VWR)]. To avoid evaporation effects, the plates were sealed with an adhesive aluminum foil (Aluminum Foils for PCR and Cold Storage; VWR)

and the temperature of PCR cycler lid was set to 30 °C above the highest temperature (max. 105 °C). Directly after heat treatment, the remaining lipolytic activity was determined as it is described in chapter 2.6.1. For determination of the thermal stability of renatured LipA or LipH alone, LipH or renatured LipA respectively was added after heat treatment and incubated at 4 °C overnight before activity measurement. The residual activities were plotted against the incubation temperature. If the resulting curve followed a two-state sigmoidal behavior, T_M values were determined by non-linear regression using Boltzmann sigmoidal fitting integrated in Graphpad Prism 5.

2.6.3. Protein stability determination by differential scanning fluorimetry

Thermal protein stability was additionally determined by differential scanning fluorimetry (DSF), measuring the intrinsic protein fluorescence changes upon unfolding. Mainly tryptophan but partially also tyrosine[127] contribute to the intrinsic protein fluorescence. The environment of the tryptophan chromophore affects heavily the appearance of the fluorescence spectrum, so that most conformational changes of the protein can be detected by fluorescence changes.[128] General, all effects that affects fluorescence can matter in DSF. The electronic constellation and polarity of the environment change λ_{max} by stabilizing or destabilizing ground or excited state or the molecular surrounding and accessibility of quenchers affect the fluorescence intensity.[129,130]

The temperature dependent emission shifts were recorded at 330 nm and 350 nm using the Prometheus NT.Plex nanoDSF device. Protein samples had a minimal concentration of 1 µM and were loaded into the measuring capillaries (Prometheus NT.Plex nanoDSF Grade Standard Capillary Chips) from a standard 396 well plate. The temperature ramp was applied from 15 °C to 95 °C with a heating rate of 0.2 °C/min. The ratio of F_{350nm} and F_{330nm} and its first derivative were calculated by the provided PR.ThermControl software. For samples with low differences in F_{350nm} and F_{330nm} the fluorescence ratio curves were smoothed by applying a simple moving average (n=200) to the data. Because of the high data point density, results were reduced by the factor of 50.

The melting points were identified by the turning points of F_{350nm}/F_{330nm} versus temperature graphs and accordingly by extrema of the first derivative.

2.6.4. Circular dichroism (CD) spectroscopy

CD spectra were recorded at JASCO J-810 spectrophotometer in 1 mm quartz glass cuvette with 300 µl of 4 µM protein samples. Measurements were always performed with freshly refolded LipA or fresh formed complex. Far-UV CD spectra (190–280 nm) were recorded under following conditions: nitrogen flow, 0.5 mm bandwidth; standard sensitivity; auto PMT voltage; 2 s response; 50 nm/min scanning speed for the full spectra with three replicates. CD spectra were blank subtracted. Secondary structure calculation was done by the secondary structure calculator inside the Spectra Manager™ Suite (Jasco) using the integrated Yang's secondary structure reference spectra.

2.6.5. Crystallization of LipAH and structure determination by X-ray diffraction

For crystallization experiments, LipA and LipH were purified after heterologous expression in *E. coli* as described in chapter 2.4.6, 2.5.2 and 2.5.5. LipA was renatured and complex was formed as it is described in chapter 2.5.6 in 10 µM TG buffer containing 250 µM $CaCl_2$ and 5 µM TCEP. Complex formation was carried out overnight to yield full complex formation. Afterwards, TCEP was washed out and the sample was concentrated by ultrafiltration (see chapter 0). Crystallization trials of LipA, LipH and LipAH complex were performed by sitting drop vapor diffusion method in CrystalQuick® 96 well sitting drop plates (Greiner). Freedom evo 150 pipetting robot (Tecan) (configuration: liquid replacing liquid handling eight tip arm with 4x 100 µl and 4x 1 µl fixed washable PTFE coated tips, plate cover) was used to pipette crystallization screens. 70 µl crystallization solution and 1 µl protein were provided in the reservoir chamber and sample chamber respectively, before 1 µl crystallization solution was mixed with the protein droplet. Half a plate column was pipetted at once from left to right. To avoid evaporation, the pipetted columns were covered between pipetting steps. After complete preparation, plates were sealed air-tight with clear adhesive foils and stored for two weeks at 19 °C without movement before first crystal observation. Crystals were observed manually under the microscope (SZH10, Olympus). For initial screens, commercially available crystallization screening kits were used (listed in Table 2.8). Self-made buffers for crystallization screens were prepared using high purity chemicals, PEGs purchased from Sigma Aldrich and pure water. All solutions were sterile filtrated by 0.2 µM pore size cellulose acetate filter (VWR). Crystal fishing and X-ray diffraction experiments were done by Dr. Joachim Granzin (Institute of Complex Systems, ICS-6: Structural Biochemistry at the

Forschungszentrum Jülich). Crystals for diffraction experiments were isolated by loop-mounting method[131] and conserved by cooling down to -173 °C within a stream of liquid nitrogen in presence of respective PEG at ratios higher than the minimal concentration which was determined experimentally using the absence of ice crystals at -173 °C as criterium. Protein crystals were transferred to cryoprotecting solution by dilution with crystallization buffer with stepwise (5 %) increasing PEG concentrations. X-ray diffraction data sets were recorded at different beamlines at the European Synchrotron Radiation Facility (ESRF, Grenoble, France). Data processing was carried out using MOSFLM[132] and structure determination was tried by molecular replacement using MOLREP.[132]

Table 2.8: Used commercially available screening kits.

Screening Kit	Distributor
Crystal Screen I	Hampton Research
Crystal Screen II	Hampton Research
Crystallization PEG Grid Screening Kit	Sigma
Crystallization Low Ionic Kit	Sigma
PEGs Suite	Qiagen
PEGs II Suite	Qiagen
The AmSO4 Suite	Qiagen
Wizard Classic 1 and 2	Rigaku

2.6.6. Distance determination by Förster resonance energy transfer

Single molecule Förster resonance energy transfer (smFRET) measurements were conducted by Dr. Jakub Kubiak (Institute for Molecular Physical Chemistry at the Heinrich Heine University Düsseldorf) on samples which were purified and labeled as described in chapter 2.5.4. The detailed method will be published soon (Manuscript in preparation). In short, multiparameter fluorescence detection (MFD)[133–135] was done using a 485 nm diode laser (LDH-D-C 485 PicoQuant, operating at 32 MHz, power at objective 40 µW) and 635 nm diode laser (PicoQuant, operating at 32 MHz, power at objective 8 µW) in interleaved pulse mode. Pulsed interleaved excitation [136] exciting freely diffusing labeled molecules that passed through a detection volume of the 60X, 1.2 NA collar (0.17) corrected Olympus objective (confocal volume occupancy: < 5 %). The emitted fluorescence signal was collected through the same objective and spatially filtered using a 100 µm pinhole, to define an effective confocal detection volume. Then, the signal was divided into parallel and perpendicular components at two different colors (“green” and “red”) through band pass filters, HQ 520/35 and HQ 720/150, for green and red respectively, and split further with 50/50 beam splitters. In total eight photon-detectors were used- four for green (τ-SPAD, PicoQuant) and four for red channels (APD SPCM-AQR-14, Perkin Elmer). HydraHarp 400 Multichannel Picosecond

Event Timer & TCSPC Module (PicoQuant) were used for data registration. Measurements were performed at room temperature (21 °C ± 1 °C).

Resulting MFD data were treated as described in Sisamakis *et al.* (2010)[135] to assign detection events to single molecules and calculate burst-wise averaged fluorescence parameters. Fluorescence intensity-based photon distribution analysis (PDA) was done according to Antonik *et al.* (2006)[137] and Kalinin *et. al* (2007)[138] using model of single Gaussian state with variable width for free LipH. When LipA was present, model of two Gaussian states with variable width was used, with one state with parameters found in free LipH fit (representing unbound fraction) and another representation. To compare data from FRET with the homology model structure, the conformational freedom of used $Alexa_{488}$ and $Alexa_{647}$ dyes were calculated as accessible volume (AV) clouds[139] using the FPSv1.2 program[140]. The algorithm implemented in FPSv1.2 uses a coarse-grained representation in which the label is approximated by a flexibly-linked sphere to compute the sterically allowed AV.[141] Here, the linkers of $Alexa_{488}$ and $Alexa_{647}$ are approximated as flexible tubes with a width of L_{width} = 4.5 Å and a length of L_{link} = 20.5 Å and 21.0 Å, respectively. Three radii were used to describe the dyes (5.0 Å, 4.5 Å, 1.5 Å) and (11.0 Å, 4.7 Å, 1.5 Å) for $Alexa_{488}$ and $Alexa_{647}$, respectively. From the accessible volumes, FPS computes R_{DA}, the mean donor-acceptor distance for each pair of AVs. Own FRET measurements were done as batch experiments with 10 nM double labeled LipH variants using the Infinite M200 pro fluorescence plate reader (Tecan) with excitation at 490 ± 10 nm and emission at 520 ± 10 nm and 670 ± 10 nm to detect donor (F_D) and acceptor (F_A) fluorescence respectively. Averaged values of nine measurements with 50x 400 Hz excitations with integration time of 40 µs were used to calculate the FRET proximity ratios (P) by equation (IV). Dye distances (R) were calculated by equation (V). Because several factors like exited state lifetimes, quantum yields and critical Förster distance were not known for the batch experiments, distance calculations were simplified by the ratio factor r which was calculated by the average of total measured complex distances from smFRET (R_{sm}) in ratio to the averaged proximity ratios of complex in batch experiments (P_{batch}) as described in equation (VI).

$$P = \frac{F_A}{F_A + F_D} \tag{IV}$$

$$R = r \sqrt[6]{\frac{1-P}{P}} \tag{V}$$

$$r = \frac{\frac{1}{n}\sum_{i=1}^{n} R_{sm_i}}{\frac{1}{n}\sum_{i=1}^{n} \sqrt[6]{\frac{1 - P_{batch_i}}{P_{batch_i}}}} \quad \text{(VI)}$$

2.6.7. NMR spectroscopy

For NMR measurements, *lipA* and *lipH* were expressed in *E. coli* using M9 medium containing ^{15}N-NH_4Cl and/or ^{13}C-glucose as sole nitrogen and carbon source respectively as it is described in chapter 2.4.6. Purification and refolding was done as it is described in chapter 2.5.2, 2.5.5 and 2.5.6. Afterwards, samples were concentrated, and buffers were exchanged by ultrafiltration.

NMR measurements were performed at concentrations of 150-600 µM in 20 mM Na-PO_4 buffer (pH 7.4) or if LipA was present in 10 mM TG buffer (5 mM TRIS, 5 mM glycine, pH 9) both containing 0.1 x protease inhibitor cocktail (S8820, Sigma Aldrich) and 3 mM NaN_3, 10 % (v/v) D_2O and 100 µM 4,4-dimethyl-4-silapentanesulfonic acid (DSS). DSS was used as a chemical shift standard, and ^{13}C and ^{15}N data were referenced using frequency ratios as previously described by Wishart *et al.* (1995)[142]. All NMR spectra were processed with TOPSPIN 3.2 (Bruker). All NMR measurements and spectra analysis were performed by Dr. Aldino Viegas (Institute of Physical Biology, Heinrich Heine University Düsseldorf) on Bruker Advance III HD spectrometers operating either at 600 or 700 MHz, both equipped with 5 mm inverse detection triple-resonance z-gradient cryogenic probes (located at the Biomolecular NMR Center, Forschungszentrum Jülich).

Structure calculations were done as it is described by A. Viegas (2012)[143]. Chemical shift assignments of the backbone atoms were obtained by ^{15}N- and ^{13}C-edited HSQC (heteronuclear single-quantum coherence) and three-dimensional HNCO, HN(CA)CO, HN(CO)CACB and HNCACB experiments. Three-dimensional ^{15}N- and ^{13}C-NOESY-HSQC (mixing time 120 and 200 ms respectively) and ^{15}N-TOCSY-HSQC (mixing time 50 ms) spectra were used for side-chain resonance assignment and NOE (Nuclear Overhauser Effect) measurements. The assignment of the ^{1}H, ^{13}C, and ^{15}N signals in the spectra was performed using CARA 1.9.24a. After assignment completion, CYANA2.1[144] was used to analyze the peak data from NOESY spectra in a semi-automated iterative manner. CARA 1.8.4.2 was used to automatically generate the NOE coordinates and intensities. The input data consisted of the amino acid sequence, assigned chemical shift list, peak volume list and backbone dihedral

angles (Φ and Ψ) derived from TALOS+ server[145]. The unambiguous NOEs assigned to a given pair of protons were converted into the upper limits by CYANA2.1. No stereospecific assignments were introduced initially. In the final steps, 12 pairs of stereospecific limits were introduced by CYANA2.1.

2.7. In silico methods

2.7.1. Homology modelling

Homology model of LipH was calculated by the Phyre2 web server[146] using the crystal structure of *B. glumae* foldase[81] (PDB ID: 2ES4, chain D) as a template. The LipAH complex was built by structural alignment of the homology model of LipH and the crystal structure of LipA (PDB ID: 1EX9)[33] with the LipAB_BG complex using Pymol. The model obtained was energy minimized with the GROMOS96 43B1 force field as implemented in Swiss-PdbViewer[147]. After several steps of energy minimization, the C_α atoms of the models were superimposed on the template structure and the model with least root-mean-square deviation (RMSD) was taken for further studies. The stereochemical parameters of the LipH and LipAH models were evaluated using PROCHECK v.3.5.4[148]. Additionally, the models were validated using qualitative model energy analysis (QMEAN)[149] and protein structure analysis (PROSA)[150].

2.7.2. Electrostatic surface calculation

For the calculation of electrostatic surface potentials, PDB files of protein structures were reformatted to PQR files using the pdb2pqr 2.0 webserver (http://nbcr-222.ucsd.edu/pdb2pqr_2.0.0/)[151,152]. Atomic charges and radii were calculated using the PARSE forcefield[153] and pK_A values were predicted by PROKA 3.1[154,155]. PQR files were used to calculate the overall protein electrostatics using the APBS plugin[156] for PyMOL Molecular Graphics System, (version 1.7 Schrödinger, LLC) with standard setting if not stated otherwise.

2.7.3. Programs for data analysis and visualization

ApE (Another plasmid editor) programmed by Wayne Davis (Department of Biology, university of Utah) was used for DNA sequence analysis, primer design and cloning. The molecular weights and extinction coefficients of proteins were calculated from known amino acids sequences using the ExPASy ProtParam tool[157]. Protein structures were investigated, and figures were made with the PyMOL Molecular Graphics System, (Version 1.7 Schrödinger, LLC). Molecule structures were drawn using ChemDraw 16 for Windows.

Structure alignments were performed with sequence alignment and structure super position algorithm that is implemented in PyMol. Protein sequence similarity searches were done by the BLASTP 2.8.0+ algorithm[158] provided on the NCBI homepage. Resulting sequence clusters were deduplicated by CD-HIT suite[159] provided by the MGA webserver[160].

Protein sequence alignments were done with ClustalW emboss stretcher algorithm, provided as web tool from EMBL (http://www.ebi.ac.uk/Tools/psa/)[161,162] with standard settings. Data analysis and graphs were done with Graphpad Prism 5 for Windows.

3. Results and discussion

In this thesis, the lipase-specific foldase of *P. aeruginosa* is called LipH, as annotated in the pseudomoas.com databank,[163] even though the gene was often referred to as *lip*B in the past.[87,90,164] The term foldase is used for the family of lipase-specific foldases (Lifs)[78] and should not be confused with the general classes of chaperons, which are sometimes also called foldases.[74]

Foldases are membrane-bound proteins that are integrated by their N-terminal hydrophobic helix into the cytosolic membrane inside the periplasm.[90,91] The common opinion, derived from different experiments, is that the transmembrane helix is not directly involved in the activation of lipases. The lipase folding reaction and the activation of lipases take place equally or, due to solubility, even more efficiently with foldases missing their transmembrane helix.[83-85,88,165] To follow up on these experiments, LipH was expressed heterologously in *E. coli* without its transmembrane domain, which was replaced by a soluble sequence with an N-terminal His_{10}-tag. The genetic construct (pEHTHis19) was adopted from Hausmann *et al.* (2008),[101] and its exact genetic description is given in Appendix 8.2. Expression and purification were performed as described in chapters 2.4.6 and 2.5.2. Because only the soluble form of LipH was used for *in vitro* experiments, this construct is referred to as LipH throughout this thesis without any additional sequence descriptives.

3.1. Structure of LipH and LipAH complex

To study the function and the underlying reaction mechanism of an enzyme, information on its structure is essential. One fast and easy method to gain structural information is homology modeling. Depending on the available structures of the corresponding enzyme family, a homology model is a reliable source for structural information that can be obtained from known amino acid sequences alone. Nonetheless, the information derived from a homology model should be interpreted with caution because it is predicted by algorithms, which may not necessarily consider important factors influencing the protein structure. In the following chapter, a homology structure of the LipAH complex structure was calculated, and different experimental approaches were used to validate the derived structure.

3.1.1. Homology model of LipAH complex

In 2006, Pauwels *et al.*[81] were able to solve the first and until now the only crystallographic structure of a lipase-specific foldase (PDB: 2ES4). It shows the soluble folding domain of a foldase (LipB) from *Burkholderia glumae* in complex with its lipase (LipA_BG). It has a unique α-helical structure enclosing almost the whole structure of its complexed lipase. This structure was used as a template for the homology model of LipH in complex with LipA_PA (calculated as described in chapter 2.7.1.). To form the complex, the homology model of LipH was calculated on the basis of the structure of LipB and then aligned with the structure of LipA_PA (PDB: 1EX9) onto the LipAB complex structure. Finally, the LipAH complex structure was subjected to energy minimization. Figure 3.1 shows the structural alignments of LipB_BG (black) with the homology model before (red) and after energy minimization (blue).

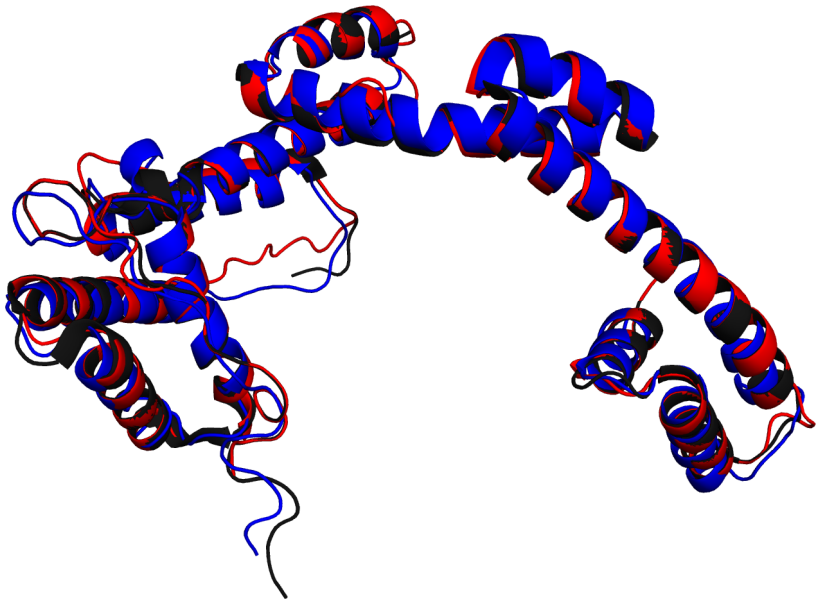

Figure 3.1: Structural alignment of LipH homology model and LipB_BG.
The structure of LipB_BG (PDB: 2ES4) is shown in black. The homology model of LipH before energy minimization is shown in red and the model after energy minimization in blue.

In addition to the conformation of some flexible loops, there are almost no structural deviations between the homology model for LipH and the crystal structure of LipB. The RMSD values of the aligned structures are 0.09 Å and 1.31 Å for the homology model before and after energy minimization, respectively. It seems that the sequence of LipH was just fitted onto the structure of LipB.

LipH and LipB share only 32.1 % sequence identity (45.6% similarity, protein sequence alignment is shown in Appendix 8.3), which is close to the minimal identity rate of 25 to 30 % that can give reliable modeling results for homology modeling.[166,167] Although sequence-

based structure prediction algorithms have shown that the whole foldase class exhibits a similar fold consisting of 70 % α-helices and 30 % random coil,[45,74,80] foldases have no globular structure and almost no ordered tertiary structure elements. From the given homology structure, the α-helical structure elements of foldases seem to be conformationally highly flexible and are stabilized in complex with the lipase. Because of the lack of additional known foldase structures for homology modeling, the low sequence identity, the low amount of tertiary structure and the fact that modeling algorithms do not include conformational influences of interaction partners, the results of homology modeling should be critically validated and experimentally proven.

3.1.2. Binding interface of LipA and LipH can influence the structure of LipH

The structures of foldases in complex seem to be dependent on interactions with their lipases. The protein sequences of LipA_PA and LipA_BG are only slightly more conserved than those of their foldases. They have 37.1 % sequence identity (51.5 % similarity; the protein sequence alignment is shown in Appendix 8.4). However, individual differences in the charge distribution on the surface of the lipases can alter the binding mechanism of foldases and hence the conformation of LipH in complex.

It has been repeatedly demonstrated that foldases are lipase-specific and that LipH and LipB are not interchangeable.[89,91] Only foldases of closely related strains can substitute for the original foldase, such as *P. aeruginosa and P. alcaligenes* or *P. wisconsinensis*.[45,91] This specificity indicates that there might be structural and mechanistic differences in complex formation between LipH and LipB. Comparing the electrostatic interfaces between LipAH_PA and LipAB_BG in Figure 3.2 shows that the specificity of these two foldases can be explained by a differing charge distribution at the complex interface. Furthermore, the complementary charge distributions of the LipA and LipH interfaces confirm the binding mode calculated by homology modeling. To visualize the whole interface, the electrostatic fields of LipB and LipH (shown in II and III) were imprinted on the surface of their cognate lipases, as shown from different perspectives (A-C). Differences between the electrostatic surfaces of LipB and LipH were observed. Whereas the two MD1s show similar, mostly negatively charged (red) electrostatic surfaces in both foldases, the charge distribution of EHD and MD2 differs between the two foldases.

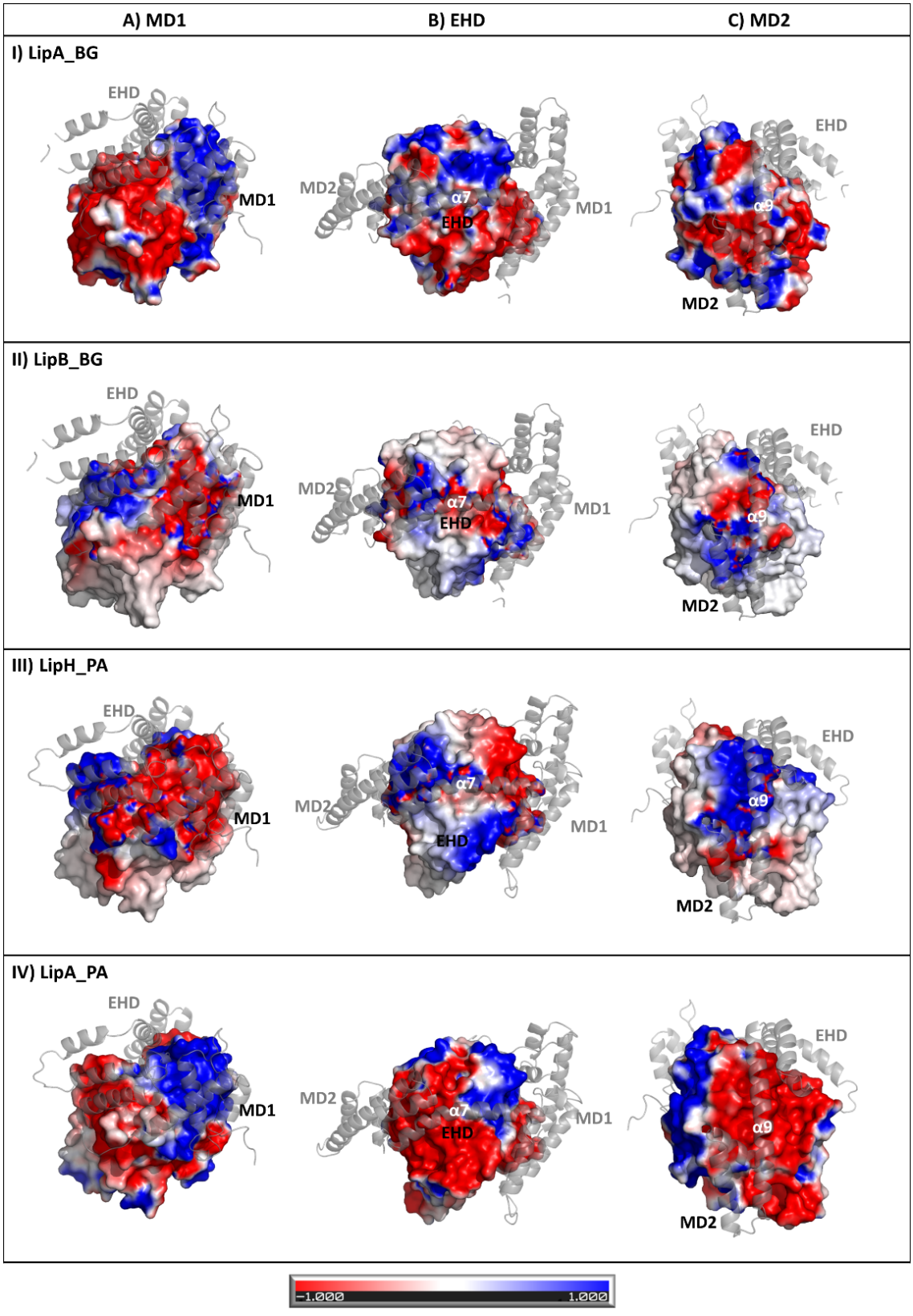

Figure 3.2: Comparison of the electrostatic interfaces of the LipAH and LipAB complexes.
The foldases are shown as transparent cartoon structures, and the lipases are shown as surface representations. The electrostatic surfaces of LipB (II) and LipH (III) are shown as imprints on the surfaces of their cognate lipases. The electrostatic surfaces of LipA_BG and LipA_PA are shown in (I) and (IV), respectively. The electrostatic surfaces are shown from different perspectives to visualize the binding interfaces of MD1 (A), EDH (B) and MD2 (C). The electrostatic surface potential is shown from 1 kT/Mol (blue) to -1 kT/Mol (red).

In particular, the interface around α-helix 9 of LipB shows a large negatively charged patch, whereas the entire interface of α-helix 9 in LipH exhibits a positively charged surface (blue). The electrostatic surfaces of the lipases are shown in I and IV, respectively. Comparison of the imprinted electrostatic surfaces of foldases with the electrostatic surfaces of their lipases shows, in both cases, mostly corresponding charge distributions (similar patches with opposite color) that should result in positive interactions with negative total free energy, favoring complex formation. These different charge distributions of foldases, fitting the charge distributions of their cognate lipases, indicate that both foldases have evolved together with their lipases.

The N-terminal half of the folding domain, especially MD1, seems to have a conserved binding mode, whereas the C-terminal part (beginning with the second half of α7) has been subject to evolutionary changes. The C-terminal part of LipB shows an elaborate charge distribution with small patches that are easily fitted to the corresponding lipase charge distribution. In contrast, the C-terminal part of LipH has an almost completely evenly charged surface that binds to a large negatively charged patch on the lipase surface. This uniformity enables different binding modes of the C-terminal part of LipH and makes it difficult to validate the exact conformation of the C-terminal part based solely on the electrostatic distribution of the interface.

3.1.3. Prolines direct the secondary structure elements in LipB_BG

A closer look at the sequence-structure relationship in LipB shows that almost all secondary structure elements of the folding domain, which LipB_BG forms in complex with LipA_BG, are directed by prolines. Figure 3.3 A shows a comparison of proline location and the α-helices that were predicted for the crystal structure of LipB_BG. Its folding domain contains eleven prolines. Ten of them are located at the beginning of ten of the eleven total helices of the LipB_BG folding domain. Only α-helix 1 does not contain a proline in its first turn. Figure 3.3 B shows the loop containing P163, the only proline that is not involved in the start of a helix, and P199, which seems to be located inside α-helix 5 but is also involved in forming the kink between α-helix 4 and α-helix 5. Prolines seem to be important structural elements. Especially in protein regions with no tertiary structure, prolines can be important for kink formation and the orientation of individual α-helical structure elements.[168]

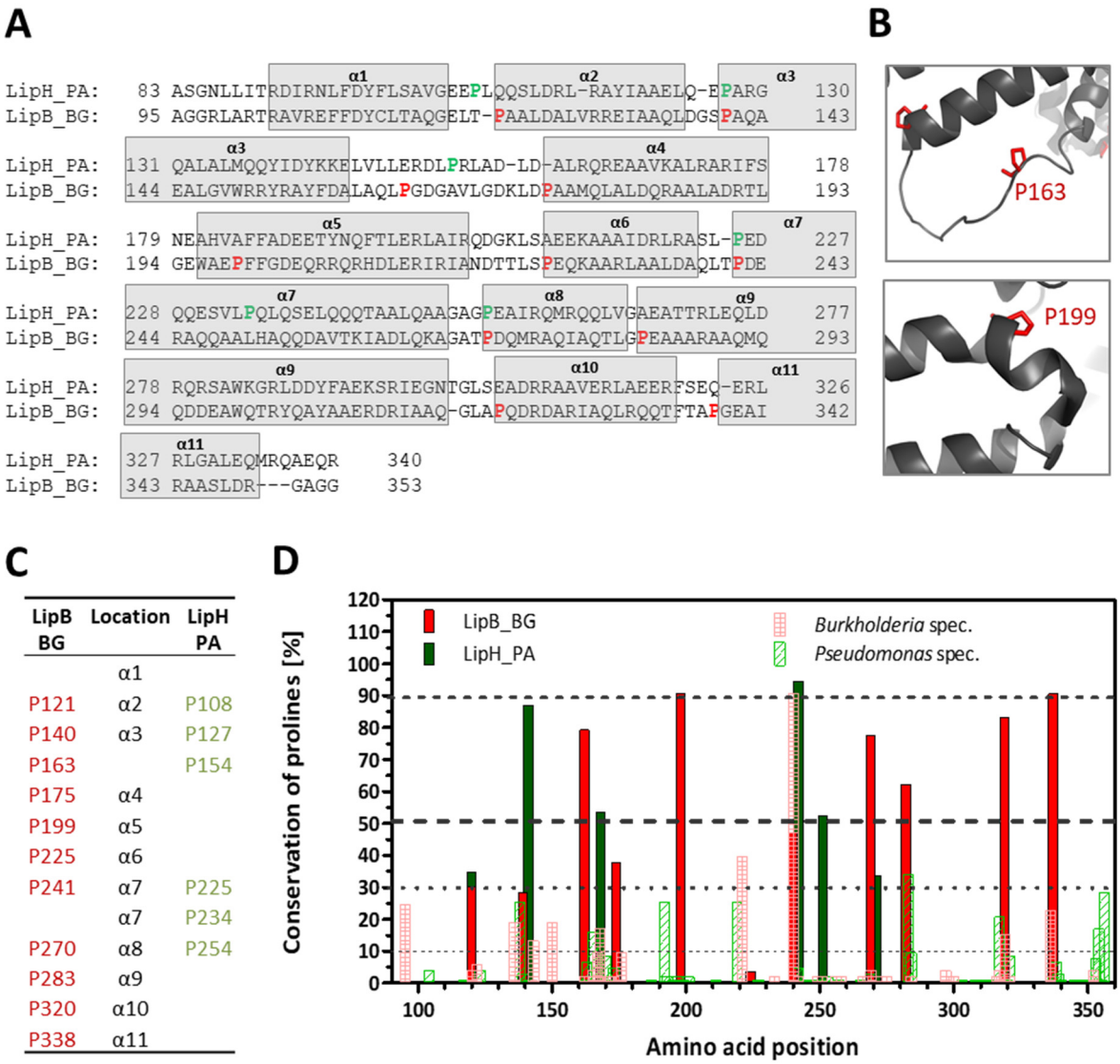

Figure 3.3: Helix-introducing role of prolines in LipB and LipH.
A) Amino acid sequence alignment of LipB and LipH. The helix content of LipB defined in its crystal structure (PDB: 2ES4) is shown as gray boxes. Prolines are highlighted in bold red (LipB) and green (LipH) letters. B) Crystal structure excerpts of the P163-containing loop (upper frame) and the P199-containing kink between helix 4 and 5 of LipAB_BG are shown (PDB entry: 2ES4). C) Table shows the prolines in LipB and LipH in comparison to their location. D) Conservation rate of prolines in the sequence space of *Burkholderia* genus and *Pseudomonas* genus as hatched bars. Prolines of LipB and LipH were highlighted additionally as filled bars.

In contrast, LipH_PA possesses only 6 prolines inside its folding domain. Four prolines are used for the introduction of α-helices 2, 3, 7 and 8, and one proline is located inside the same large flexible loop of LipB_P163. Interestingly, P234 is located in the middle of α-helix 7, exactly where LipH starts to bind to the large negatively charged patch of LipA (see chapter 3.1.2). All prolines and their locations are summarized in Figure 3.3 C. Although several predicted structure elements in LipH_PA are also directed by prolines, some large regions, such as α-helices 4, 5, 6, 9, 10 and 11, contain no prolines, whereas α-helix 7 is even interrupted by an additional proline.

To examine the proline-helix relationship observed in LipB, the conservation rates of prolines within the same genus were determined. Figure 3.3 D shows the conservation rates of prolines in LipB and LipH compared to their genus. These conservation rates were calculated from sequence clusters derived from the protein BLAST sequence search (546 hits for LipB and 452 hits for LipH). These clustered sequences were deduplicated by the CD-Hit suite, removing all sequences with >90 % similarity, leaving a set of 53 divergent sequences in the genus *Burkholderia* and 107 in the genus *Pseudomonas* (the association numbers of the gene sequences used are given in Appendix 8.5).

These sequences were aligned to LipB and LipH, and the rates of prolines occurring at a defined position were plotted against the amino acid position (filled bars). For better comparison of the conservation rates of prolines in *Burkholderia* and *Pseudomonas*, the amino acid positions in LipH were corrected to the amino acid positions in LipB according to the sequence alignment in Figure 3.3 A. The positions of prolines in LipB (shown in red filled bars) are highly conserved within the *Burkholderia* genus (between 30-90 %). The selection pressure for the proline positions can be assumed from the fact that prolines with lower conservation rates, such as P^{121}, P^{141} and P^{225}, are often replaced by neighboring prolines within one to four positions in the sequence (hatched bars). Only a small number of prolines (mostly in 1 of the 53 sequences) occur at different positions in the *Burkholderia* sequence cluster. In the *Pseudomonas* sequence cluster, prolines seem to be similarly highly conserved with the same near-range variations. Some of the prolines of LipB that are missing in LipH occur partially in the *Pseudomonas* sequence cluster. New proline positions occur only in a small number of sequences and in distinct ranges.

This conservation rate shows the importance of prolines for the function of foldases in the *Burkholderia* and *Pseudomonas* genera. Although secondary structural elements can be initiated without a proline, prolines can be important for structural elements without any long-range contacts formed by tertiary structure elements. Unfortunately, without more solved structures of foldases, the pattern of prolines deduced from sequence analysis serves only as an indicator of structural divergence.

3.1.4. Fold of MD1 is conserved

The conserved electrostatic surfaces of MD1 in both foldases (see chapter 3.1.2) indicate the conserved structure and binding mode of this domain. Sequence alignments of each domain show that MD1 has the highest identity rate of all domains (see Table 3.1).

Rosenau *et al.* (2004)[45] postulated a foldase-specific sequence motif within MD1 that is highly conserved among all foldase families. It is defined as $Rx^1x^2FDY(F/C)L(S/T)A$ (x can be any residue) and located inside α-helix 1 at the interface of the foldase and lipase. The precise role of that sequence motif is still unknown, but Shibata *et al.* (1998)[87] demonstrated the importance of some amino acids in the motif for lipase folding, inactivating LipH from *P. aeruginosa* by mutating the tyrosine or the serine/threonine residues.

Table 3.1: Sequence alignments of the LipH and LipB domains.

	Lengths	Identity [%]	Similarity [%]
TMD	42	21.4	31.0
VD	41	34.1	43.9
MD1	83	37.3	51.8
EHD	123	33.3	45.5
MD2	75	29.3	48.0

The conservation of the binding mode of MD1 is further confirmed by the experiments of El Khattabi *et al.* (1999).[91] They investigated the exchangeability of different regions between LipH and LipB by constructing chimeric foldases and observed that MD1 of LipB can be replaced by MD1 of LipH, resulting in a chimeric foldase that is able to activate LipA_BG *in vivo.* Other constructed chimeras were not active, and it was not possible to demonstrate that MD1_BG can replace MD1_PA. Unfortunately, the construction of these chimeric foldases seems to have been based on an incorrect sequence alignment. Reproduction of the chimeric sequences *in silico* (data not shown) showed that several amino acids were deleted in most of the chimeras and that they were most likely inactive because of missing structural components, so the inactive chimeras do not prove different binding modes.

MD1 consists of 3 α-helices (approx. 56 amino acids) and is the largest globular tertiary structure in LipH. Neha Verma (Institute for Pharmaceutical and Medicinal Chemistry, Heinrich Heine University Düsseldorf) was able to demonstrate by molecular dynamics simulations that, in contrast to most of the secondary structure elements, these three helices of MD1 remain stable in the free foldase.[169]

To determine the structure of MD1 and investigate the interactions between LipA and LipH, the structure of LipH was examined by NMR. The NMR experiments were performed in collaboration with Dr. Aldino Viegas (Institute of Physical Biology, Heinrich Heine University Düsseldorf). Because of the low amount of tertiary structure of LipH, many atoms show similar chemical shifts, leading to crowded areas that hinder the assignment of individual signals. Thus, peak assignment and structure prediction were not performed on the full-length folding

domain of LipH but on LipH fragments. Therefore, NMR measurements and structure predictions for MD1 (spanning residues L66-L146) and EHD(α7,8)-MD2 (spanning residues E226-R340) fragments encoded on pETLipHMD1 and pETLipHEHDMD2, respectively, were performed as described in chapter 2.6.7.

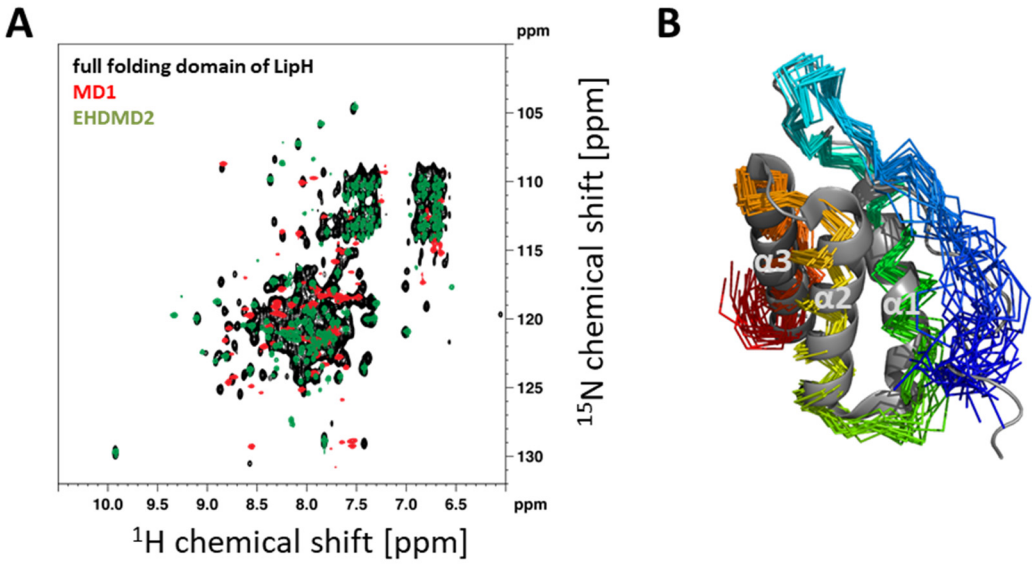

Figure 3.4: Structure prediction of MD1 by NMR.
A) Superimposition of ^{1}H,^{15}N-HSQC NMR spectra of the full-length folding domain (black) and MD1 (red) and EHD(α7,8)-MD2 (green) fragments. B) Structural alignment of the 20 best structure predictions from NMR measurements are shown as rainbow-colored ribbon (N': blue -> C': red) with MD1 of *Burkholderia glumae* (PDB: 2ES4) (gray cartoon).

Figure 3.4 A compares the ^{1}H,^{15}N-HSQC spectra of the MD1 and EHD(α7,8)-MD2 to the spectrum of the complete folding domain (encoded on pETLipHΔVD expression plasmid). Both fragment spectra look similar to that of the complete folding domain, indicating that the LipH fragments have a similar fold to that of the complete folding domain. The crowded peak areas at approximately 7-8/112 ppm are mostly caused by signals from the EHD(α7,8)-MD2 fragment. MD1 had a good peak distribution that made it possible to perform a full backbone assignment and structure calculation. The calculated structure of MD1 was deposited in the Protein Data Base[170] with the PDB entry ID 5OVM. The 20 best structure predictions are shown in Figure 3.4 B as rainbow ribbons (blue: N-terminal to red: C-terminal) aligned to the MD1_BG structure (gray cartoon). The predicted structures are structurally very similar to each other and show a maximal RMSD variation of 0.95 Å. In comparison to the MD1_BG structure, the average RMSD is 2.66 Å, which shows slightly more structural deviation than the homology modeling derived MD1_PA structure with an RMSD value of 0.64 Å. The N-terminal unstructured region shows a high degree of freedom, causing the high RMSD. However, as shown in Figure 3.4 B, the overall structure of free MD1_PA resembles the

structure MD1_BG. These findings are consistent with the molecular dynamic simulations performed by Neha Verma and to the conserved electrostatic complex interface of MD1 and open the question of whether MD1 has a special role in the folding of LipA. The highly conserved folding motif is located in helix α1, which faces the lipase binding site. The roles of MD1 and of the folding motif in the complex formation and activation of LipA are investigated more closely in chapter 3.9.

3.1.5. Dimensions of the LipAH complex by FRET

Although the structure of MD1 was validated by solution NMR, as described in chapter 3.1.4, the structure of the other two folding domains remained elusive. To obtain more information about the complex structure and to validate the overall conformation of LipH in complex, the dimensions of LipH in complex and the orientations of single sites in LipH were measured by fluorescence resonance energy transfer (FRET). Therefore, LipH was labeled with $Alexa_{488}$ and $Alexa_{647}$ dyes at defined positions on the outer surface, enabling the determination of the distance between these points. The dyes were regiospecifically attached to LipH by thiol reactive maleimide groups and cysteine mutations, which were introduced into LipH as described in chapter 2.5.4. In total, all 6 possible distances were measured between 4 points (P1 to P4: Q137, A215, E268, R296), as shown in Figure 3.5 A in red.

A)

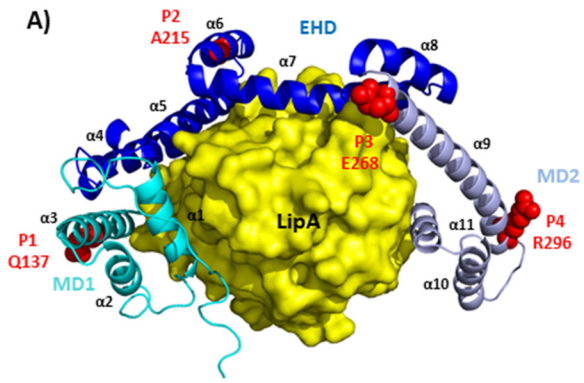

B)

Label positions	Mutation sites	$\langle R_{DA} \rangle_E$ [Å] AV_model	$\langle R_{DA} \rangle_E$ [Å] FRET
P1-2	137-215	59	62±8
P1-3	137-268	61	52±7
P1-4	137-296	90	80±8
P2-3	215-268	51	65±9
P2-4	215-296	66	66±9
P3-4	268-296	53	53±8

Figure 3.5: FRET label positions and data comparison.
A) Amino acids mutated to cysteines for labeling are shown as red spheres on the LipAH homology model. LipA is shown as a surface representation in yellow. MD1, EHD and MD2 of LipH are shown as cartoon representations in cyan, dark blue and light blue, respectively. B) Distances of dye simulations (AV_model) and FRET measurements. $\langle R_{DA} \rangle_E$ describes the averaged dye distances in Å.

Measurements and distance calculations were performed by Dr. Jakub Kubiak (Institute for Molecular Physical Chemistry at the Heinrich Heine University Düsseldorf) as described in chapter 2.6.6. The four labeling points cover the whole folding domain of LipH, and determining the distances between these points makes it possible to determine the positions

of the domains relative to each other. The table in Figure 3.5 B shows the simulated distances derived from the homology model and the distances measured by FRET. Deviations resulted from uncertainties in the dye orientation.

The exact structure of MD1 is known from NMR experiments. The distance between P1 and P2 shows that helices α 4-6 of EHD are most likely aligned similarly to those s in the homology model. However, the α-helices encompassing P3 and P4 seem to be aligned differently. The P1-P3 and P1-P4 distances are shorter than expected, whereas the P2-P3 distance is longer than calculated. The P1-P4 distance is difficult to resolve without a high degree of uncertainty.[171] The electrostatic interface of α-helices 10 and 11 and LipA (see chapter 3.1.2), which defines the position of P4, shows that binding occurs at a specific location defined by a complex complementary charge distribution. Furthermore, the binding of MD2 is mostly directed by a salt bridge formed between R327 of LipH and E58 of LipA, which is highly conserved.[81] The P3-P4 distance, between label positions that are both located in helix α9, is similar to the expected value, suggesting that helix α9 may adopt the structure predicted by homology modeling. If the structural elements were rigid, it would be possible to postulate a shifting of position P3 and helix α9 along the surface of LipA in the direction of MD1, bringing P3 closer to P1 and further away from P2. However, because the structural elements are not rigid, there are an infinite number of possible conformations, and several factors can influence the distance determination for P3. The dyes are attached via a large flexible linker, and a slight turn of the helix to which the dye is attached can substantially alter the location of the center point of the dye.

The similarity of the simulated and measured distances between these 4 points of the LipH structure further validates the homology structure of LipH. Together with the solved structure of MD1 and the electrostatic interface, which shows a defined binding location for α-helices 10 and 11, these distance results make it is possible to validate the homology model and narrow its uncertainties to the region surrounding P3 beginning with the proline in helix α7.

3.1.6. Crystallization of LipAH complex

To finally solve the uncertainties about the actual structure of LipH in complex and to expand the available structures of foldases, crystallization experiments with the LipAH complex were conducted as described in chapter 2.6.5. LipA and LipH were purified separately, and the complex was formed *in vitro* by the incubation of preactive LipA, derived by denaturation and renaturation, with an equimolar amount of LipH. After incubation overnight, the freshly

prepared complex was concentrated to 16 mg/ml, at which point it started to precipitate. The precipitate was removed by centrifugation before use. For an initial crystallization screening, commercially available crystallization screening kits (Table 2.8, page 35) with a broad spectrum of conditions were used to find suitable conditions for crystallization. In total, 768 crystallization conditions were tested. After two weeks of incubation, the first crystal formation with different morphologies ranging from small needles to hexagonal columns was observed. Most crystals were not usable for diffraction experiments because of their small size or their irregular morphology. However, some of them seemed to be single crystals of appropriate size. They were selected for diffraction experiments but showed no diffraction or poor diffraction patterns. After three months, additional crystal formation was observed from the same screening trial. It was possible to derive a diffraction pattern from one of the chosen crystals with a resolution of 4 Å. This crystal was obtained from 0.1 M TRIS, pH 8.5 with 30 % PEG 1000 and showed a hexagonal column shape with trigonal symmetry and a primitive cell of 65x65x280 Å.

Conditions of the initial screening that showed crystallization, were combined and slightly varied to reproduce and refine crystal formation. In general, the LipAH complex seemed to crystalize in conditions that stabilize preactive LipA, as described in chapter 3.3. A low-ionic-strength buffer with basic pH seems to stabilize the complex enough to enable crystallization. Short to medium chain length polyethylene glycol (PEG) served as an effective precipitation agent. The conditions that stabilized preactive LipA the most (5 mM TRIS, 5 mM glycine, pH 9) with varying concentrations of PEG showed no crystallization, but the addition of salts, an increase in buffer strength or a decrease in pH lowered the solubility and induced crystallization. Crystal formation was not consistent; reproduction with one defined condition often yielded only precipitation or unsatisfactory crystal formation. Thus, crystals were always obtained in fine screening setups with varying pH, salt and PEG concentrations. However, most crystals that seemed to be suitable exhibited little or no diffraction. In total, it was possible to collect diffraction patterns of 4 crystals with resolutions between 3.6 – 4 Å (Table 3.2). All of them showed similar symmetry and primitive cell size.

From these diffraction datasets, it was not possible to resolve the structure by molecular replacement using the homology model of the complex, LipH alone, or the structure of LipA in its open conformation (PDB code: 1EX9) or in its closed conformation derived from homology modeling (personal communication Dr. Joachim Granzin). Therefore, an attempt was made to solve the phase problem for structure determination by multiwavelength

anomalous diffraction phasing[112] with selenomethionine-labeled LipAH complex. LipA and LipH were expressed as described in chapter 2.4.7 in a methionine auxotrophic *E. coli* strain with exogenously added selenomethionine and purified as described above. This selenomethionine-labeled LipAH complex crystallized under similar conditions to the unlabeled complex, and it was possible to derive crystals under the same conditions. However, similar to the unlabeled complex, most crystals showed little or no diffraction, and it was not possible to derive a diffraction pattern of the selenomethionine-labeled complex during the time of this project.

Table 3.2: Crystallization conditions of diffracting crystals.

#	Buffer	pH	Salt	PEG	Resolution
1	0.1 M TRIS	8.5	---	30 % (w/v) PEG 1000	4 Å
2	0.1 M TRIS	8.5	---	19 % (w/v) PEG 4000	4 Å
3	0.1 M TRIS	9	---	22 % (w/v) PEG 4000	3.6-3.9 Å
4	0.1 M TRIS	8.5	0.2 M $CaCl_2$	25 % (w/v) PEG 4000	3.6-3.9 Å

Pauwels (2008)[172] reported the formation of similar hexagonal column-shaped crystals of the LipAB_BG complex with a resolution of 3-5 Å. However, the actual crystal structure was derived from a single crystal with a monoclinic shape, which occurred after several months. Reproduction of that crystal shape was not possible. The structure was derived by multiwavelength anomalous diffraction phasing of a selenomethionine-labeled hexagonal column-shaped crystal and molecular replacement with the diffraction dataset of the monoclinic crystal.

A potentially important difference between LipAH_PA and LipAB_BG crystallization is that Pauwels performed complex formation with native LipA_BG, which was directly copurified with LipB from the supernatant and not by renaturation of the lipase from the denatured state. This difference might be why molecular replacement with LipA or LipH model structures yielded no results. FRET measurements showed a different conformation of LipH in the complex, which was explained by a different binding mode of LipH compared to LipB. However, it is also possible that preactive LipA exhibits conformational differences from native LipA. The characteristics of these two states of LipA are investigated in the following chapters to examine whether the measured conformational differences in LipH are caused by structural differences in LipA or by different binding modes of LipH compared to LipB and to gain insights into the mechanism of LipH-mediated LipA activation.

3.2. Purification of native and preactive LipA

To investigate the properties of LipH and its mechanism of action, the behavior of both the substrate, preactive LipA, and the proposed product of the foldase reaction, native mature LipA, should be characterized, therefore both conformations should be obtained in high purity. Therefore, published protocols for purification of these two LipA conformations were compared and tested for their applicability. A new purification method was developed for the mature state of LipA, which facilitates the isolation of LipA from large supernatant samples. Furthermore, the protocol for the purification of preactive LipA was improved, and increased yield and purity were obtained.

3.2.1. Homologous production of mature LipA in *P. aeruginosa*

For the production of mature LipA, the T7-RNA polymerase expression system of the *P. aeruginosa* PABST7.1 strain and the T7 promoter-controlled *lipAH* (full-length) gene cassette on pBBR2LipAHff were used. pBBR2LipAHff, a derivative of pBBR1MCS/PA *lipAH* from Janosch (2002),[100] was constructed during this project because the strain PABST7.1 can spontaneously develop resistance against chloramphenicol (communication in the laboratory), circumventing selection by the plasmid-encoded chloramphenicol resistance of pBBR1MCS/PA *lipAH.* To ensure a genetically stable strain for *lipAH* expression, the resistance cassette of the plasmid pBBR1MCS1/PA *lipAH* was exchanged against the kanamycin resistance cassette of pBBR1MCS2 by restriction and ligation at the XhoI and SfiI restriction sites (further called pBBR2/PA *lipAH*). Furthermore, sequencing of the *lipAH* gene cassette of available pBBR1MCS/PA *lipAH* plasmids showed that *lipH* carried three mutations: L6del, A31T (GCG->ACG) and E145A (GAA->GCA). To restore the native *lipH* gene, the mutated *lipH* was exchanged with *lipH* from *P. aeruginosa* PA01. For this purpose, *lipH* was amplified by PCR using the primers NdeI_lipH_FW (P#3) and BamHI_lipH_RV (P#4) with isolated genomic *P. aeruginosa* PA01 DNA as a template. The resulting fragment and the pBBR2/PA *lipAH* were hydrolyzed by NdeI and BamHI, purified by preparative agarose gel electrophoresis and ligated by T4-DNA ligase (yielding the pBBR2lipAHff expression plasmid). The influence of mutated *lipH* on LipA production was demonstrated by comparison of the lipolytic activities in the supernatants of pBBR2/PA *lipAH*- and pBBR2lipAHff-containing cultures (Figure 3.6).

On average, the lipolytic activity of wild-type *lipH* (pBBR2lipAHff)-containing PABST7.1 cultures was 6 times higher than that of the mutated *lipH* (pBBR2/PA LipAH)-containing

cultures. The exact influence of the three mutations was not further investigated. Because of the locations of these mutations, the lowered LipA secretion could be attributable to several effects. The amount of full-length LipH could be lowered by inefficient secretion and membrane integration caused by the L6 deletion. The E145A mutation is located on the outside of MD1, but a conformational change causing lower activation efficiency cannot be excluded. The mutation A31T, located in the variable domain, might affect the interaction of LipH with other proteins involved in the secretion of LipA.

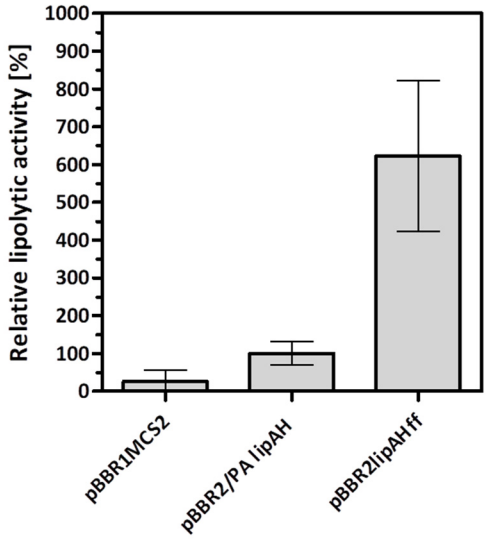

Figure 3.6: Comparison of LipA activities in *P. aeruginosa* PABST7.1 supernatants.
Relative lipolytic activities of supernatants from *P. aeruginosa* PABST7.1 transformed with pBBR1MCS2, pBBR2/PA *lipAH* and pBBR2lipAHff. Supernatants were taken from fresh overnight cultures grown from inoculation with single colonies. Activities were normalized to the activity of the supernatant of *P. aeruginosa* PABST7.1 pBBR2/lipAH. Bars represent the average ± standard deviations of 5 biological replicates measured in 2 independent experiments.

The preparative production of native LipA with PABST7.1/pBBR2lipAHff was performed as described in chapter 2.4.8 after comparing different expression protocols described in the literature.[17,86,98,173,174] The expression of the *lipAH* operon in LB at 37 °C for 40 h without induction by IPTG yielded the highest lipolytic activity. Induction with IPTG without the use of glucose in the cultivation media yielded only low amounts of lipolytic activity, possibly caused by overloading the secretion apparatus. Aerobic growth conditions seemed to be important; therefore, cultivation was performed in Erlenmeyer flasks with a flask to culture volume ratio of at least 25. Comparison of the lipolytic activity of the supernatant with the specific activity of purified LipA (see chapter 3.2.2) gave a yield of 80 ± 6 mg/l LipA. Rosenau (2001)[173] reported a possible yield of up to 150 mg/l with a pUCPKS-based plasmid in tryptophan-phosphate-based medium with induction. Therefore, it might be possible to further increase the yield of mature LipA by controlling the induction rate and optimizing the expression conditions. However, the amount of LipA was sufficient for preparative purification, and optimization was not performed at this point.

3.2.2. Improved purification procedure of mature LipA from supernatant

The last published protocol for the purification of LipA from *P. aeruginosa* supernatants dates back to Liebeton *et al.* (2000).[17] They described a two-step procedure of size exclusion chromatography (SEC) followed by ion-exchange chromatography (IEC). For SEC purification, the sample size that is applied to the column is a critical factor for protein separation; therefore, the first step requires intensive concentration of the supernatant. Exopolysaccharides secreted from *P. aeruginosa*[175] make it difficult to concentrate the supernatant with ultrafiltration devices on a large scale. Therefore, optimization of the purification procedure was attempted by testing whether the SEC purification step could be circumvented. IEC is suitable to concentrate the protein of interest from large sample volumes, but it requires low ionic strength and appropriate pH of the sample to favor the effective binding of the desired protein and to prevent the binding of impurities. The use of low-salt medium or minimal medium to produce LipA in *P. aeruginosa* yielded only unsatisfactory growth and low amounts of secreted LipA. Dialysis made it possible to reduce the ionic strength of supernatants of *P. aeruginosa* culture expressing *lipA* grown in LB medium to a level suitable for IEX. Unfortunately, without pH adjustment, the binding sites of the resin were saturated quickly by protein and impurities. At low pH (pI of LipA: 5.8[34]), the binding of impurities was reduced, but LipA showed increased aggregation. In conclusion, IEC is not applicable for the purification of LipA from supernatants without extensive adjustments. Another purification method to concentrate the protein of interest from large volumes is hydrophobic interaction chromatography (HIC). This method has often been successfully used for the purification of lipases from supernatants.[176–178] The interactions of the resin and proteins are strengthened by high salt concentrations, and LipA, as an amphiphilic protein,[179] should have higher binding affinity than most protein and protein-like impurities. As described in chapter 2.5.7, HIC enabled the development of a faster and easier method for the large-scale purification of LipA from supernatants than the published method of Liebeton *et al.*[17]

Octyl sepharose FF (GE Healthcare) resin, described as a strongly binding hydrophobic material that causes less denaturation than phenyl-substituted resins, was used in this protocol.[180] The presence of 3 M NaCl was used to strengthen hydrophobic interactions during column loading, as 3 M NaCl had no influence on the activity of LipA in the supernatant for several hours at room temperature (data not shown). During washing, the NaCl content

was reduced to 150 mM to remove weakly bound impurities. Below 150 mM NaCl, LipA eluted slowly, detectable by an increase in lipolytic activity in the flow-through.

Because LipA still eluted very slowly in the absence of NaCl, ethylene glycol was added as a hydrophobic agent for elution. Figure 3.7 shows samples of crude supernatant containing LipA, concentrated 10 times, and the pooled fractions of purified LipA. It was possible to remove most protein-like impurities with a single HIC purification step. Interestingly, the addition of SDS-PAGE buffer to supernatant samples, if not performed directly before boiling, led to the disappearance of the LipA protein band, indicating the presence of a protease that can digest LipA when it is unfolded by SDS. Purified LipA samples showed long-term stable protein bands after the addition of SDS buffer (data not shown), indicating that the main protease impurities were removed during purification.

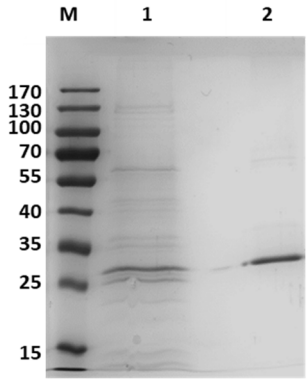

Figure 3.7: SDS-PAGE of crude culture supernatant and purified native LipA.
12 % reducing analytic SDS-PAGE gels of (1) 10-fold concentrated supernatants of *P. aeruginosa* PABST7.1 pBBR2lipAHff culture and (2) purified native LipA. (M) Protein size marker.

Ethylene glycol-containing buffer stabilized LipA at -20 °C for long-term storage but showed influences on the activity and stability at high temperatures; therefore, ethylene glycol had to be removed or diluted intensively before further experiments. It would also be possible to remove ethylene glycol with the remaining visible impurities by adding an additional SEC or IEC purification step as polishing. Additionally, without dialysis of the culture supernatant prior to salt addition, the final samples showed a brownish color, which is most likely caused by hydrophobic small-molecule impurities that would also be removable by an additional chromatographic step, circumventing the need for prior dialysis. Further improvements of the purification protocol were not performed at this point.

Purified native LipA showed very high specific activity, which was determined to be 141 µkat/mg (4.26 mkat/µmol) (chapter 2.5.8 and 2.6.1) and is comparable to the activity of 760 µkat/mg determined by Stuer *et al.* (1986).[34]

3.2.3. Improved procedure for the purification of LipA from inclusion bodies

The preactive state of several lipases is derived by chemical denaturation and refolding of the native state purified from the supernatant or from heterologously expressed inclusion bodies.[84,89,165,181,182] Because of the high yield of inclusion bodies and the lack of a reported difference in quality, throughout this thesis, preactive LipA was derived from inclusion bodies after heterologous expression in *E. coli* BL21 (DE3) using the pLipA-SS expression plasmid.[101] In this plasmid, LipA is encoded under the control of the T7-promotor without its N-terminal signal sequence, resulting in the production of LipA inside the cytoplasm as inclusion bodies, which were purified according to a protocol modified from that of Hausmann[92] through cell lysis and thorough washing by centrifugation and suspension (chapter 2.5.5). Hausmann overcame problems with protein contamination in the final sample by expression in minimal media and by using lauroyl sarcosine to eliminate membrane fragments during purification.
The experiments in this study showed that it is possible to obtain electrophoretically pure LipA inclusion bodies from cultures grown in LB medium without using detergents (see Figure 3.8, lane 9). The use of 1 % (w/v) lauryl sarcosine, which was applied by Hausmann during the washing steps, greatly reduced the yield of LipA. Most of the inclusion bodies were dissolved and removed with the supernatant after centrifugation during washing. Furthermore, the usage of detergents includes the risk of contaminating the purified samples, which might influence the refolding behavior of LipA.

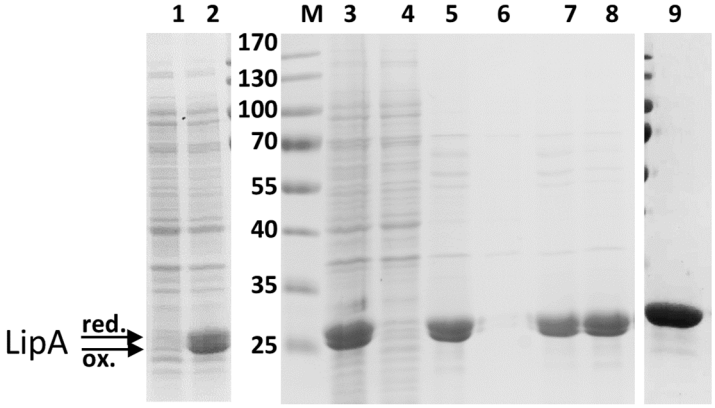

Figure 3.8: Expression and purification of LipA as inclusion bodies in *E. coli* BL21 (DE3).
12 % nonreducing analytic SDS-PAGE gel showing expression with samples (1) before and (2) after induction; fractions obtained from purification with 10 mM DTT: (3) insoluble fraction, (4) soluble fraction after cell lysis, (5) inclusion bodies after first washing step, (6) first wash phase, (7) inclusion bodies after second washing step, (8) inclusion bodies after third washing step; and (9) LipA in urea purified with 1 mM TCEP in wash buffer. The formation of the disulfide bridge causes a small shift, and the reduced (red.) and oxidized forms (ox.) are marked by arrows. (M) Protein size marker.

A more severe mechanism that retains contamination is the formation of intermolecular disulfide bridges during purification. The behavior of the two cysteines of LipA (C183 and C235), which form an intramolecular disulfide bridge in the native mature state of LipA, was not investigated by Hausmann during purification under nonreducing conditions. Therefore, the formation of the disulfide bridge was investigated during expression and purification by nonreducing SDS-PAGE. The two states of LipA can be distinguished by the faster migration of the oxidized form during SDS-PAGE.[101] Lane 2 of Figure 3.8 shows that the disulfide bridge was formed only partially in the inclusion bodies during expression, leaving reactive cysteines that could still covalently bind to other proteins during purification.

The use of 5 mM of the redox agent dithiothreitol (DTT) during purification led to only partial reduction of the disulfide bridges during washing (shown in lanes 3 to 8 by the increased intensity of the band of reduced LipA), and contaminants were still visible in the final sample. The use of 1 mM tris(2-carboxyethyl)phosphine (TCEP) during purification, as an irreversible reducing agent,[183] led to the full reduction of cysteines; therefore, no contaminations were observed (shown in lane 9).

By modifying the protocol of Hausmann, it was possible to obtain pure LipA inclusion bodies electrophoretically without the use of detergents, which might have influenced the refolding of LipA. The recovery rate of inclusion bodies was highly increased without the use of detergents, and LipA was not lost during washing steps (lane 6). The use of TCEP during purification can disrupt all disulfide bridges making LipA available solely in the reduced conformation and thereby resulting in enhanced purity.

3.3. Renaturation and stabilization of preactive LipA

To derive the preactive conformation of LipA from purified inclusion bodies, they are chemically denatured by the addition of urea (or guanidium hydrochloride) and renatured by dilution (or dialysis).[24,101,184–188] The reproducibility and efficiency of the renaturation procedure is a critical factor for the investigation of foldase-mediated lipase folding.

The underlying procedure for the renaturation of LipA and its activation by LipH of *P. aeruginosa* (also denoted as refolding) was developed in the work of Schneidinger (1997)[188] and has been only slightly modified since then.[92] In this procedure, denatured LipA is diluted at least 10 times into refolding buffer (50 mM TRIS pH 8, 45 % (v/v) glycerol, 3.5 mM $CaCl_2$, 0.7 mM lauroyl maltoside) containing LipH and incubated at 30 °C for 3 h. The efficiency of this refolding procedure is estimated to be 20-25 %.[189,190] Hausmann observed that efficient refolding requires glycerol.[92] Shibata *et al.* (1999)[89] used 0.5 % Triton X-100 instead of glycerol. El Khattabi *et al.* (2003)[38] used neither glycerol nor detergents, but both have postulated that Ca^{2+} is necessary for complex formation.

The role of each chemical used for LipA refolding seems to be not fully understood.

The experiments in this study showed that glycerol and detergents were not needed for the efficient refolding of LipA. Although activity was gained without glycerol, the thermal stability of the preactive state was decreased; therefore, the activity could be regained only if the refolding was done at 4 °C (data not shown). Most biochemical and biophysical measurements are disturbed by high amounts of glycerol or the presence of detergents or are not feasible at 4 °C. To be able to investigate the refolding reaction more closely, an improved renaturation procedure and buffer composition were needed.

3.3.1. Preactive LipA is pH and salt sensitive

Accordingly, the influence of single buffer components on the renaturation efficiency and the thermal stability of preactive LipA were tested. The denatured LipA was renatured in varying buffer compositions, divided into aliquots and incubated at different temperatures for 1 h before an equimolar concentration of LipH was added. After incubation at 4 °C overnight to achieve full complex formation, the stability of preactive LipA was determined by the lipolytic activity of the remaining activatable LipA in the LipAH complex (the detailed procedure is described in chapter 2.6.2). Figure 3.9 A shows the influence of $CaCl_2$ at concentrations ranging from 0 to 2 mM on the thermal stability of preactive LipA. $CaCl_2$ had a strong influence on the

stability of preactive LipA. With increasing concentrations of $CaCl_2$, the stability decreased. But also, in the absence of $CaCl_2$, the preactive state was not stable at room temperature. The refolding efficiencies for different buffer compositions could normally be determined by the activity level of the stable plateau at low temperatures. However, in this experiment, the melting curves of LipA showed no plateau at the lowest incubation temperature.

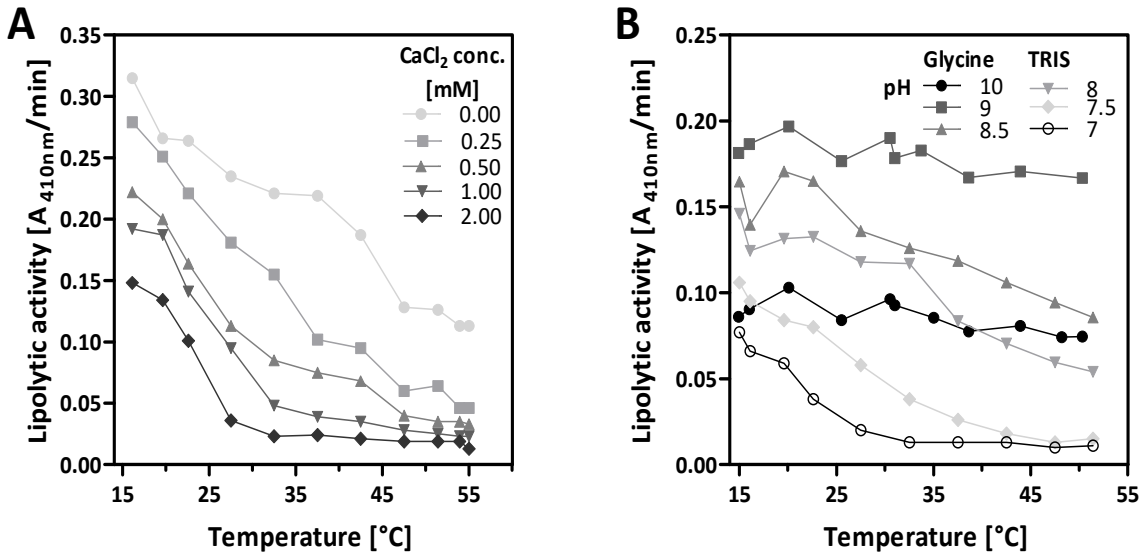

Figure 3.9: $CaCl_2$ and pH influence the thermal stability of preactive LipA.
First, 100 nM LipA was renatured in A) 50 mM TRIS buffer pH 8 containing different amounts of $CaCl_2$ and B) 10 mM TRIS or glycine buffer with different pH values. Samples were divided and incubated at different temperatures for 1 h. Foldase was added at an equimolar ratio to LipA. After incubation at 4 °C overnight, the activities were measured.

Because of the instability of preactive LipA in the absence of $CaCl_2$, the influence of pH was determined in a second experiment. The buffer strength was reduced to 10 mM because it was observed that at high buffer concentrations or in the presence of NaCl, LipA precipitates during renaturation (data not shown). In Figure 3.9 B, the thermal stability of preactive LipA is shown in a pH range from 7 - 10 in plain TRIS and glycine buffers. The thermal stability increased with increasing pH. The highest stability of preactive LipA was measured in buffers at pH 9 and 10, where the recovery of preactive LipA was higher than 90 % after incubation at 50 °C for 1 h.

The refolding efficiency at pH 9 was the highest. At pH 10, the activity was decreased to approximately 50 % of that at pH 9, possibly caused by reduced renaturation efficiency during the dilution of LipA or lower refolding efficiency resulting from lowered affinity between LipA and LipH. This experiment cannot distinguish between these two effects.

3.3.2. Preactive LipA has high thermal stability in salt-free TG buffer

The salt content of refolding buffer seems to play a role in the stability of LipA. Plain TRIS and glycine buffers also contain a small amount of salts, resulting from pH adjustment, usually with HCl or NaOH. The amount of acid or base that has to be added to reach a specific pH can be determined by titration experiments or calculated using the Henderson-Hasselbalch equation. For example, TRIS has a pK_A of 8.05 at 25 °C,[191] and therefore TRIS buffer adjusted to pH 8 with HCl contains chloride ions at a concentration that is almost 50 % of the TRIS concentration. At pH 9, it still contains more than 20 % chloride ions compared to the TRIS concentration. Glycine has pK_A values of 2.34 for the carboxyl group and 9.6 for the amino group and a pI value of 5.97.[192] A glycine buffer at pH 9 contains almost 20 % sodium ions compared to the buffer concentration. A buffer free of additional salts can be derived by mixing 5 mM TRIS and 5 mM glycine in pure water (TG buffer). This buffer composition adjusts itself to pH 9 at room temperature without the need to adjust the pH with the addition of further acid or base. The thermal stability of preactive LipA in TG buffer was investigated more closely with the same experimental setup used in chapter 3.3.

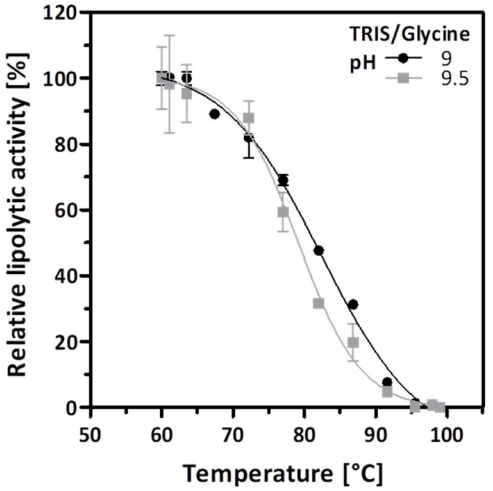

Figure 3.10: Thermal stability of preactive LipA in TG buffer.
Denatured LipA was renatured in 10 mM TRIS/glycine (TG) buffer at pH 9 and 9.5 and a final concentration of 100 nM. Samples were divided and incubated in a temperature gradient for 1 h. Afterwards, LipH was added in an equimolar ratio compared to LipA. After incubation at 4 °C overnight, the lipolytic activities were measured. The values shown represent the average ± standard deviations of triplicate samples. Melting temperatures were calculated by nonlinear regression using a Boltzmann sigmoidal fit.

Figure 3.10 shows the melting curves of preactive LipA in TG buffer and in TG buffer adjusted (with NaOH) to pH 9.5. At pH 9 and 9.5, the preactive state had high thermal stability; denaturation began ($T_{M\text{-}5\ \%}$) at 63 °C, and full inactivation ($T_{M\text{-}100\ \%}$) occurred at 98 °C. The $T_{M\ 50\ \%}$ differs slightly between 82 °C at pH 9 and 79 °C at pH 9.5, respectively. At pH 10, the stability of preactive LipA was lower than that at pH 9.5. Denaturation started below 60 °C and reached 100 % at 84 °C (data not shown).

To exclude the possibility that renaturation at different pH values caused different stable conformations of preactive LipA, denatured LipA was renatured in TG buffer and further diluted into TG buffers adjusted with acetic acid to pH 7-8.5 before incubation in a

temperature gradient. The remaining activities measured after incubation with foldase showed a similar decrease in stability with decreasing pH, as shown in Figure 3.9 B (data not shown). Conclusively, renaturation in buffers with different pH values does not cause a measurable change in stability, and it can be reasoned that pH mainly affects the stability of preactive LipA.

3.3.3. Aggregation tendency might be caused by evolution

Curve progressions of the thermal stability measurements of preactive LipA in Figure 3.9 indicate aggregation behavior rather than thermal unfolding, as no defined melting transition is observed. This aggregation increased with increasing calcium chloride concentration and decreasing pH. Purified native LipA showed similar sensitivity to calcium chloride and pH (shown in Appendix 8.7) as preactive LipA. Therefore, this property is most likely not due to the misfolding of preactive LipA during renaturation but rather to an intrinsic characteristic of LipA. There are several possible reasons for this aggregation behavior. It could be caused by hydrophobic forces. LipA is described as an amphiphilic enzyme that can bind LPS or other hydrophobic detergents.[179] Similar to many other lipases, LipA possesses a hydrophobic substrate binding pocket that is covered by a lid in its inactive state.[33,193,194] This lid prevents the uncontrolled exposure of the hydrophobic parts in the absence of possible substrates and activate the lipase by opening the substrate binding pocket and exposing the active site in contact with micelle surfaces.[195] This so-called interfacial activation mechanism seems to be very sensitive in LipA, and it was observed that the presence of hydrophobic substances can cause a permanent open substrate binding pocket.[174,196] This uncontrolled opening of the substrate binding pocket of LipA could cause inactivation by aggregation at the hydrophobic substrate binding pocket. The pH and salts can influence the electrostatics that are responsible for the control of lid opening or the strength of hydrophobic interactions.[197]

Another possible reason for this aggregation behavior is the general electrostatic characteristics of LipA. LipA exhibits an interesting surface charge distribution (shown in Figure 3.2 on page 45), with large evenly charged patches. These charged patches can serve as interaction points between two LipA molecules. The pH can influence the net sum charge of these patches and, in turn, the affinity of LipA molecules for each other. Ions, especially divalent cations such as calcium and magnesium, have the ability to bind to the protein surface and bridge two negative charges that would otherwise contribute to repulsions.[198] The

addition of glycine to the buffer had a stabilizing effect, most likely by direct interaction with LipA and shielding of these surface charges.[199]

In fact, LipA has evolutionary evolved to bind to alginate structures in the extracellular space,[174,200] which protects it from proteolytic degradation, denaturation and diffusion from the cell.[174,201] Tielen *et al.* (2013)[174] postulated that this binding occurs specifically between several positively charged amino acids on the surface at the opposite site from the active center and the negatively charged carboxyl groups of alginate. Considering the high binding capacity of alginate for divalent cations,[202] it is possible that the effective concentration of divalent cations is greatly reduced inside these alginate structures or even that the cations are used to strengthen the binding by crosslinking the negative charges of alginate and LipA. This assumption is supported by the finding that EDTA helped to isolate LipA from alginate.[34] Therefore, LipA did not have selective pressure to develop a surface charge distribution that prevents *in vitro* aggregation in the presence of calcium and the absence of alginate structures.

3.4. Complex formation is not influenced by the new buffer system

The experiments in chapters 3.3.1 and 3.3.2 revealed buffer conditions in which thermal treatment of renatured LipA had no effect on its activation by LipH. This property made it possible to investigate the refolding reaction at room temperature without any essential additives, such as glycerol or detergents, lowering the risk of artificial effects caused by detergents and temperature-induced changes during incubation, sample handling and measurements. Because the buffer composition for LipA refolding was changed, the basic parameters for the LipH-mediated LipA refolding should be determined and compared with literature data. The progress of LipA activation by LipH was monitored over time by measuring the increasing lipolytic activity. Therefore, a sample of 100 µM equimolar mixture of renatured preactive LipA and LipH was freshly prepared and incubated at room temperature. To avoid diffusional influences on the sample taking, the samples were steadily mixed on an Eppendorf rotational shaker at 500 rpm. The measured activation process against reaction time is shown in Figure 3.11 A.

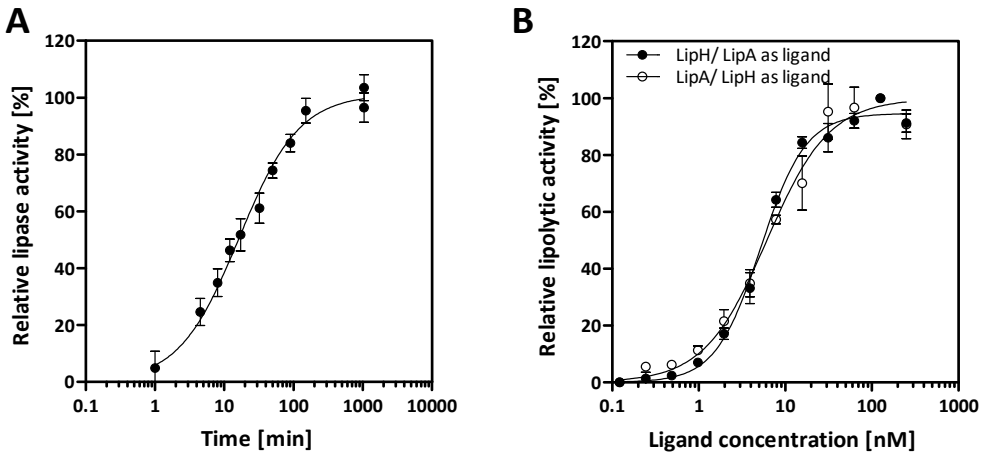

Figure 3.11: Determination of the activation and affinity constant.
(A) Time course of the activation of LipA by LipH at equimolar concentrations of 100 µM. The samples were incubated with slight agitation at room temperature. Activities were normalized to activity at the plateau phase, which was set to 100 %. The activation constant of 17 min was determined by nonlinear regression using the "One Site Binding (hyperbola)" fit. (B) The affinity between LipA and LipH was measured by preparing dilution series of LipA and LipH, respectively, and the addition of a constant amount of the other interaction partner (1 nM) to each dilution series. Samples were incubated at 4 °C overnight before activity measurement. Activities were normalized to the activity at the plateau phase, which was set to 100 %. The half effective concentrations were calculated using the "One site - Specific Binding with Hill slope" fit.

The half activation constant was determined by one site binding (hyperbola) fit to be 17 min. The complex formation should follow a second order reaction rate, which means that the reaction rates are dependent on the start concentration of free LipA and LipH and slows down

with progressing reaction. After approximately two hours, the activation is almost complete but reaches full saturation only after incubation overnight. El Khattabi *et al.* (2000)[85] determined a half activation constant for the LipAB_BG complex formation of 10 min under slightly different conditions (37 °C, probably 33 nM LipA and a 5 times excess of LipB). Shibata *et al.* (1998)[89] reported the full activation of LipA_PA by LipH in under 1 hour, obtained in an equimolar mixture of LipA and LipH with a concentration of 290 nM in a more complex buffer system (20 mM Tris–HCl, pH 8.0, 0.2 M NaCl, 5 mM CaCl2, 0.5 mM EDTA, and 0.5 % (v/v) Triton X-100) at room temperature.

A more important characteristic of protein-protein interactions is their affinity, often expressed as the dissociation constant, which describes the equilibrium state between association and dissociation rates. Because the LipAH complex formation is thought to be irreversible *in vitro,*[45,74,81,85,88,92,93] the affinity is described as half the effective concentration (EC_{50}) of ligand that is needed to saturate half of the interaction partner. This constant was determined by the titration of one protein with the other (the protein with constant concentration is designated as the interaction partner and the protein with variable concentration as the ligand). For this purpose, dilution series of LipA and LipH as ligands in a range of 0.1 nM to 250 nM were prepared, and 1 nM of the respective interaction partner was added to all samples. After incubation overnight to reach the equilibrium state, the resulting activities were measured.

Figure 3.11 B shows the resulting ligand concentration-dependent increase in activity. The half effective concentrations were between 5 and 6 nM for both titration curves. Approximately 100 nM of LipA or LipH is needed as a ligand to saturate 1 nM of the corresponding interaction partner. This ratio of 1:100 decreased with increasing concentration of the interaction partner and reached 1:1 at concentrations above 100 nM (data not shown). This affinity is in agreement with the high affinity of 5 nM that was observed for the LipAB_BG complex (Pauwels *et al.* 2006)[81] by surface plasmon resonance (SPR). Ogino *et al.* (2013)[182] determined the affinity of the LipAH complex from *P. aeruginosa LST-03 (LipA-LST3* is 99 % identical to LipA) to be 0.558-1.34 µM, also by SPR. This value seems to be very high compared to the affinity that was determined in the experiment above and contradicts previous published results of Ogino *et al.* (2008),[24] in which they were able to demonstrate full complex formation by activity assays at nearly equimolar ratios at concentrations below 0.5 µM. Comparison of these two experiments shows that different buffer compositions were used (activity-buffer: 20 mM Tris–HCl, pH 8.0, SPR-buffer: 10 mM HEPES, pH 7.4, 150 mM NaCl

and 0.005 % Tween 20). The buffer composition used for SRP experiments contained Tween 20 as a detergent, which may have influenced the mostly nonpolar interactions[81] of foldases with lipases. Furthermore, the stability experiments of preactive LipA, conducted in chapter 3.3.1, indicate that immobilized LipA was not fully stable during their binding experiments, lowering the binding affinity of LipH. Heil (2012)[203] was able to determine the dissociation constant (K_D) of LipAH_PA using Biolayer Interferometry as probably 1.72 nM (originally specified as 0.16 nM, but recalculation from the given k_{on} and k_{off} rates with the given formula for K_D and estimated sign error in the given k_{off} potency yielded 1.72 nM), but unfortunately without providing biochemical details of the measurement, which makes comparison impossible. Comparison of the titration curves, shown in Figure 3.11 B, can also give information about the amount of renatured LipA that is activated. To calculate the renaturation efficiencies solely by the activity gained by activation of preactive LipA with the specific activity of native LipA can lead to wrong assumptions, even if full complex formation is reached because several foldases showed an inhibiting effect on the lipolytic activity if added to native lipases.[88,93,188]

Ihara *et al.* (1995)[88] even observed a reduction in lipolytic activity to 40 % for LipL from *Pseudomonas spec.* strain 109 in the presence of an equimolar amount of its lipase-specific foldase LimL. The maximal activity reached during the titration of LipH with LipA in the saturation plateau should correspond to the activity of 1 nM LipAH complex, excluding multiturnover catalysis of LipH and assuming that misfolded LipA does not bind to LipH with significant affinity. Under these conditions, the difference in the maximal reached activities of the LipAH titration curves should correlate with the amount of non-activatable preactive LipA. The LipA titration curve reached 84±2 % of the activity of the LipH titration curve, showing that 16±2 % of renatured LipA was not activated. Of course, the activity at complex saturation is influenced by many factors; for example, the amount of LipA at such low concentrations can be influenced by absorption at hydrophobic surfaces during sample handling, or the activity of the saturated complex can be decreased by an excess of inactive LipA; therefore, this value should be seen as a rough estimation. The specific activity measured in this experiment was 16 µkat/mg lipase, which is just 11 % of the specific activity of native LipA (see chapter 3.2.2). Even with an inhibitory effect of LipH, this value is lower than expected and can be caused by several factors, which are discussed in the following chapters. In summary, the complex formation and activation of LipA by LipH seem not to be influenced by the modified buffer

conditions, and the complex formation time constant and the affinity are comparable to previously published results.

3.5. Role of divalent ions during complex formation

Calcium ions exhibit a negative effect on the stability of preactive LipA but are essential for the activity of LipA. Therefore, the role of calcium cations was investigated in more detail. In contrast to previous literature,[38,85,89,204] it was possible to demonstrate that calcium is not needed for complex formation and that LipH interacts with and opens the calcium binding site of both preactive and native LipA, resulting in fast exchange rates of calcium. To compare the effect of cations that bind to the metal binding center with other unspecific binding, the affinity of LipA to several biologically relevant cations was analyzed.

3.5.1. Calcium is not needed for complex formation

LipA requires a calcium ion for its activity. Ca^{2+} is coordinated octahedrally by side chain carboxy groups of D209 and D253, backbone carbonyl groups of Q257 and L261, and two water molecules close to the active site.[33] This metal binding site is highly conserved among bacterial lipases of families I.1 and I.2.[33] Because of its distance from the active serine of 15 Å, it is most likely not involved in the catalytic mechanism, but it is thought to be important in stabilizing the structure of the active site by coordinating H251 of the catalytic triad at the right position.[33]

Because of the crosslinking experiments of *Shibata et al.* (1998),[89] in which they observed an inhibition of complex formation in the absence of calcium, an additional role of calcium for the complex formation was discussed.[38,85,204] This discussion was further complicated by the observation of El Khattabi *et al.* that LipA_BG does not need calcium for refolding or activity.[38,85] The requirement of calcium for complex formation of the LipAH_PA complex and not only for the activity of LipA was never again experimentally proven but continued to be cited.[41,74,172,173,203] Later, *Ogino et al*. (2013)[182] were able to show that the activity of LipA from *P. aeruginosa LST-03* (99 % identical to LipA from *P. aeruginosa PA01*) can be gained if calcium is added after complex formation.

In this thesis, most complex formation experiments were performed without calcium. The possibility of copurifying LipA over the affinity tag of LipH in the absence of calcium (shown in Figure 3.24, page 95) and a time-dependent increase in activity, which can be measured with the presence of calcium only during the activity assay (shown in Figure 3.11, page 66), clearly prove that foldase does not need calcium for complex formation. Accordingly, calcium ions most likely play a role in the active state of LipA.

3.5.2. Complexed preactive LipA binds calcium with high affinity

Because of the sensitivity of preactive LipA to calcium, the concentration of calcium should be as low as possible, to reach saturation of the metal binding but not to influence the stability of preactive LipA. Therefore, the effective concentration of calcium was determined by titration experiments and the resulting lipolytic activity. A LipAH complex sample formed overnight without calcium was divided, and calcium was added at different concentrations in a dilution series. After incubation at room temperature for 15 min, the activity was measured (data shown in Appendix 8.8).

The half effective concentration (EC_{50}) of 51 µM was determined from the saturating activity curves at increasing calcium concentration. This value is comparable to the calcium dissociation constant of *Staphylococcus hyicus* lipase,[205] which is 55 µM (different calcium coordination: four aspartate side chains and one glycine carbonyl group[206]), and has been considered high-affinity binding for lipases.[207] Saturation of the curves was observed at 250 µM, showing that a concentration of 250 µM during complex formation is sufficient to saturate the metal binding site of the LipAH complex at room temperature.

3.5.3. Exchange rates of calcium are higher than expected

Titration experiments for calcium affinity determination revealed that the equilibrium calcium binding, established during incubation, shifts if substrate without $CaCl_2$ is added for activity measurement (Figure 3.12 A). The activity curves of samples 20-fold diluted during the activity assay (10 µl sample and 190 µl substrate), with substrate but without $CaCl_2$ and with substrate containing the same amounts of $CaCl_2$ as used for incubation, were different. However, accounting for the dilution factor by plotting the activities against the final calcium concentration during the activity assay led to nicely overlapping curves (Figure 3.12 B). This fast exchange rate of calcium made it possible to saturate the metal binding pocket of the LipAH complex by the addition of 1 mM $CaCl_2$ during the activity measurement. At this concentration of Ca^{2+} in the substrate, the activities of samples preincubated with or without $CaCl_2$ were indistinguishable.

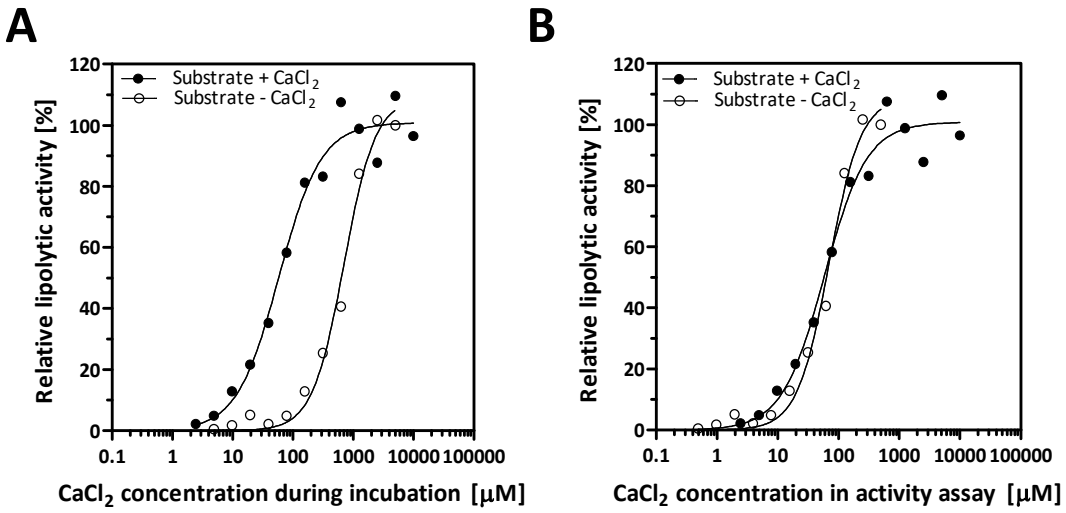

Figure 3.12: Shifting equilibrium of calcium binding caused by dilution.
Relation between $CaCl_2$ concentration and the activity of LipA in complex with LipH. A sample of the LipAH complex was diluted with buffers containing different $CaCl_2$ concentrations and incubated for 30 min on ice. To determine the lipase activity, substrates with and without $CaCl_2$ in equal concentrations to the samples were used. The activities were normalized to the average value of the highest activity and plotted against the $CaCl_2$ during incubation (A) and against the final concentration of $CaCl_2$ during activity measurement (B). Curves were fitted using the equation for "One site - Specific binding with Hill slope".

3.5.4. Foldase opens the calcium binding pocket of lipase

The fast exchange rates of Ca^{2+} indicate a loss of bound metal ions, which is rather unexpected for LipA because the structure of its metal binding pocket revealed that the calcium ion is not solvent accessible and should be bound tightly. Experiments by Shibata *et al.* (1998)[89] supported these assumptions. They observed similar fast exchange rates of calcium inside the metal binding pocket of preactive LipA in complex with LipH by a fast decrease in activity upon the addition of EDTA, while native LipA was much more resistant to EDTA.

This difference can be caused by structural differences between preactive and native LipA, caused by the refolding of LipA or by interactions with LipH, which might be able to open the metal binding pocket. Shibata *et al.* did not measure the influence of EDTA on native LipA complexed by LipH. To investigate whether LipH is able to open the metal binding pocket of LipA, this missing experiment was complemented here. Figure 3.13 shows the influence of EDTA on the activity of native LipA and native LipA in complex with LipH. EDTA had a significant influence only on the complex, reducing the activity on average to approximately 30 % of that of untreated native LipA. Therefore, it can be concluded that the foldase affects the accessibility of the metal binding pocket in preactive and native LipA.

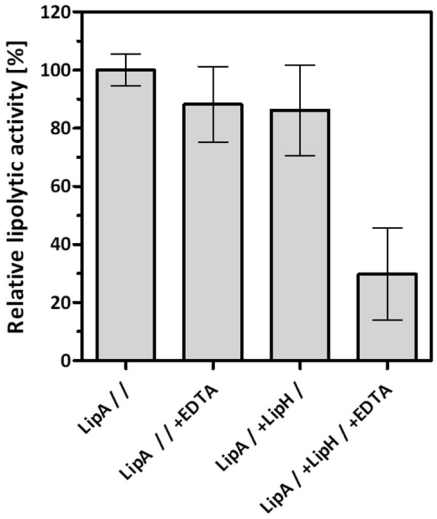

Figure 3.13: Influence of LipH and EDTA on the activity of native LipA.
The influences of LipH and EDTA on the activity of native LipA were determined after incubation for several hours. "/" indicates the single additions and incubation steps. First, 2 nM native LipA in TG buffer was supplemented with 100 nM LipH and incubated on ice for 3 h. Afterwards, 2 mM EDTA was added and further incubated on ice for 2 h before remaining activities were determined. Activities are normalized to a control LipA sample. The results of three independent measurements are shown.

3.5.5. LipA promiscuously binds divalent cations

Ca^{2+} is considered to be the native cation for LipA.[33] However, different divalent cations can substitute for Ca^{2+}.[92] To test the ability of LipA to use other divalent cations, the activity of the LipAH complex was measured in the presence of different divalent cations that have biological relevance for proteins and can adopt octahedral coordination geometry[208] (Figure 3.14 A). Preactive LipA in complex with LipH showed similar activity in the presence of Mg^{2+} and increased activity in the presence of Mn^{2+} in comparison with Ca^{2+}. In the presence of Cu^{2+}, Co^{2+} and Ni^{2+}, LipA retained 50 % of activity compared with Ca^{2+}-complexed LipA. For Zn^{2+}, no activity was observed. The high activity in the presence of Mn^{2+} may be caused by an effect on the pNPP activity assay. At high Mn^{2+} concentrations, a rapid degradation of pNPP accompanied by the formation of white precipitation, indicating interactions of Mn^{2+} with the product, was observed.

The promiscuous binding of metal ions by bacterial lipases and modulation of their activities was previously described in the literature. Hausmann (2008)[92] observed only approximately 20 % and 39 % remaining activity of the LipAH complex with Mg^{2+} and $Mn^{2+,}$ respectively, if cations were added at an effective concentration of 10 mM during refolding. $CuSO_4$ showed no activity in the same experiment. Glogauer *et al.* (2011)[209] showed that subfamily I.1 lipase LipC12 (47 % identity with LipA) had approximately 50-60 % in the presence of Mn^{2+}, Cu^{2+}, Co^{2+} and Ni^{2+} and no activity for Zn^{2+}. Mg^{2+} yielded only 4 % remaining activity. Additionally, Rashid *et al.* (2001)[210] were able to show for a subfamily I.3 lipase from *Pseudomonas spec*. strain

KB700A that for the activity was not greatly affected by the presence of Mg^{2+} and Mn^{2+}, that little activity was observed in the presence of for Co^{2+} and Cu^{2+}, and almost no activity was observed for Zn^{2+}.

These measured values provide an indication of how well LipA can incorporate other divalent metal cations, but they can be influenced by stability effects and possibly affected by the catalytic activities of LipA. More detailed information can be derived by titration experiments to determine the EC_{50} and the resulting catalytic activities of LipA (Figure 3.24 B). The EC_{50} for the affinity of calcium was measured as previously described for the affinity of calcium in chapter 3.5.2.

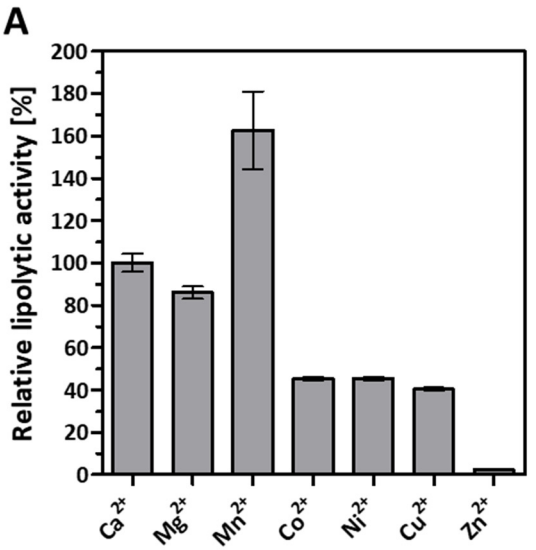

B

Cation	EC_{50} [µM]	B_{max} [ΔA_{410}/min]
Ca^{2+}	51	0.74
Mg^{2+}	114	0.46
Mn^{2+}	51	0.45
Co^{2+}	185	0.23
Ni^{2+}	>250	--
Cu^{2+}	>250	--
Zn^{2+}	--	--

Figure 3.14: Effects of divalent cation on the activity of the renatured LipAH complex.
A) First, 1 µM LipA foldase complex was diluted to 5 nM in buffer containing 1 mM divalent cations as chloride salts, and activity was measured with substrates containing the same divalent cations. The graphs represent the average activity of three independent experiments normalized to the activity with $CaCl_2$. B). Half effective concentrations (EC_{50}) of divalent cations for LipA activation, determined as described in Appendix 8.7.

Mn^{2+} and Ca^{2+} have the same EC_{50} of 51 µM. Mg^{2+} and Co^{2+} have lower affinities of 114 µM and 185 µM, respectively. The EC_{50} values of Cu^{2+} and Ni^{2+} were not quantifiable because the affinities were too low that saturation could not be reached in the cation concentration range used (≤ 1 mM). The concentration was kept below 1 mM because the LipAH complex stability was not given at higher concentrations. The affinity for Zn^{2+} was, because of missing activity, also not determinable.

The affinity of the cations used to bind to the metal binding center of LipA seems to follow the preference for cations to bind hard or soft coordination partners, based on the HSAB principal

of Pearson,[211,212] which reports that hard Lewis acids prefer hard Lewis bases and the other way around. The metal binding center of LipA coordinates Ca^{2+} solely by oxygens. Ca^{2+} and Mg^{2+} are hard Lewis acids and prefer oxygen as coordination partners. The tendency to bind to soft Lewis bases (such as nitrogen) increases with increasing group of the transition metals ($Mn^{2+}<Co^{2+}<Ni^{2+}<Cu^{2+}<Zn^{2+}$). Furthermore, the affinity is influenced by the preference to form complexes in octahedral geometry. For example, Zn^{2+} a poorly incorporated divalent cation in LipA but is predominantly found in tetrahedral complexes.[208] The high measured effective concentration of Mg^{2+} can be caused by a hydration rate four orders of magnitude higher than that of Ca^{2+}, which was often observed to lower the association rate of Mg-protein complexes.[213]

B_{max} values indicate the catalytic activities of LipA with bound cations if possible influences on the activity assay are ignored. Ca^{2+} enabled the highest activity, followed by Mg^{2+} and Mn^{2+} with approximately 60 % activity and Co^{2+} with 31 % activity compared to Ca^{2+}. It seems that the structural integrity and therefore the catalytic activity depends on the bound ion and that Ca^{2+} as a native cation for LipA causes the highest catalytic activity of LipA.

3.6. Preactive state is not near-native

The renaturation of lipases from a chemically denatured state yields the globular preactive state, which was defined as near-native because no structural differences compared to the native state were observed by physicochemical methods and because incubation with foldase yields an active conformation. El Khattabi *et al.* (2000)[85] observed by CD spectroscopy for the renatured LipA_BG no difference in secondary structure content and no difference in tryptophan fluorescence at room temperature. However, it was also observed that refolded lipases are more sensitive to trypsin digestion than their native state.[85,90] Pauwels *et al.* (2012)[214] complemented this observation with a detailed investigation of proteolytically degraded LipA_BG by mass spectrometry. They found several hot spots for proteolytic digestion in the near-native state of LipA_BG that are not accessible for proteolytic digestion in the native state. Most of these cleavage sites were located at the surface of the lipase, and only a minor amount was located inside the globular structure and most likely caused by secondary cleavage events. Together with the observation that the near-native state exhibits only a minor redshift in its intrinsic tryptophan fluorescence, Pauwels *et al.* confirmed that the near-native state refolds into a globular structure that is similar to the native state. They also observed that the near-native state has a higher hydrodynamic radius and a higher capacity to bind ANS, a dye for probing the accessibility of positively charged amino acids.[215] These findings, together with the high proteolytic sensitivity, clearly show that the near-native state differs from the native state in its fine structure.

The results of the experiments described in this chapter support these structural differences and even indicate that these differences are larger than expected. Furthermore, incompletely renatured LipA showed effects during thermal treatment, demonstrating the high structural flexibility of the renatured state. Together with differential scanning fluorometry (DSF), it was possible to demonstrate that these minor differences in fine structure can lead to very large stability differences and that renatured LipA does not fold into a near-native state that has only to be activated to reach the native conformation.

3.6.1. Thermal treatment induces conformational changes – an example

In chapter 4.3.2, the thermal stability of preactive LipA was determined by the remaining fraction of activatable LipA. However, from these experiments, it is not possible to draw a conclusion about the conformational thermal stability of preactive LipA. Reversible thermal

unfolding does not change the amount of activity and accordingly cannot be detected by these experiments. Preactive LipA was derived from a chemically unfolded conformation and was forced to fold into the lowest-energy reachable state upon removal of the denaturant. In conclusion, it is highly likely that LipA is able to refold into the preactive state again after its partial unfolding during thermal treatment. Such reversible structural changes were observed during stability experiments with improperly renatured preactive LipA samples. Figure 3.15 A shows an excellent example of the activation of a thermally treated preactive LipA sample of poor quality obtained from an old slightly turbid LipA stock, which was frozen and thawed many times and renatured by dilution to high LipA concentrations without the usual thorough mixing. This procedure should have led to a high amount of improperly folded LipA molecules that were trapped in unproductive folding side pathways, caused by interactions with other molecules or from incompletely denatured starting points.

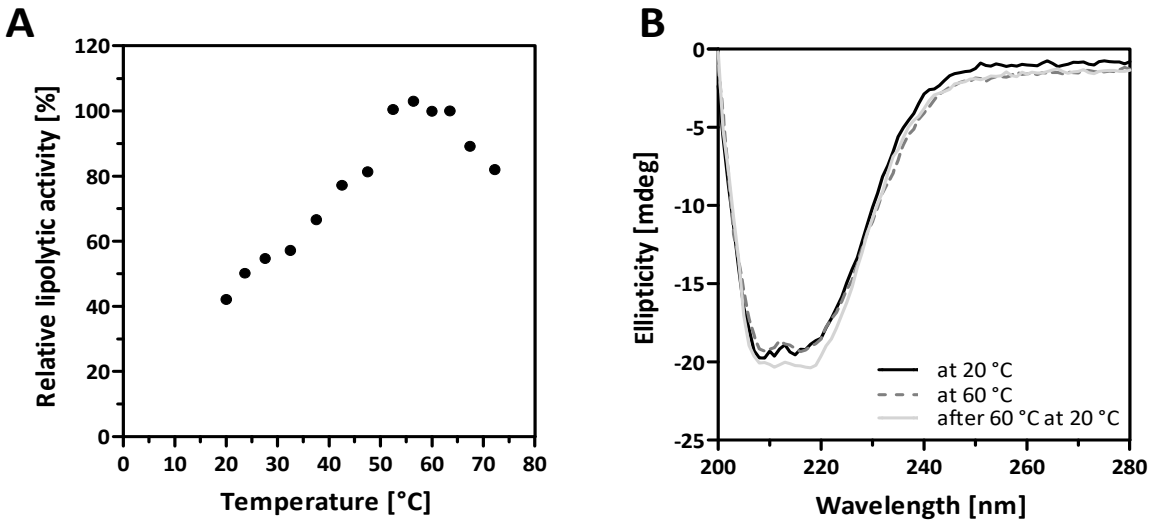

Figure 3.15: Thermally induced conformational changes in preactive LipA.
4 µM LipA was renatured improperly in 10 mM TG buffer. A) Sample was further diluted to 100 nM, divided into aliquots and incubated at different temperatures for 1 h. Afterwards, equal molar amounts of foldase were added to the samples. After incubation at 4 °C, the overnight activities were measured. B) CD spectra of the 4 µM sample were recorded at 20 °C after 1 h at 60 °C and cooled again to 20 °C after 1 h.

Obviously, thermal treatment of poorly refolded samples increased the amount of LipA that can be activated. This effect increased at higher temperatures. The increase in end activity indicates that LipA undergoes conformational changes during thermal treatment. The higher energy makes it possible to overcome the energetic barriers that keep molecules trapped inside local energetic minima, reentering the folding pathway, which leads to activatable conformations. Above 63 °C, the amount of LipA that can be activated decreases with

increasing temperature, as observed in chapter 3.3.2, most likely caused by irreversible unfolding.

To further examine structural changes, the same sample was investigated by CD spectroscopy (Figure 3.15 B). However, these structural changes occur mainly at the tertiary structure level. Comparison of the far-UV CD spectra recorded at 20 °C and 60 °C showed no change in the range from 200 nm to 240 nm and hence in the secondary structure of LipA. However, the spectra above 240 nm show an increase in the negative CD signal upon heating to 60 °C, which remains constant after cooling to room temperature again. Additionally, the ellipticity between 210 and 230 nm decreases slightly. The similarity between these three CD spectra, especially in the far-UV range (200 - 240 nm), shows that secondary structure elements of LipA are stable during heat treatment. Changes in the near-UV range (above 240 nm) mostly reflect the environment of aromatic amino acids,[216] indicating that structural changes occur in the tertiary structure. These rearrangements of tertiary structure elements at elevated temperatures induce a small change in secondary structure after cooling down, which was calculated as a 2 % transition from random coil to α-helix.

3.6.2. DSF reveals structural flexibility of preactive LipA

Because thermal treatment of preactive LipA seems to induce changes in the tertiary structure with only minor changes in secondary structure, the structural flexibility of preactive LipA was further investigated by differential scanning fluorometry (DSF). DSF detects conformational changes in proteins by the intrinsic fluorescence of their aromatic amino acids and is therefore a good complement to CD spectroscopy and activity measurements. Tryptophan and to a small extent tyrosine contribute to the intrinsic fluorescence of a protein at 330 nm and 350 nm. The emission characteristics of tryptophan are highly dependent on the electrostatic properties of the environment and shift to higher wavelengths depending on the polarity of the surrounding. In DSF, this redshift is monitored by the ratio of fluorescence at 350 nm and 330 nm to correct for other temperature-induced effects, such as changed quantum yields or fluorescence quenching.[128,130] LipA contains two tryptophans (W28 and W198), which are located inside the hydrophobic core in the loop before α-helix 1 and at the end of β-strand 7, which is located next to the central β-sheet.[33] Hence, it should be possible to observe the unfolding of the globular structure of LipA by its intrinsic fluorescence.

The melting curve of preactive LipA measured by DSF (Figure 3.16) confirms the structural flexibility and diversity of preactive LipA because no defined melting point can be observed.

Prior incubation at 60 °C for 1 h increased the amount of preactive LipA for activation and should therefore induce higher conformational uniformity of the sample. Only minor changes in the melting behavior were observed, but the results confirmed that preactive LipA can refold reversibly after partial thermal unfolding.

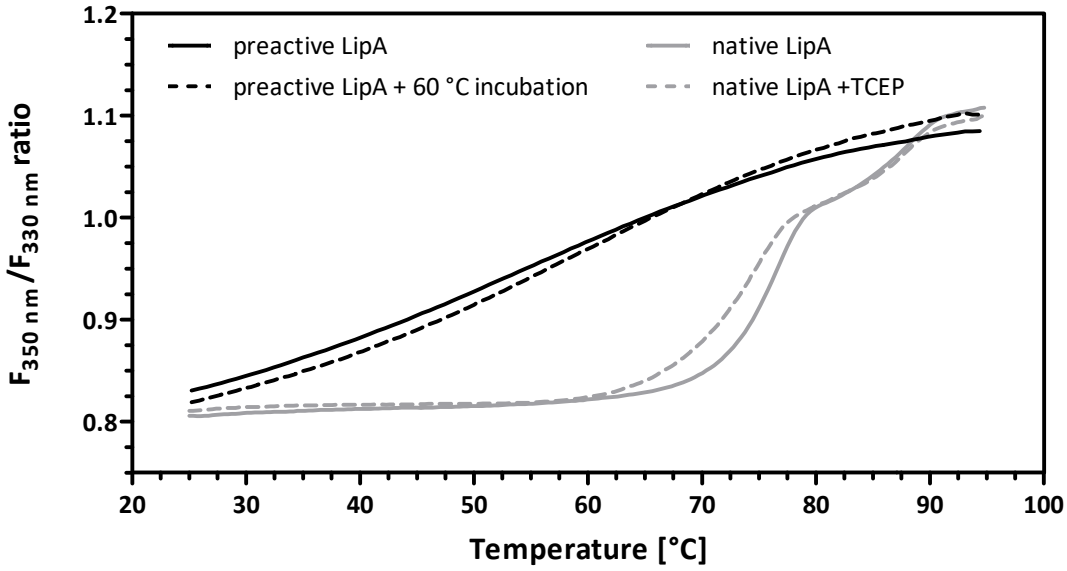

Figure 3.16: Melting curves of preactive and native LipA measured by DSF.
Fluorescence signal ratio (350 nm/330 nm) versus temperature of preactive LipA (2 µM) samples renatured and incubated on ice or at 60 °C for 1 h and native LipA (2 µM) with and without 500 µM TCEP.

In contrast, the melting curve of native LipA showed a defined melting with two transition points. Melting started at 60 °C with the first transition at approximately 76 °C and the second transition at approximately 88 °C. It can be argued that the disulfide bridge in LipA, which is not formed in freshly renatured preactive LipA, stabilizes the globular structure of native LipA. Therefore, the unfolding of native LipA was tested in the presence of TCEP, but only minor differences in the first transition point, which was shifted lower by approximately 3 °C, were observed.

Apparently, the difference in thermal stability is not caused by the cleaved disulfide bridge but by other conformational differences. The structural changes in preactive LipA, which do not show a defined transition point, indicate that renatured LipA folds into a globular structure but with no defined tertiary structure. Hence, unfolding of the tertiary structure occurs at different temperatures because of the structural inhomogeneity of renatured preactive LipA, and unfolded LipA is able to fold into the preactive state after thermal treatment at 60 °C.

3.7. Influence of LipH on LipA

The significant difference in the structure of preactive LipA and the structure of native LipA raises the question of whether the renatured state of LipA is a real folding intermediate on the route to native LipA, as previously postulated.[214] Complex formation and activation should convert preactive LipA into native LipA, and both conformations should show similar properties in complex. To answer this question, the behavior of preactive and native LipA in complex with LipH was investigated by DSF and by their lipolytic activity. Both methods consistently showed that LipH has a destabilizing effect on the globular structure of preactive and native LipA. The complex of native LipA and LipH unfolded at lower-temperature than free native LipA.

This inactivation process seems to overlap partially with the release of the intact globular structure of both LipA states from complex. Ca^{2+} and other divalent cations had a stabilizing effect on the preactive and native LipA in complex, most likely caused by structural rearrangements during the binding of a divalent cation to the metal binding site. In addition to stabilization, several other interesting observations lead to the assumption that divalent metal ions additionally influence the complex by allosteric effects. Because the behavior of the LipA states in complex were significantly different, it must be assumed that the preactive state of LipA is not converted into the native state by LipH.

3.7.1. Behavior of LipA in complex measured by DSF

To investigate the behavior of preactive and native LipA in complex, the properties of LipH should also be considered. Therefore, the thermal stability of LipH was determined by activity and DSF as described in chapters 2.6.2 and 2.6.3. Thermal inactivation, shown in Appendix 8.9, occurred at temperatures above 80 °C and reached 90 % at 100 °C. The DSF melting curve (Figure 3.17) revealed a conformational change starting at 30 °C with a $T_{M\text{-}50}$ of 49 °C. For better comparison of the transitions, the first derivatives of the fluorescence ratios are also shown (Figure 3.17, lower graph).

LipH contains only one tryptophan (W283) and six tyrosines in its folding domain. Because of the low amount of tertiary structure, W283 is only partially buried inside the structure of MD2, which results in high fluorescence at 350 nm with only a small redshift upon unfolding of LipH. Because W283 is located at α9 and covered by R327 of α11 in LipH, this unfolding event most likely reflects the unfolding of MD2.

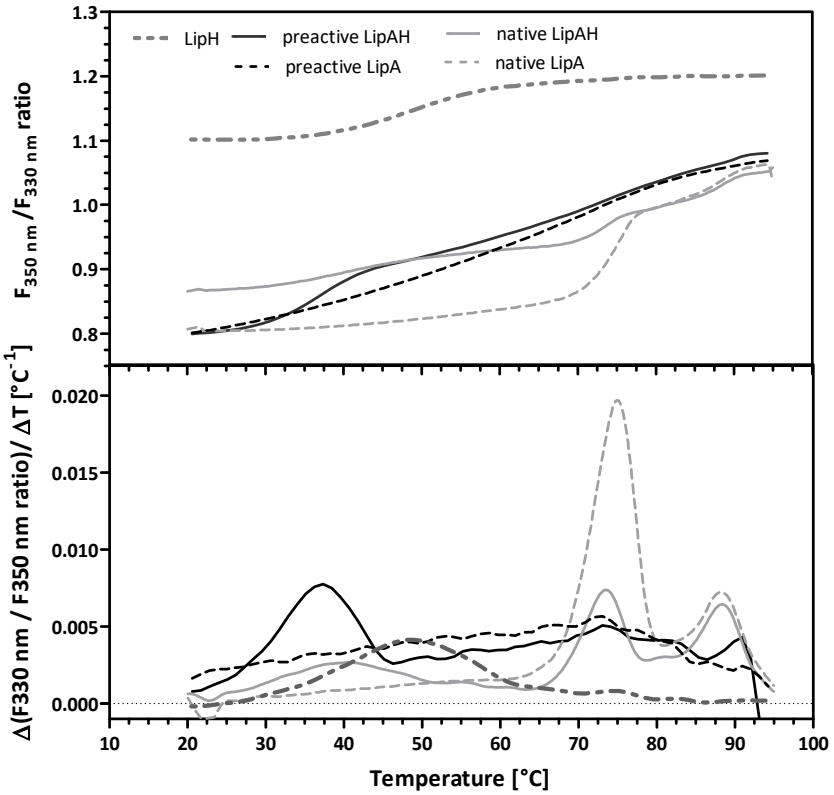

Figure 3.17: Melting of preactive and native LipA in complex with LipH measured by DSF.
Renatured preactive LipA and purified native LipA (2 µM) were incubated with and without an equimolar amount of LipH at 4 °C overnight in TG buffer for complex formation. Fluorescence signal ratios (350 nm/330 nm) versus temperature are shown in the upper graph, and their first derivatives are shown in the lower graph.

To compare the influence of LipH on preactive and native LipA, samples of free preactive and native LipA, which were treated equally as complex samples, were measured together with complex samples. The melting of free preactive and native LipA is comparable to the melting shown previously in Figure 3.16. Free native LipA showed slightly different fluorescence ratio values at high temperatures and a slight increase at low temperatures before the characteristic double transition occurred. The high fluorescence ratio of LipH can influence the initial fluorescence values of complex samples, as observed in the case of the native LipAH sample, whose initial fluorescence is redshifted (higher ratio of fluorescence 350 nm and 330 nm) compared to that of free native LipA.

Because the preactive LipAH and preactive LipA samples show similar initial fluorescence ratio values, it might be possible that incubation overnight with foldase influences the folding of native LipA. Complex formation can also change the fluorescence ratio of LipH, burying its solvent-accessible amino acids inside the complex interface. Differences in the complex

conformations of preactive and native LipA or incomplete complex formation can therefore also change the beginning fluorescence ratio.

The spectra of both LipA states are influenced by LipH. Native LipA in complex shows a slight transition at 40 °C and a reduced intensity of the characteristic double transition. The unfolding of preactive LipA in complex seems to be slightly delayed compared to that of free preactive LipA but occurs in a strong transition at 36 °C, followed by the same fluorescence ratio progression as preactive LipA alone without the characteristic double transition observed for the native LipA.

The transitions of both complexes occur in the range of the folding transition of LipH; thus, the transitions of LipH might influence the conformations of preactive and native LipA. It is also possible that the redshifts were caused solely by the transitions of LipH without any influence of the structure of preactive and native LipA. However, from the curve progression, preactive and native LipA in complex with LipH differ in their behavior, indicating that LipH is not able to convert the preactive into the native state.

3.7.2. Conformational changes in LipH lead to inactivation of LipA

To further investigate the thermally induced conformational changes in preactive and native LipA in complex observed by DSF, their thermal stability was further measured by their lipolytic activity. First, the thermal inactivation of native LipA seems to be independent of its structural stability. Whereas DSF showed high stability up to 60 °C, thermal inactivation started at 43 °C (Figure 3.18), which means that the loss of activity of LipA results from small structural changes that occur before the overall structure unfolds. The same phenomenon was already observed for the *B. glumae* lipase (LipA_BG) by Invernizzi *et al.* (2009).[217] They tested the influence of pH and organic solvents on the thermal stability of LipA_BG by ESI-MS in comparison to its activity and were able to demonstrate that inactivation occurs independently of large structural changes in the globular structure. It might be possible that the loss of the calcium ion causes the inactivation of LipA, but because of the high aggregation behavior of LipA in the presence of calcium, it was not possible to measure a delayed inactivation caused by calcium chloride (Appendix 8.7). By ESI-MS, Invernizzi *et al.* were able to demonstrate that the inactivated but still folded state still binds a calcium ion in their experiments.

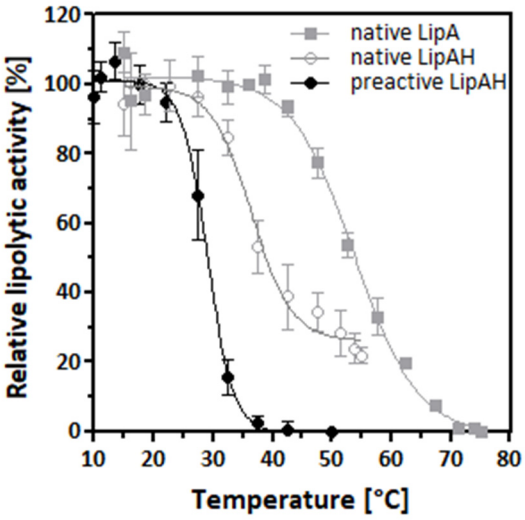

Figure 3.18: Thermally induced inactivation of free native LipA and LipAH complexes.
The complex was formed by the incubation of 100 nM native LipA or preactive LipA with 250 nM LipH overnight at 4 °C. Free native LipA was used at a concentration of 2 nM. The samples were divided and incubated at different temperatures for 1 h. Afterwards, the remaining lipolytic activities were determined. Melting temperatures were calculated by Boltzmann sigmoidal fit.

As already shown by DSF experiments, the stability of preactive and native LipA is influenced by LipH. The preactive LipAH complex starts to lose its activity at approximately 25 °C with a T_{M-50} of 29 °C and T_{M-100} of 37 °C. As in the DSF results, the native LipAH complex is slightly more stable, and inactivation starts at approximately 30 °C with a T_{M-50} of approximately 37 °C. Interestingly, complete inactivation of native LipA in complex with LipH was not possible. The inactivation of native LipA in complex overlapped with the melting behavior of free native LipA starting at 43 °C. This behavior might be caused by incomplete complex formation or by the release of native LipA from the complex before it starts to unfold. The inactivation of preactive LipA was partially reversible if samples were incubated at low temperatures between thermal treatment and activity measurement. An example of the resulting curve progression is shown in Appendix 8.10. This restoration of activity followed a similar time dependency to that of the complex formation shown in chapter 3.4. The level of regained activity was dependent on the concentration of complex used and decreased with increasing complex concentration (data not shown). If preactive LipA was used in excess, it was possible to regain full activity, leading to the conclusion that denatured LipA was released from the complex and replaced by preactive LipA refolded into a complex-competent state after thermal treatment. Even at high equimolar concentrations of LipA and LipH, as in Appendix 8.10. (2 µM), a partial restoration of activity was observed. Accordingly, there might be two processes leading to loss of activity. Thermal energy loosened the interactions between LipA and LipH causing LipA to be released from the complex as a stable globular structure, which leads in the case of preactive LipA to a loss and later restoration of activity and in the case of native LipA to a delayed melting curve.

However, the complex release can cause misbalanced interactions of LipA and LipH, leading to unfolding of the globular structure of LipA and permanent loss of activity in both states.

3.7.3. Binding of divalent cations increases the stability of the LipAH complex

The measurements in chapter 3.7.2 were performed in the absence of Ca^{2+}. Native LipA has a calcium ion bound in its metal binding center, which could cause a major difference in stability. Therefore, the stability of the preactive LipAH complex in the presence of calcium chloride was tested through its remaining activity after thermal treatment, as described in previous chapters. Ca^{2+} was observed to have a stabilizing effect on the complex with a maximal T_{M-50} shift of 6.4 °C. In the absence of calcium chloride, the LipAH complex starts to melt at approximately 25 °C with a sharp melting curve and a turning point at 29.0 °C. In the presence of 250 µM calcium chloride, the melting starts at approximately 29 °C and has a T_{M-50} of 35.4 °C. (Figure 3.19 A). This T_{M-50} shift was found to depend on the calcium concentration: incubation with different amounts of calcium chloride influences the resulting shift. The correlation of the calcium concentration and the T_{M-50} are shown in Figure 3.19 B. The observed T_{M-50} shifts were further validated by DSF measurements, and the calculated values are summarized in Figure 3.19 D. The half effective concentration was determined to be 21 µM (14 µM from DSF measurements), which is lower than the EC_{50} of 51 µM determined for the incorporation of calcium into the metal binding pocket (see chapter 3.5.2). This difference could be explained by temperature effects causing faster diffusion, a more open metal binding pocket or a slower unfolding process than in the binding of calcium. The melting behavior of the preactive LipAH complex was additionally measured in the presence of Mg^{2+}, Mn^{2+}, Zn^{2+} and Na^{+} cations. Zn^{2+} was chosen because it showed no activity increase and therefore possibly no binding, and Na^{+} was chosen as a control to exclude a general effect of the ionic strength or counterions. In the presence of Na^{+}, no T_{M-50} shift was observed by activity measurement (DSF fitting resulted in a T_{M-50} shift of 0.2 °C). The presence of Mg^{2+} and Mn^{2+} yielded lower shifts of 2.3 °C and 5.2 °C than the presence of Ca^{2+}, with a slight difference (-0.6 °C and -0.9 °C, respectively) between the activity and DSF measurement. The half effective concentrations were all similarly reduced compared to the EC_{50} constants of metal binding affinity. Concentrations of Mn^{2+} above 125 µM decreased the stability of LipA in complex, influencing the fitting of B_{max} and thus reducing the calculated EC_{50} value. Zn^{2+} caused a concentration-dependent destabilization of the complex, which was observed by the loss of

activity at low temperatures and the loss of fluorescence signal in DSF measurements (shown in Figure 3.20 B); thus, thermal shifts were not evaluable.

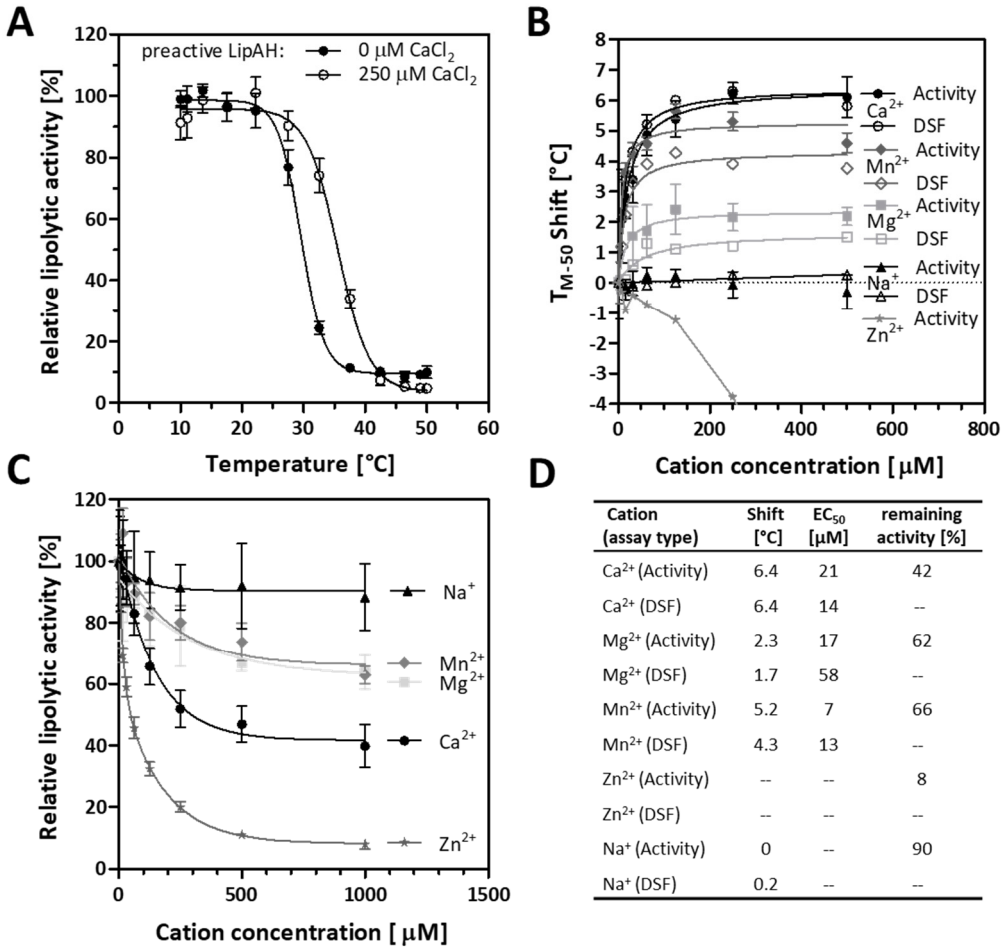

Cation (assay type)	Shift [°C]	EC_{50} [µM]	remaining activity [%]
Ca^{2+} (Activity)	6.4	21	42
Ca^{2+} (DSF)	6.4	14	--
Mg^{2+} (Activity)	2.3	17	62
Mg^{2+} (DSF)	1.7	58	--
Mn^{2+} (Activity)	5.2	7	66
Mn^{2+} (DSF)	4.3	13	--
Zn^{2+} (Activity)	--	--	8
Zn^{2+} (DSF)	--	--	--
Na^{+} (Activity)	0	--	90
Na^{+} (DSF)	0.2	--	--

Figure 3.19: Influence of cations on the thermal stability of the preactive LipAH complex.
A) Shift in the melting curve caused by 250 µM $CaCl_2$: 1 µM LipAH complex was diluted to 50 nM in TG buffer containing defined amounts of cations as chloride salts and incubated at different temperatures for 1 h in non-low binding PCR plates. Activity was measured immediately afterwards. Data are normalized to the plateau phase at low temperatures. Curves are fitted with Boltzmann sigmoidal fit. B) (Activity) Influence of divalent cations on T_{M-50} shift measured by lipolytic activity as shown in A. T_{M-50} values are plotted against the concentration. (DSF) Melting transitions derived by DSF measurement with 1 µM LipAH samples in the presence of divalent cations. Curves were fitted with the "one site binding (hyperbola)" fit. C) Percentage activity decrease caused by cations derived from the stable plateau phase at low temperatures. D) Summary of results shown in B and C derived from data fitting.

Mn^{2+} showed the same effect as Zn^{2+} but with a lesser intensity. This effect might be caused by the high tendency to bind to amines and allosteric destabilizing effects (see chapter 3.5.5). Interestingly, the DSF melting curves showed an additional transition of preactive LipAH in the presence of 250 - 500 µM $CaCl_2$ at 79 °C and 90 °C (shown in Figure 3.20 A), which look similar to the double transition of native LipA (shown in Figure 3.17). Therefore, it might be possible that the binding of a calcium ion leads to a structural rearrangement of the foldase-induced transition of preactive to native LipA. However, because of the destabilizing effect of LipH and

the high sensitivity of LipA to divalent cations, it is not possible to isolate and characterize this conformational state of preactive LipA. However, the DSF melting behavior of the preactive LipAH sample at low temperatures differs significantly from the melting of the native LipAH complex, and therefore structural differences between those two states exist even in the presence of calcium.

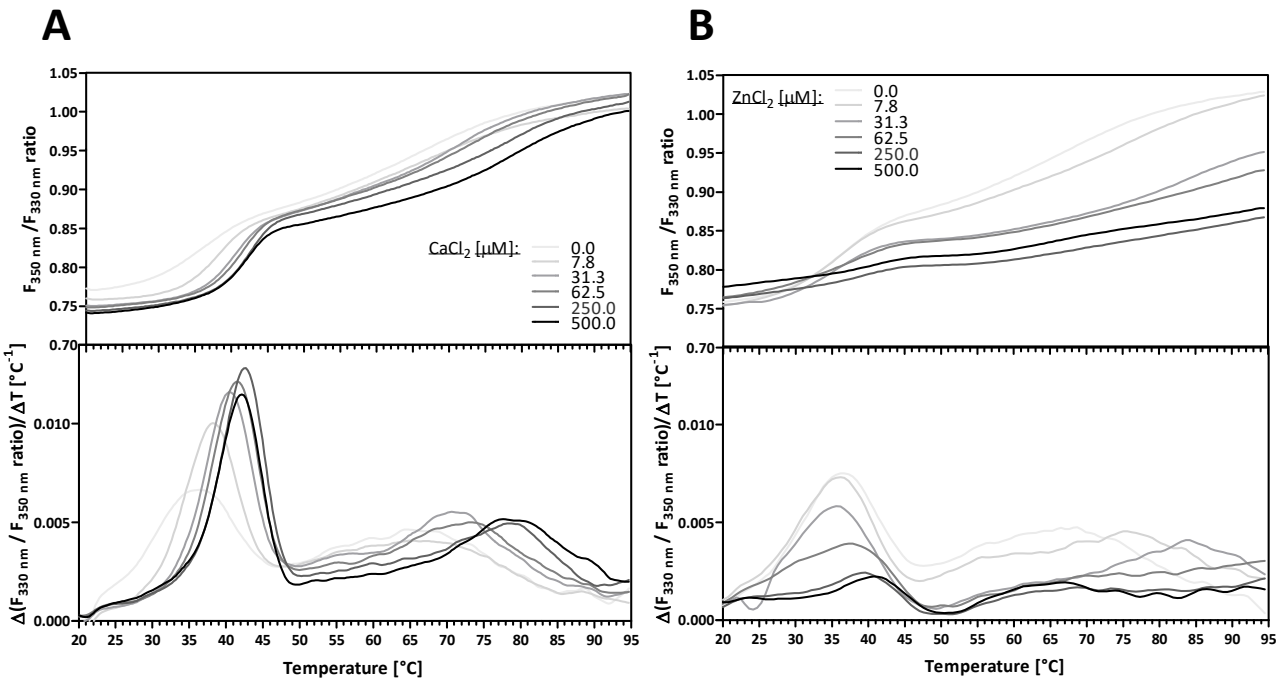

Figure 3.20: DSF melting curves of preactive LipAH in the presence of $CaCl_2$ and $ZnCl_2$.
Then, 2 µM renatured preactive LipA was incubated with an equimolar amount of LipH at 4 °C overnight in TG buffer for complex formation. For DSF measurements, calcium chloride and zinc chloride were added in concentrations between 0 and 500 µM. Fluorescence ratios (350 nm/330 nm) versus temperature and the first derivatives of the ratios were derived by DSF.

Additionally, native LipA in complex with LipH showed a higher melting temperature in the presence of calcium (Figure 3.28, page 99). The melting temperature of native LipA in complex in the presence of 100 µM $CaCl_2$ shifted from 36.5 °C to 40.5 °C. Although this shift of + 4 °C was lower than that of preactive LipA in complex in the presence of 100 µM $CaCl_2$ (+ 6 °C), native LipA in complex was more stable than preactive LipA in complex. This thermal shift is rather unexpected because native LipA already has a calcium ion bound in its metal binding center. However, as shown in chapter 3.5.4, LipH is able to open this metal binding center, and the presence of calcium can delay the loss of the bound ion and therefore the destabilization.

The different effects observed with various divalent cations show that there might be additional allosteric effects influencing the complex formation and stabilization in the

presence of divalent cations. Another indication of allosteric effects is shown in Figure 3.19 C. In addition to the delayed inactivation of preactive LipA in complex and thus the stabilization of activated LipA bound by LipH, the presence of divalent cations caused a concentration-dependent decrease in the overall activity of the melting curves. This activity decrease was derived from average activity values of the plateau phase at temperatures between 10 °C and 20 °C against the cation concentration used. This effect was omitted in Figure 3.19 A by the normalization of the lipolytic activity of the plateau phase at low temperatures to 100 %, and the values in Figure 3.19 C can be taken as a normalization factor. The presence of 1 mM $CaCl_2$ decreased the activity to 42 %. The presence of 1 mM $MgCl_2$ or $MnCl_2$ decreased the activity to 62 % or 66 %, respectively. NaCl resulted in a slight decrease to 90 %. $ZnCl_2$ reduced the activity to 8 %. Therefore, LipH protects LipA from aggregation in the presence of cations, (except for Zn^{2+}), which are stabilizing the complex, leading to a delayed melting behavior, but they also cause a decrease in activity at temperatures in which the complex should be stable. To explain this effect, it must be considered that for these experiments, the LipAH complex was formed at concentrations of 1 µM and diluted to 50 nM for heat treatment to allow transfer of the samples after heat treatment from the PCR plate to the MTP in an appropriate volume for activity measurement. Because the Ca^{2+} concentration-dependent decrease of activity was not observed, without prior dilution of the complex sample before thermal treatment (shown in Appendix 8.10), this activity decrease must be caused by an equilibrium shift during dilution and partial release of LipA from the complex during incubation time. This analysis showed that the complex formation is a reversible reaction, contradicting the general opinion that the complex cannot dissociate *in vitro,*[45,74,81,85,88,92,93] and is therefore investigated more closely in chapter 3.8. How calcium influences the reversibility of complex formation is further investigated in chapter 3.8.3.

3.8. Dynamics of complex formation

Complex formation of LipA and LipH from *P. aeruginosa,* as in other bacteria, is thought to be irreversible *in vitro*.[45,74,81,85,88,92,93] The assumption that foldase and lipase form a 1:1 complex and do not dissociate after the activation of LipA is mostly based on the following observations: a) no free active lipase was observed and b) an excess of lipase does not yield an increase in activity by multiple turnover catalysis cycles of foldase.

To determine the affinity of LipA and LipH, as described in chapter 3.4, complex formation must be a dynamic equilibrium. If the reaction of complex formation would be a one-way reaction, it should always reach saturation when the time constant is long enough. Furthermore, data shown by Ogino *et al.* (2008)[182] and Heil (2012)[203] for the affinity determination by SPR and biolayer interferometry, respectively, also showed a dissociation phase after removing the free interaction partner from the system. The FRET measurements with LipAH from *P. aeruginosa*, performed in collaboration with Dr. Jakub Kubiak (chapter 3.1.5), were possible only with an excess of LipA because the complex, which was formed at high concentrations, dissociated almost instantly after dilution to concentrations needed for single-molecule FRET measurements (5-10 nM) (personal communication Dr. Jakub Kubiak).

Based on these observations and on the results of experiments in this study indicating the release of LipA from the complex, the dynamics of complex formation were investigated more closely.

3.8.1. Dissociation of the LipAH complex after dilution

To test if LipA is released from the LipAH complex, the stability of the complex was tested by its activity after dilution. Dilution of the complex to a concentration close to or below the affinity constant of LipA and LipH (see chapter 3.4) should shift the equilibrium, increasing the amount of free LipA and LipH and therefore reducing the measurable activity, if the LipAH complex dissociates and LipA is released in an inactive conformation. To determine the amount of free LipA and complexed LipA without depending solely on comparison of lipolytic activity values at different complex concentrations, the half effective concentration (EC_{50}) values for complex formation were used to compare the amount of complexed LipA. As described in chapter 3.4, the amount of ligand that is needed to saturate the binding to its interaction partner is dependent on their affinity. The molar ratio of the needed ligand

compared to the interaction partner increases with decreasing concentration of the interaction partner.

Therefore, dilution series were prepared as described for the affinity determination in chapter 3.4. Specific amounts of LipH were titrated with a dilution series of LipA and incubated overnight at 4 °C to achieve equilibrium complex formation. Afterwards, the effect of dilution on the lipolytic activity was measured to determine if the equilibrium of complex formation was shifted.

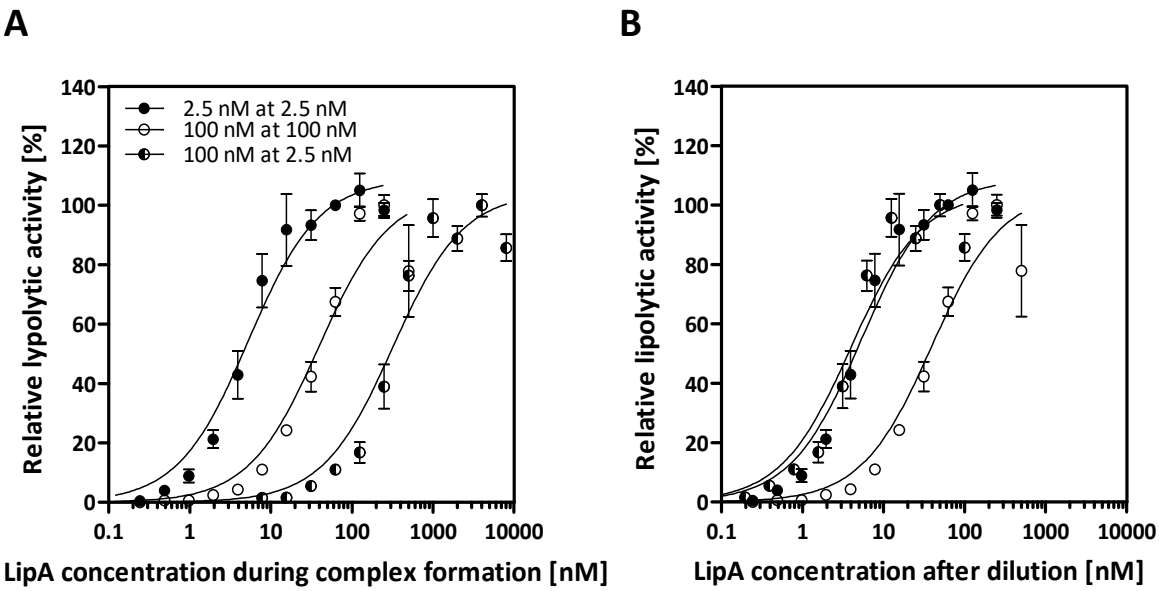

Figure 3.21: Dissociation of LipAH complex after dilution, measured by activity.
Dilution series of LipH (as interaction partner) with different concentrations of LipA (as ligand) were prepared in 250 µM $CaCl_2$ containing TG buffer and incubated overnight to reach equilibrium complex formation. A) The dilution series with a 2.5 nM interaction partner was measured undiluted (2.5 nM at 2.5 nM). The dilution series with 100 nM interaction partner was diluted to 2.5 nM (100 nM at 2.5 nM) and incubated for 3 h at room temperature before activity measurement. To measure the high activity of the undiluted 100 nM dilution series (100 nM at 100 nM, gum arabic and sodium deoxycholate was added to the substrate as described in Hausmann *et al*. (2007).[218] B) Activities of figure A were corrected by the dilution factor for ligand concentration.

Figure 3.21 A shows the activity results of titration curves with 2.5 nM and 100 nM concentrations of LipH. The titration curve with 2.5 nM LipH reaches its half activation point at approximately 6 nM LipA, similar to the affinity determination in chapter 3.4. The titration curve of 100 nM LipH yields a half activation point at approximately 50 nM. The curve with 100 nM LipH diluted to 2.5 nM shows a half activation point at approximately 320 nM. If the curve of the diluted sample is corrected by the dilution factor of 40 (2.5/100 nM), the titration curves of 2.5 nM and the diluted 100 nM curve overlap (Figure 3.21 B). This result shows that the equilibrium of complex formation shifts upon dilution and that complex formation is

dynamic with a steady exchange of LipA. Furthermore, LipA is released in an inactive conformation.

3.8.2. Exchange of preactive LipA in complex

To further study the dynamic equilibrium of complex formation, the possibility of an exchange of LipA molecules in the LipAH complex was investigated. An inactive LipA mutant in which the active Ser82 is mutated to alanine was used to investigate the possibility of replacing $LipA_{WT.}$

The purified $LipA_{S82A}$ mutant was renatured and used for complex formation with LipH at a concentration of 1 µM. At this concentration, the amounts of free $LipA_{S82A}$ and LipH should be negligible. After incubation overnight, the complex was diluted to 1 nM, and renatured $LipA_{WT}$ was added in excess at a concentration of 100 nM, followed by 3 h incubation and activity measurement. Samples of LipH and diluted $LipA_{S82A}H$ without the addition of LipA were used as controls. Figure 3.22 A shows the resulting activities. It was possible to regain approximately 90 % of the activity by replacing the $LipA_{S82A}$ in the complex with LipH with renatured $LipA_{WT}$.

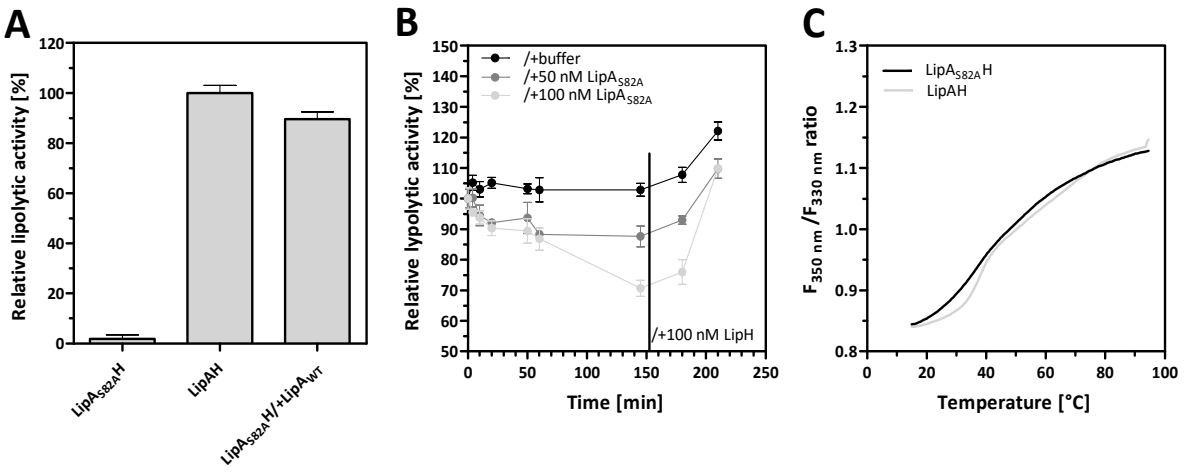

Figure 3.22: Exchange of preactive LipA in complex.
A) A sample of the $LipA_{S82A}H$ complex was diluted from 1 µM to 1 nM. Then, 100 nM $LipA_{WT}$ was added to replace the inactive $LipA_{S82A}$. Activity was measured after incubation for 3 h at RT. B) Then, 50 nM $LipA_{WT}H$ WT complex was supplemented with 50 and 100 nM $LipA_{S82A}$ to replace active $LipA_{WT}$ in the complex. The activity was monitored over time, and after 150 min, 100 nM LipH was added to restore the activity of the replaced $LipA_{WT}$ (marked by vertical line). C) DSF melting curves of 1 µM $LipA_{S82A}H$ and $LipA_{WT}H$ complex.

Because it cannot be ensured that the complex between $LipA_{S82A}$ and LipH forms similarly to the $LipA_{WT}H$ complex, the replacement of $LipA_{WT}$ by $LipA_{S82A}$ was tested. Therefore, 50 nM

$LipA_{WT}H$ complex was supplemented with 50 nM or 100 nM $LipA_{S82A}$ and with buffer as a control, and the activity decrease was monitored over time (Figure 3.22 B). After 145 min, the activity level decreased by approximately 10 % and 30 % in the presence of 50 nM and 100 nM $LipA_{S82A,}$ respectively. This result shows that $LipA_{S82A}$ is able to replace $LipA_{WT}$ in complex with LipH. To exclude the possibility that the decrease in activity is caused by the instability of LipA in the presence of an excess of other LipA molecules and to show that the activity of replaced $LipA_{WT}$ can be restored, 100 nM LipH was added after 150 min (marked by a vertical line). It was possible to observe an increase in activity, indicating that replaced $LipA_{WT}$ is still able to be activated by LipH.

The expected activity decrease due to the addition of $LipA_{S82A}$ in the first step of this experiment was lower, as expected. From the calculated ratios of $LipA_{WT}$ and $LipA_{S82A}$, the remaining activity should have been 50 % and 33 % for the samples with 50 nM and 100 nM $LipA_{S82A}$, respectively.

This behavior can be caused by an unfinished exchange process after 145 min and by the fact that complex formation was not complete at the starting concentration of 50 nM, as observed in the control sample, which also showed an increase in activity upon the addition of LipH addition in the second step, indicating the presence of free LipA and LipH, which was also able to bind $LipA_{S82A}$.

Furthermore, DSF showed that the $LipA_{S82A}H$ complex is not as stable as the $LipA_{WT}H$ complex (Figure 3.22 C). The melting of the $LipA_{S82A}H$ complex started at lower temperatures than that of the $LipA_{WT}H$ complex, indicating a lower affinity and binding strength of $LipA_{S82A}$ compared to those of $LipA_{WT}$.

With these experiments, it was possible to demonstrate that complex formation is a dynamic equilibrium that underlies a steady exchange and that LipA is released in an inactive conformation and not as an active native state.

3.8.3. Calcium changes the conformation of LipH

Calcium and other divalent cations showed several effects on complex formation, stability and lipolytic activity. In chapter 3.7.3, a stabilizing effect of Ca^{2+} on the complex and an activity decrease in the presence of Ca^{2+} were observed in the stable temperature range. It was possible to demonstrate that this effect was caused by prior dilution of the complex, which disequilibrates the complex formation and leads to the release of LipA. Because of the multiple effects caused by calcium, it is difficult to determine the specific effect on complex formation

without observing artifacts of LipA destabilization. Therefore, the conformational effect of calcium on LipH was measured using the FRET mutants from chapter 3.1.5. Neha Verma (Institute for Pharmaceutical and Medicinal Chemistry, Heinrich Heine University Düsseldorf) and Dr. Jakub Kubiak (Institute for Molecular Physical Chemistry at the Heinrich Heine University Düsseldorf) observed by MD simulation and FRET that LipH undergoes conformational changes during the binding of LipA. In the free form, it exists in a more compact conformation with fast conformational changes that enable the binding of LipA.[169] The titration of LipH with LipA in two different buffer systems showed that calcium has an effect on the average conformation of free LipH that may influence the rates of complex formation and dissociation.

A

buffer	10 % glycerol 0 µM $CaCl_2$		0 % glycerol 250 µM $CaCl_2$	
label positions	complex [Å]	free [Å]	complex [Å]	free [Å]
P12	61	63	60	66
P13	53	46	54	63
P14	76	72	74	71
P23	65	59	66	69
P24	70	60	67	67
P34	54	51	55	54

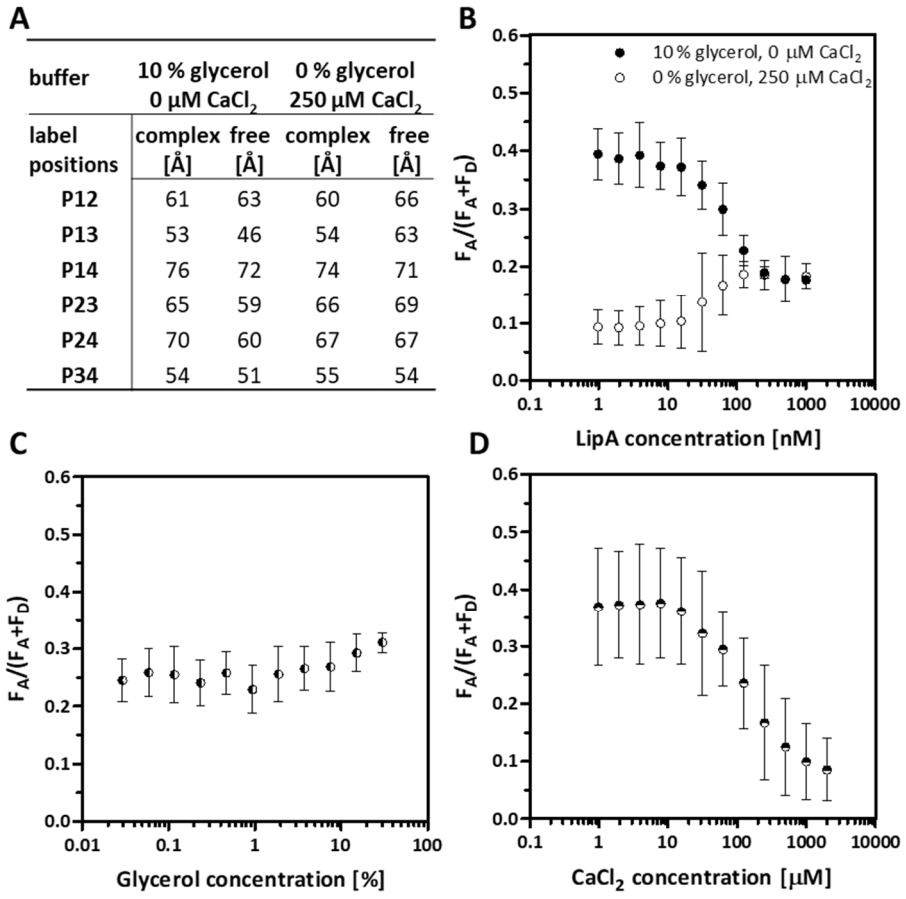

Figure 3.23: Influence of buffer on the conformation of LipH.
A) Dye distances derived from average FRET efficiency measurements of labeled LipH variants in free and complexed forms in two different buffer systems. B) Underlying FRET efficiencies from a LipH titration curve for the LipH P13 (Q137C-E268C) variant in two different buffer systems. C) Influence of glycerol on the FRET efficiency of the LipH P13 variant. D) Influence of $CaCl_2$ on the FRET efficiency of the LipH P13 variant.

Figure 3.23 A shows the average dye distances of free and complexed LipH, derived by batch FRET efficiency measurements as described in chapter 2.6.6. For complex titration,

10 % (v/v) glycerol and 250 µM $CaCl_2$ containing 10 mM TG buffers were used. The FRET efficiencies were measured after incubation overnight at 4 °C and for 1 h at room temperature to measure fluorescence at constant ambient temperature. The distances measured for the saturated complex show similar values in both buffer systems, which are comparable with the distances measured by single-molecule FRET (chapter 3.1.5).

The average distances for free LipH show conformational changes in the two buffer systems. The P12 and P34 distances, describing the conformation of MD1+α-helix 4,5 and α9+MD2, respectively, remain almost constant, whereas the distances of variants P13, P23 and P24, describing the positions of MD1 and MD2, show a more open average conformation in the presence of $CaCl_2$ in comparison to glycerol-containing buffer. To exclude the possibility that glycerol causes a conformational change, the effect of glycerol concentration and $CaCl_2$ was tested by titration of the LipH P13 variant. The resulting FRET efficiencies are shown in Figure 3.23 C and D in comparison to the measured FRET efficiencies of the LipAH titration curves shown in Figure 3.23 B. Glycerol had only a minor effect on the FRET efficiencies, but calcium caused a strong concentration-dependent decrease in the FRET efficiencies and therefore, on average, a larger distance between P1 and P3, which can be interpreted as an opening of LipH. This opening can influence the complex formation and release rate so that the calcium-dependent activity decrease measured in chapter 3.7.3 can be caused by higher release rates during the thermal incubation.

3.9. Characterization of LipH$_{Y99A}$ mutant

A bachelor thesis[219] conducted in the framework of this thesis used an alanine screen investigated the importance of single amino acids of LipH at the complex interface for the secretion of LipA. Single alanine mutations at the complex interface almost always showed inhibitory effects on the secretion of LipA in *P. aeruginosa* as measured by the lipolytic activity of supernatants. Most of them yielded activities that were not distinguishable to those of from cultures incapable of secreting LipA (containing an empty vector). Because these results were rather unexpected and it was not possible to distinguish whether the missing lipase activity was caused by impaired secretion or impaired LipA activation, the foldase activity of LipH alanine variants was tested *in vitro*. Therefore, several of these mutations were introduced into the *lipH* gene on pEHTHis19, and the resulting variants were tested for their ability to activate renatured LipA *in vitro* by the addition of cell lysates of LipH variants producing *E. coli* cultures to approximate a high excess of refolded LipA in TG buffer. Complex formation was performed overnight at 4 °C, and the ability of LipH variants to activate LipA was determined by the resulting lipolytic activity. Only LipH$_{Y99A}$ showed no activity, and the remaining mutants showed similar or slightly decreased activity levels, which could be caused by differences in expression level (data not shown). For further characterization of LipH$_{Y99A}$, it was purified and compared with LipH$_{WT}$.

3.9.1. LipH$_{Y99A}$ still binds LipA

To confirm the inability of LipH$_{Y99A}$ to activate renatured LipA, a purified LipH$_{Y99A}$ variant was used for the refolding of LipA (shown in Figure 3.24 A). Under conditions where LipH WT is able to refold LipA, no activity was detectable for the LipH$_{Y99A}$ mutant. Shibata *et al.* (1998)[87] already reported that the Y99C and Y99H mutants are unable to activate LipA, but for these mutants, they did not observe complex formation. To test if LipH$_{Y99A}$ is still able to form a complex with renatured LipA, LipA was copurified through the affinity tag of LipH (Figure 3.24 B). After complex formation overnight at concentrations of 4 µM, the samples were applied to a Ni-NTA column. After a wash step with TG buffer, the complex was eluted from the column and analyzed by SDS-PAGE. A sample without LipH served as a control for nonspecific binding of LipA to the Ni-NTA resin (lane 1). The amount of LipA copurified with LipH$_{Y99A}$ (lane 3) was much higher than that purified from the control sample without LipH.

These results show that $LipH_{Y99A}$ is able to form a complex with LipA but with a slightly weaker interaction strength than that of $LipH_{WT}$ (lane 2).

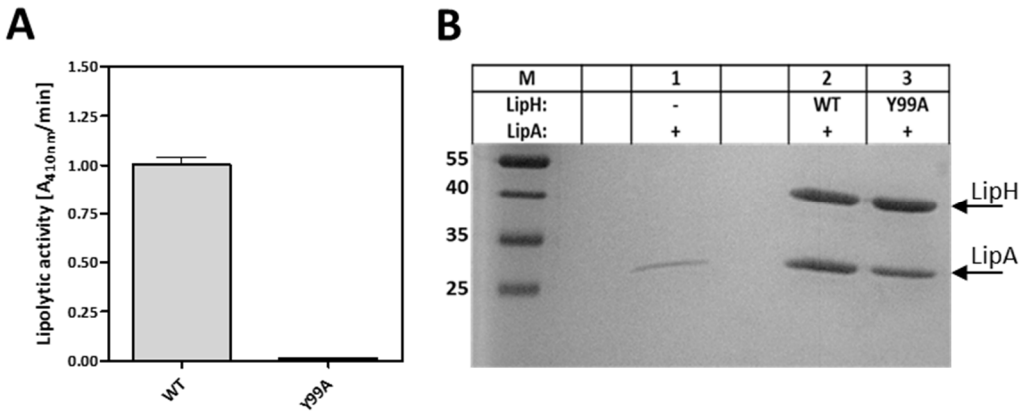

Figure 3.24: Activation and copurification of LipA by $LipH_{WT}$ and $LipH_{Y99A}$.
A) Lipolytic activity of LipA in complex with LipH WT and LipH Y99A mutant after complex formation overnight at 4 °C at 1 µM. Activity was measured with 10 nM. B) 16 % SDS-PAGE: Complex formation was tested by copurification of LipA through the His_{10}-tagging of $LipH_{WT}$ and $LipH_{Y99A}$ mutant after complex formation overnight at 4 °C and 4 µM.

3.9.2. Structure of $MD1_{Y99A}$

To investigate the reason for the inability of $LipH_{Y99A}$ to activate renatured LipA, the solution NMR structure of $MD1_{Y99A}$ was solved as described for $MD1_{WT}$ in chapter 2.6.7 by Dr. Aldino Viegas. Figure 3.25 A shows the 20 best structure predictions derived by NMR as rainbow ribbons (blue: N-terminal to red: C-terminal) aligned to the $MD1_{WT}$ homology model (gray cartoon). Among these 20 predicted structures, only slight variance was observed, as indicated by the low maximal RMSD variation of 0.56 Å. Similar to the solution NMR structures of $MD1_{WT}$, the predicted structures of $MD1_{Y99A}$ resembled the structure of the MD1 homology model with an average RMSD of 2.12 Å, with the flexible N-terminal strain (L66-D82) the main cause of the high RMSD values.

Comparison of the predicted structures of $MD1_{WT}$ (see Figure 3.4 B, page 50) and $MD1_{Y99A}$ shows that Y99 seems to be important to keep this flexible strand in place and to prevent it from binding to α-helices 1 and 2, as the average conformation of this flexible strand is bent towards the main core structure of $MD1_{Y99A}$. In the structure of MD1_BG, a conserved hydrogen bonding network was identified that seems to prevent this bending, as shown in Figure 3.25 B and C.

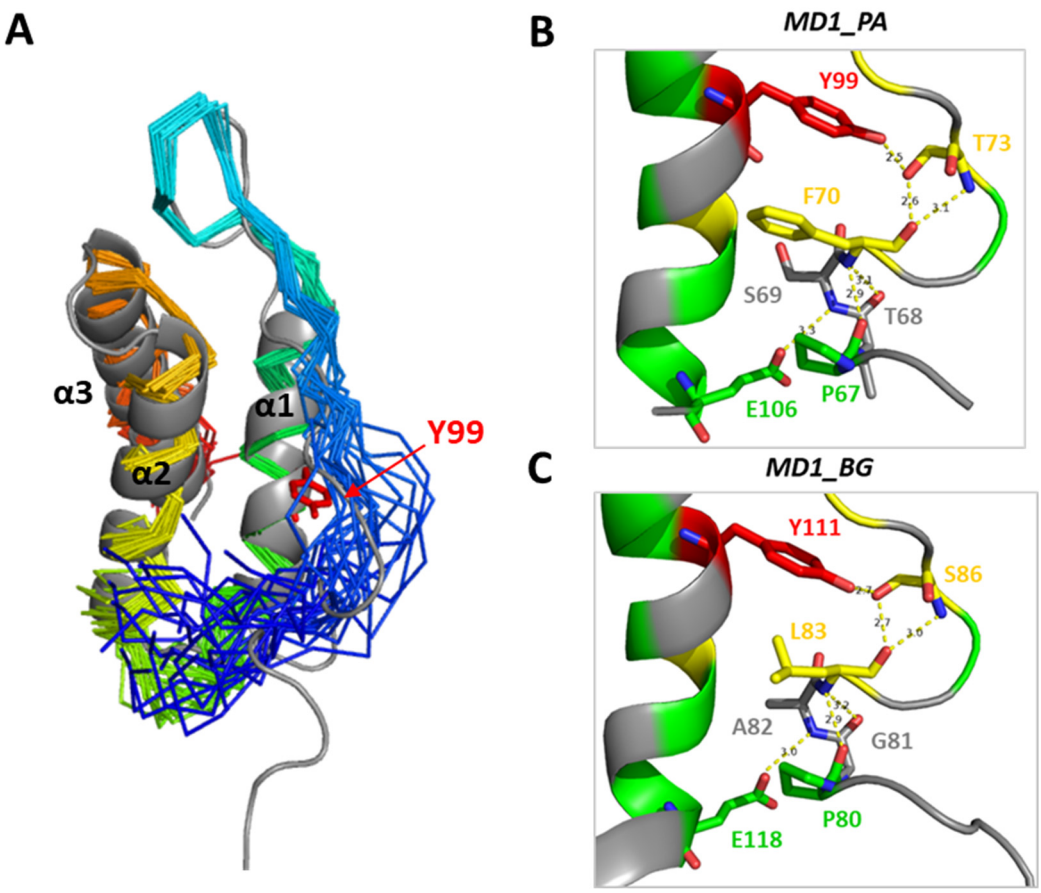

Figure 3.25: Predicted structure of MD1$_{Y99A}$ and its structural role.
A) Structural alignment of the 20 best structure predictions from NMR measurements as rainbow-colored ribbons (N': blue -> C': red) with homology model MD1 (gray cartoon). Y99 is shown as red sticks. Interactions of tyrosine in MD1 of (A) the *P. aeruginosa* homology model and (B) the *B. glumae* crystal structure (PDB:2ES4). Backbone is shown as a cartoon structure. Positions with conserved residues are shown in green and positions with similar residues in yellow. The tyrosine is shown in red. Amino acids involved in the hydrogen network are shown as sticks. Distances are shown in Å.

Y99 interacts with the hydroxyl group of T73 (S86 in MD1_BG). This interaction is further stabilized by the carboxyl group of F70 (L83 in MD1_BG). Amino acids P67 to S69 (P80 to A82 in MD1_BG) form a hydrogen bonding-stabilized loop whose position is further fixed by E106 (E118 in MD1_BG). This loop forms from 4 of the total 20 polar interactions of the LipB LipA_BG interface, found in the crystal structure of LipAB_BG complex.[81] These interactions are visualized in Figure 3.26 A. The backbone amides of A82, A84 and H87 of this flexible loop form hydrogen bonds to R313, N312 and Y4 in LipA_BG, respectively. In the LipAH complex, these interactions are also found between the backbone amides of the nonconserved amino acids S69, R71 and S74 of LipH and the conserved amino acids R279, N278 and Y3 in LipA_PA (Figure 3.26 B).

A

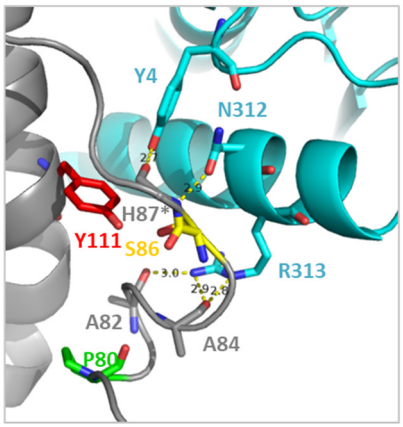

B

LipB	LipA_BG	LipH	LipA_PA
A82	R313	S69	R279
A84		R71	
H87	N312	S74	N278
	Y4		Y3

Figure 3.26: Influence of Y99 on interactions with LipA.
A) Interactions of MD1_BG with LipA_BG (shown in cyan). * means that the side chain of H87 is not shown for better visualization. B) Table of MD1_BG backbone residues involved in interaction with LipA in comparison to interactions found in the LipAH complex.

Therefore, Y99 seems not to be directly involved in the activation of LipA but is responsible for maintaining the structure and position of the flexible N-terminal strain of MD1. The introduction of an alanine mutation induces a conformational change in this flexible strand and a bending toward α-helices 1 and 2. This interaction circumvents the interaction of the stabilized loop with LipA, which is a major interaction of LipH with LipA, considering that only 20 hydrogen bonds are found between LipA_BG and LipB. These interactions take place at structural elements in the N- (Y3) and C-terminus (R279, C': L285) of LipA and are 21 - 25 Å away from the active site serine. However, the loop of the N-terminus forms the β-strand (starting with V9) neighboring the β-strand at whose end the active serine is located. This β-strand is also involved in the formation of the oxyanion hole by coordinating the position of M16. The beginning of the C-terminal helix (α9) is involved in the formation of the calcium binding pocket (see also chapter 3.5.1).[33]

3.9.3. Behavior of LipH$_{Y99A}$ in DSF

The behavior of the LipH$_{Y99A}$ and LipAH$_{Y99A}$ complexes was further investigated by DSF. LipH$_{Y99A}$ showed a slight blueshift in intrinsic fluorescence compared to LipH$_{WT}$ (Figure 3.27 A), which can be caused by deletion of the solvent-exposed tyrosine at position 99, increasing the ratio of buried to solvent-exposed fluorescent amino acids. The transition at approximately 49 °C observed for LipH$_{WT}$ is still present and is not influenced by the Y99A mutant, confirming the assumption that this transition is caused by the unfolding of MD2 rather than MD1 (see chapter 3.7.1).

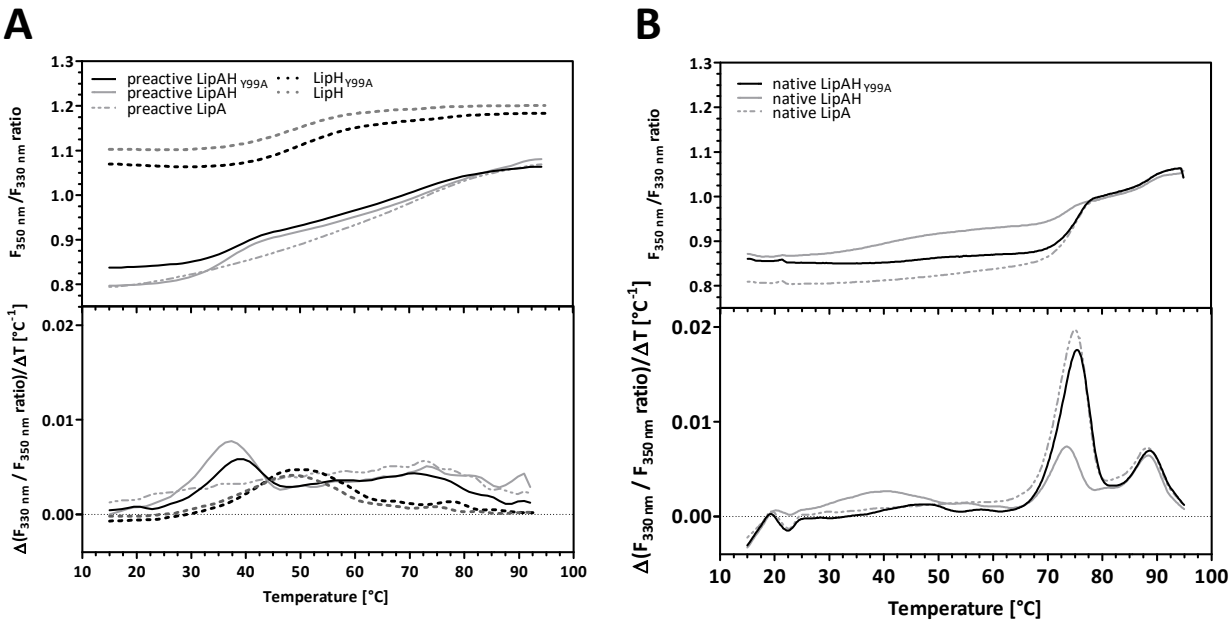

Figure 3.27: Influence of LipH$_{Y99A}$ on DSF melting of preactive and native LipA.
DSF melting curves of 2 µM LipH$_{Y99A}$ both free and complexed with an equimolar concentration of LipA: A) with renatured preactive LipA, B) with native LipA. DSF melting curves of LipH$_{WT}$ samples and free LipA from Figure 3.17 are shown for comparison. Fluorescence signal ratios (350 nm/330 nm) versus temperature and the first derivatives of the ratios were derived by DSF.

The LipAH$_{Y99A}$ complex with renatured LipA shows a similar melting transition at approximately 36 °C compared to the LipAH WT complex, confirming the ability of LipH$_{Y99A}$ to form a complex with LipA. The redshift in the initial fluorescence of the LipAH$_{Y99A}$ complex in comparison to that of the LipAH$_{WT}$ complex indicates that LipH$_{Y99A}$ most likely binds in a different mode, leaving several fluorescent amino acids at the interface exposed to the solvent. This redshift was already observed in chapter 3.9.2 for the native LipAH complex, and it was mentioned that LipH does not bind native LipA in the same way as preactive LipA. The mutation Y99A seems to weaken the binding of LipH$_{Y99A}$ to native LipA, as the melting curve of native LipAH$_{Y99A}$ was almost identical to that of native LipA alone. As mentioned in chapter 3.9.2, Y99A interrupts the interactions of MD1 with the C-terminal α-helix 9 of LipA, which covers one of the two tryptophans (W198) in LipA. It seems that these interactions were responsible for the partial unfolding of native LipA during complex decomposition under DSF measurement.

3.9.4. Influence of LipH$_{Y99A}$ on the calcium binding of LipA

The mutation Y99A in LipH affected the structure of MD1 and disrupted several interactions with LipA, but LipH$_{Y99A}$ still forms a complex with LipA. DSF revealed a different binding mode

with LipA compared to that with $LipH_{WT}$. Because it was postulated that this different binding mode can influence the metal binding center of LipA by eliminating interactions of MD1 with the C-terminal helix of LipA or direct interactions of the metal binding center with the beginning of EHD, the influence of calcium on the thermal stability of $LipAH_{Y99A}$ was measured. For the $LipAH_{WT}$ complex, calcium showed a measurable stabilizing effect (chapter 3.7.3). Because of the missing activity of the $LipAH_{Y99A}$ complex, the influence of calcium on the complex stability was measured by DSF.

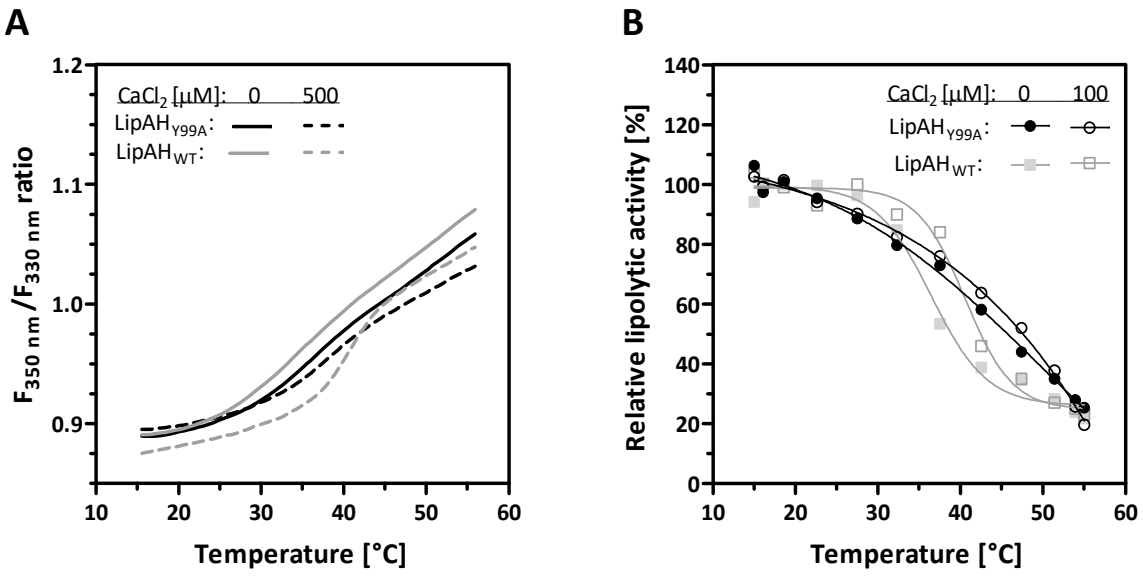

Figure 3.28: Influence of calcium on the thermal stability of the $LipAH_{Y99A}$ complex.
A) Thermal stability of the renatured LipAH complex (1 µM) in the absence and presence of 500 µM $CaCl_2$ measured by DSF. for comparison, the behavior of the $LipAH_{WT}$ and $LipAH_{Y99A}$ complex. B) Stability of the native LipAH complex in the absence and presence of 100 µM $CaCl_2$ measured by their remaining activity after thermal treatment. For comparison, native $LipAH_{WT}$ and $LipAH_{Y99A}$ complex. The complex was formed with 100 nM native LipA and 250 nM LipH (WT or Y99A). Samples were divided and incubated in a temperature gradient for 1 h. Afterwards, the remaining lipolytic activity was determined. A graph of 0 µM $CaCl_2$ was already shown in Figure 3.18.

Figure 3.28 A shows the DSF melting curves of renatured $LipAH_{Y99A}$ in comparison to renatured $LipAH_{WT}$ in the presence and absence of 500 µM $CaCl_2$. In contrast, the renatured $LipAH_{WT}$ complex shows a $T_{M\text{-}50\ \%}$ shift of 6.4 °C (chapter 3.7.3), and the $LipAH_{Y99A}$ complex shows no shifted transition. Because native LipA in complex with LipA also showed a shifted transition point, which was measured by the remaining activity after thermal treatment, the effect of calcium on the native LipAH complex was also tested (Figure 3.28 B).

No stabilizing effect of calcium was observed. These results confirm that the Y99A mutation in LipH influences the interactions with the metal binding center of LipA. It may be possible that $LipH_{Y99A}$ is not able to open the metal binding center of LipA, which is why LipA does not

incorporate a calcium ion and shows no increased thermal stability. This possibility would also explain the inability of $LipH_{Y99A}$ to activate renatured LipA, as LipA needs Ca^{2+} for activity. Another possible explanation could be that the calcium binding center of LipA is still open and can bind calcium, but the interactions of LipH, which lead to thermal stabilization, are disrupted. Interestingly, the inactivation of native LipA in complex with $LipH_{Y99A}$ in Figure 3.28 B started at lower temperatures than inactivation of the $LipAH_{WT}$ complex and showed no defined melting transition. DSF melting in Figure 3.27 B showed no influence of $LipH_{Y99A}$ on the globular structure of LipA, but it seems that $LipH_{Y99A}$ is still interacting and destabilizing the structure elements responsible for the active conformation of native LipA.

4. Conclusion

Over the past 30 years, several scientists and research groups have contributed to the understanding of the secretion process of lipases and the role of lipase-specific foldases during lipase activation. The results presented in this thesis further characterize the process of lipase-specific foldase-assisted folding and the activation of a lipase *in vitro* using LipA from *P. aeruginosa* as a model protein. Additionally, these results provide new insights into the specific role of lipase-specific foldases in the *in vivo* secretion of lipases.

4.1. Proposed role of foldase during folding of LipA *in vivo*

Because lipases are able to fold into a globular structure after chemical denaturation and because foldases are able to activate these globular states by forming stable complexes with them *in vitro*, it was assumed that preactive LipA is formed as a stable conformation before it is bound by LipH *in vivo,* implying that lipase activation is uncoupled from lipase folding.[74,85,220]

During this thesis, studies on the complex formation of LipA and LipH showed that renatured LipA can indeed be activated upon contact with LipH (chapter 3.4), although surprisingly renatured LipA and native LipA differ significantly (chapter 3.6). Whereas native LipA seems to fold into a stable globular structure, with many cooperative interactions that prevent thermal unfolding, the renatured LipA folds into a globular structure with a similar hydrodynamic radius[215] but with an unstable tertiary structure.

Binding to LipH changed the stability of both LipA states, but the properties of these species were still clearly distinguishable (chapter 3.7). Furthermore, complex formation was shown not to be a one-way reaction *in vitro,* as renatured LipA is most likely released in an inactive or at least a very unstable conformation. Thus, LipH is not able to convert the preactive state of LipA into the native state *in vitro,* as previously thought (chapter 3.8).

Together with the observation that the inactivation of native LipA and its structural stability seem to be independent of each other (chapter 3.7.2), the assumption that the renatured state is an intermediate on the route to the native state should be questioned. The preactive state formed by renatured LipA might be a trapped folding conformation that is artificially held in a catalytically active state by LipH. Basically, only five amino acids, the catalytic triad and the oxyanion hole, have to adopt proper conformations to enable catalytic activity in LipA.

The finding that the activity of the renatured LipAH complex was only 11 % of that of native LipA indicates different properties of these two states (chapter 3.4).

Yang *et al*. (2000)[204] mentioned that the *in vitro* refolding of proteins starting from a peptide strand in the form of a random coil proceeds by different mechanisms from the folding during the translation process, which starts from the N-terminus and proceeds in a rather slow process to the C-terminus. In the case of secreted proteins, the mechanism of folding is even more complicated, and the translated protein is actively transported across the membrane with the help of several other proteins.[49] Inside the periplasm, the secretory peptide chain, still bound by its signal sequence to the cytoplasmic membrane, starts to fold into its globular structure during transport over the inner membrane. The translocation does not occur in a continuous process, such as protein biosynthesis, but in a sequential transport of 20 to 30 amino acids at a time.[53,55,56] This process gives LipA the possibility to fold in much more defined ways compared to the *in vitro* renaturation process.

Interestingly, the literature only describes procedures for the *in vitro* activation of lipases by foldases, including chemical denaturation and renaturation steps.[38,83,88,165,221] Hobson *et al*. (1995)[93] were able to show that the foldase of *Burkholderia cepacia* is able to bind to its lipase, which was produced in the absence of its foldase, but activity was only gained if this lipase was chemically denatured and renatured. Apparently, foldases are able to bind to the stable globular states of uninitiated mature or native LipA but are not able to disrupt this highly cooperative fold to activate the uninitiated mature state of LipA. The DSF results also indicated different binding modes of LipH to native LipA and renatured LipA (chapter 3.7.1).

The foldase activity of LipH seems to be dependent on the structural flexibility of renatured LipA. Considering that this flexibility is caused by the artificial folding pathway due to denaturation and renaturation, it is highly likely that *in vivo*, foldases interact with lipases much earlier on their folding pathway during the translocation process before lipases reach a stable globular state.

Similar to the complex structure of α-lytic protease with its pro domain, the *B. glumae* LipAB complex structure shows a high water content at its interface. These ordered water molecules can serve as adapter molecules that allow the interface to interact with different conformational states. For the α-lytic protease, it was shown that the preactive state exhibits a higher surface complementarity and therefore higher affinity to the pro domain compared to the native state and the pro domain.[77,81,85,222]

Aboubi (2008)[86] was able to demonstrate that the mutation of S48P inside the variable domain of LipH and the truncation of the variable domain lead to the accumulation of pre-LipA (containing its signal sequence) during the expression of *lipA* in *P. aeruginosa* PABST7.1. Furthermore, he was able to demonstrate global inhibition of protein secretion in this strain, most likely due to blockage of the Sec-pathway. This result indicates that LipH interacts with LipA early during the secretion process and not only after it is folded into a stable globular structure with a cleaved signal sequence.

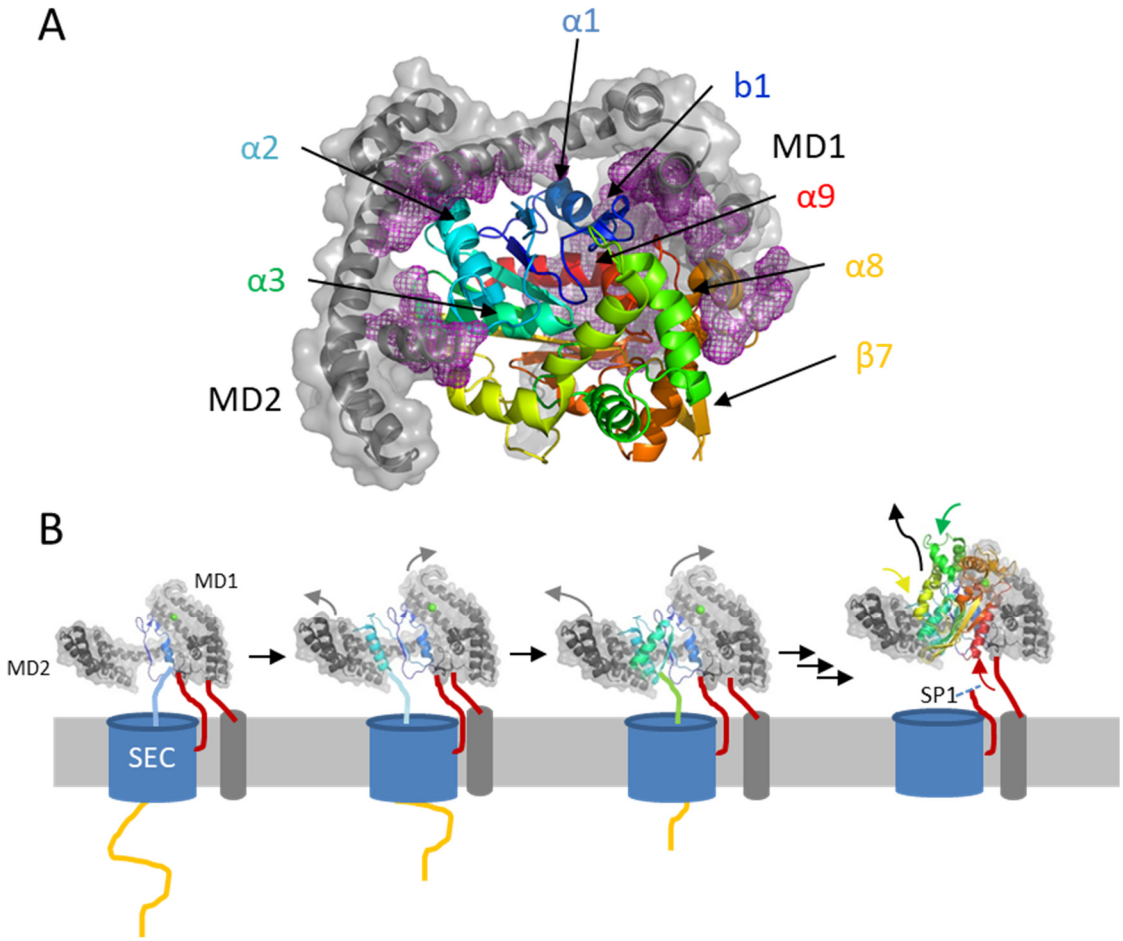

Figure 4.1: Hypothetical model of foldase-assisted LipA secretion.
A) Interaction interface of LipAB_BG. LipB is shown as gray surface/cartoon representation. LipA is rainbow-colored (N' to C': blue to red). Residues of LipB within 4 Å of LipA are shown as magenta mesh. Annotations of secondary structure elements are according to Nardini *et al*. (2000).[33] B) Hypothetic sequential binding of LipA during its secretion over the SEC pathway. Signal peptides of LipA and VD of LipB are shown in red. Calcium binding spots in LipA are shown as green spheres. After secretion and complete folding, the signal sequence of LipA is cleaved by signal peptidase (SP1), and LipA is released as a stable structure into the periplasm or further transported to the XCP machinery.

Analysis of the structure of the LipAB_BG complex (Figure 4.1 A) shows that LipB interacts mainly with the N-terminal part of LipA (N' to C': blue to red). The first half of EHD interacts with β-strand 1 and α-helix 1 of LipA. The second half of EHD and MD2 binds to α-helices 2 and 3 of LipA (all these structural elements are formed by the first 100 amino acids). Only

β-strand 7 and α-helices 8 and 9 (formed by the last 80 amino acids of LipA_BG) are bound by MD1.[33,81] It can be concluded that most structure elements of LipA_BG that interact with LipB are formed early during the secretion process, possibly accounting for the initial recognition and binding of foldase to the secretory chain of its lipase.

Similar to the periplasmic chaperone PpiD,[223] lipase-specific foldases might be able to recognize the partly translocated lipase and sort the single structure elements in the right position for the activated state until the C-terminal part of LipA is secreted and folded into the active, highly stable globular structure of native LipA. During folding, LipA loses its structural flexibility, lowering the affinity for its foldase, which leads to the final release of the lipase from the complex (as shown schematically in Figure 4.1 B). This coupled secretion-folding of LipA would also circumvent the possibility of the aggregation and proteolytic digestion of preactive lipases floating freely inside the periplasm before their activation by foldases, which was described for lipases produced in the absence of foldases.[90]

Comparison of the lipase-specific foldase-aided folding of lipases with the folding mechanism of other steric chaperons, such as the prodomain of subtilisin of *Bacillus amyloliquefaciens*, show similar behavior. Subtilisin, folded in the absence of its prodomain, showed a secondary structure similar to the native state but no or little defined tertiary structure, with a hydrodynamic radius between the size of unfolded and native state.[224,225] The addition of the prodomain *in trans* leads to the formation of a stable tertiary structure and the activation of subtilisin. The activation rates of subtilisin by its prodomain, added *in trans,* were much slower than activation *in cis*, on time scales not appropriate for the living cell.[224,225] Therefore, the pro domain of subtilisin most likely acts during the secretion of prosubtilisin, initializing the folding before the catalytic domain of subtilisin can reach a kinetically stable globular state.

In the case of lipase-specific foldases, it might also be possible to observe the transitions of preactive lipases to their native states on longer time scales. The experiments conducted in this thesis characterized the lipase-specific foldase-aided folding of LipA in its early stages with incubation times no longer than 24 h. However, the time course of LipA activation by foldase measured *in vitro* is too slow to be appropriate for an organism that is able to divide every 25 min under optimal conditions.[226]

It is interesting that most other intermolecular steric chaperones that influence the tertiary structure of their target proteins are produced as N-terminal sequence extensions[227] and are always translated or secreted before the substrate, enabling their function immediately

during folding. This early interaction with steric chaperones guarantees the most efficient folding of their substrate, preventing misfolding or proteolytic degradation.

Lipase-specific foldases are intermolecular chaperones, and it has often been asked why it was favorable to develop the chaperone dependent secretion process of lipases.[45,90] In contrast to the steric chaperones of proteases, it is not known for certain whether lipase-specific foldases inhibit the activity of lipases during complex formation to protect against enzyme activity inside the cell.[85,88] However, this protection is not needed because lipases are not able to degrade phospholipid membranes on their own.[228]

It might be possible that microorganisms have solved a great conflict in a very elegant way by the development of periplasmic lipase-specific foldases. Secreted lipases have to withstand harsh conditions outside the cell and must fold into a compact, highly cooperative fold to be protected from proteolytic digestion. On the other hand, to be efficiently secreted across the inner membrane, lipases have to fold into loosely packed conformations after translation to enable structural disintegration during transport of the unstructured peptide chain over the Sec channel. These long-lived, loosely packed folding intermediates seem to be a basic characteristic of secretory proteins.[229] Once transported across the inner membrane, lipase-specific foldases provide an environment for refolding that blocks off the kinetically trapped folding route to the preactive state and enables the route to the highly stable native state. Foldases, acting as intermolecular chaperons, make it possible to recycle them for multiturnover catalysis and avoid the need for proteolytic cleavage afterwards.

5. Summary

Secreted bacterial lipases frequently show interesting properties for use in biocatalysis, such as promiscuous reactivity and high stability. Unfortunately, the complexity of the secretion process, which involves many accessory proteins, hampers efficient heterologous and homologous expression, limiting the availability of lipases and therefore their applicability as biocatalysts. One of the major bottlenecks in the production of many secreted lipases is their dependency on lipase-specific foldases, which function as steric chaperones that help lipases overcome an energetic barrier on their folding pathway to the active conformation.

In the absence of foldases, lipases aggregate into insoluble inclusion bodies that can be activated by foldases after they have been chemically unfolded and refolded into a so-called preactive state. It is generally accepted that this *in vitro*-derived preactive conformation is formed on the *in vivo* folding pathway as well. However, the molecular mechanisms of the *in vivo* and *in vitro* foldase-assisted activation of lipases are barely understood.

In this thesis, the lipase-specific foldase (LipH) and lipase (LipA) from *Pseudomonas aeruginosa* PA01 was used as a model system to investigate foldase-assisted lipase activation. After a detailed biochemical and biophysical characterization of the refolding and activation processes of LipA *in vitro,* the results put into question the hypothesis about the preactive LipA state as a real folding intermediate *in vivo.* A great aggregation tendency and unstable tertiary structure make the preactive state unlikely to exist as free molecules inside the periplasm. Furthermore, preactive LipA in complex with LipH showed catalytic activity, but comparison of the structural stability and characteristics with the native state of LipA, isolated from *P. aeruginosa* supernatants, demonstrated clear differences, leading to the assumption that LipH is not able to convert preactive LipA into the native conformation. For the first time, it was possible to demonstrate that the LipAH complex is able to dissociate and that there is a steady exchange of LipA molecules inside the complex during the refolding reaction *in vitro*. As a consequence, the release of active lipase and multiturnover catalysis of foldases has never been observed, because preactive LipA falls back into an inactive conformation after dissociation from LipH. *In vivo,* LipH may interact with LipA during the secretion process, before LipA folds into the globular preactive state, to block this pathway and to assist in folding into a highly stable native conformation. The active conformation of preactive LipA in complex with LipH might be an artificial state that does not occur *in vivo.*

6. Zusammenfassung

Sekretierte bakterielle Lipasen zeigen häufig Eigenschaften, wie promiskuitive Reaktivität und hohe Stabilität, die sie besonders interessant für den Einsatz in der Biokatalyse machen. Die Komplexität des Sekretionsprozesses, an dem oft viele akzessorische Proteine beteiligt sind, erschwert häufig die effiziente heterologe und homologe Expression von Lipasen. Hierdurch ist ihre Verfügbarkeit und somit auch ihre Einsetzbarkeit als Biokatalysatoren häufig jedoch eingeschränkt. Einer der größten Engpässe bei der Produktion vieler sekretierter Lipasen ist ihre Abhängigkeit von den Lipase-spezifischen Foldasen, die als sterische Chaperone den Lipasen auf dem Faltungsweg zu ihrer aktiven Konformation helfen.

In Abwesenheit von Foldasen aggregieren Lipasen häufig zu unlöslichen Einschlusskörperchen, die durch Foldasen aktiviert werden können, nachdem sie chemisch entfaltet und in einen sogenannten präaktiven Zustand zurückgefaltet wurden. Es wird im Allgemeinen vermutet, dass diese *in vitro* erhaltene präaktive Konformation auch auf dem *in vivo* Faltungsweg existiert. Jedoch sind die molekularen Mechanismen der *in vivo* und *in vitro* Foldase-unterstützten Aktivierung bisher kaum verstanden.

In dieser Arbeit wurde die Lipase-spezifische Foldase (LipH) und die Lipase (LipA) von *Pseudomonas aeruginosa* PA01 als Modellsystem zur Untersuchung der foldase-unterstützten Lipase-Aktivierung verwendet. Eine detaillierte biochemische und biophysikalische Charakterisierung der Rückfaltung und der Aktivierung von LipA *in vitro* führte zu der Annahme, dass der präaktive Zustand kein Intermediat auf dem *in vivo* Faltungsweg darstellt. Eine starke Aggregationstendenz und eine instabile Tertiärstruktur des präaktiven Zustandes machen seine Existenz im Periplasma sehr unwahrscheinlich. Präaktive LipA im Komplex mit LipH zeigte zwar katalytische Aktivität, aber ein Vergleich ihrer strukturellen Stabilität mit der vom nativen Zustand zeigte deutliche Unterschiede. Dies führte zur Schlussfolgerung, dass LipH nicht in der Lage ist den präaktiven Zustand in die native Konformation zu überführen. Zum ersten Mal konnte gezeigt werden, dass während der *in vitro* Rückfaltungsreaktion der LipAH-Komplex dissoziiert und ein stetiger Austausch von LipA-Molekülen erfolgt. Jedoch fällt der aktivierte Zustand von LipA nach der Dissoziation von LipH wieder in eine inaktive Konformation zurück und liefert damit eine Begründung, warum es bisher nicht möglich war einen Mehrfachumsatz durch LipH zu beobachten. Aufgrund dieser Ergebnisse wurde die Hypothese aufgestellt, dass LipH *in vivo* viel früher im Sekretionsprozess mit LipA interagiert

und dafür verantwortlich ist, dass LipA sich direkt in den stabilen nativen Zustand falten kann und die Faltung in den sogenannten präaktiven Zustand verhindert wird.

Der durch LipH aktivierte präaktive Zustand von LipA scheint nur eine künstlich aktive gehaltene Konformation zu sein, die keine Rolle auf dem *in vivo* Faltungsweg zu spielen scheint.

7. References

1. McGovern PE, Zhang J, Tang J, Zhang Z, Hall GR, Moreau RA, Nunez A, Butrym ED, Richards MP, Wang C -s., Cheng G, Zhao Z, Wang C. Fermented beverages of pre- and proto-historic China. *Proc. Natl. Acad. Sci.* **101,** 17593–17598 (2004).
2. Li X, Harbottle G, Zhang J, Wang C. The earliest writing? Sign use in the seventh millennium BC at Jiahu, Henan Province, China. *Antiquity* **77,** 31–44 (2003).
3. Manchester KL. Louis Pasteur (1822–1895) — chance and the prepared mind. *Trends Biotechnol.* **13,** 511–515 (1995).
4. Kühne W. Ueber das Verhalten verschiedener organisierter und sog. ungeformter Fermente. *Verhandlungen des Naturhistorischen-Medicinischen Vereins zu Heidelb. Band 1* 190–193 (1877).
5. Sumner JB. The chemical nature of enzymes. in *Nobel Prize Lectures Chemistry 1942-1962* 115–120 (Elsevier Publishing Company, 1964).
6. Pahoja VM, Sethar MA. A review of enzymatic properties of lipase in plants, animals and microorganisms. *J. Appl. Sci.* **2,** 474–484 (2002).
7. Jaeger K-E, Eggert T. Lipases for biotechnology. *Curr. Opin. Biotechnol.* **13,** 390–397 (2002).
8. Blow DM, Birktoft JJ, Hartley BS. Role of a buried acid group in the mechanism of action of chymotrypsin. *Nature* **221,** 337–340 (1969).
9. Cantu DC, Chen Y, Reilly PJ. Thioesterases: A new perspective based on their primary and tertiary structures. *Protein Sci.* **19,** 1281–1295 (2010).
10. Dodson G, Wlodawer A. Catalytic triads and their relatives. *Trends Biochem. Sci.* **23,** 347–52 (1998).
11. Jaeger KE, Reetz MT. Microbial lipases form versatile tools for biotechnology. *Trends Biotechnol.* **16,** 396–403 (1998).
12. Liese A, Seelbach K, Buchholz A, Haberland J. Processes. in *Industrial Biotransformations* (eds. Liese, A., Seelbach, K. & Wandrey, C.) 147–514 (Wiley-VCH Verlag GmbH & Co. KGaA, 2006).
13. Hasan F, Shah AA, Hameed A. Industrial applications of microbial lipases. *Enzyme Microb. Technol.* **39,** 235–251 (2006).
14. Fischer M. Die Lipase Engineering Database: systematische Analyse familienspezifischer Eigenschaften und der Sequenz-Struktur-Funktionsbeziehung von α/β-Hydrolasen. (Doctoral dissertation, University of Stuttgart, 2004).
15. Henke E, Pleiss J, Bornscheuer UT. Activity of lipases and esterases towards tertiary alcohols: Insights into structure-function relationships. *Angew. Chemie Int. Ed.* **41,** 3211–3213 (2002).
16. Joerger RD, Haas MJ. Alteration of chain length selectivity of a *Rhizopus delemar* lipase through site-directed mutagenesis. *Lipids* **29,** 377–384 (1994).
17. Liebeton K, Zonta A, Schimossek K, Nardini M, Lang D, Dijkstra BW, Reetz MT, Jaeger K-E. Directed evolution of an enantioselective lipase. *Chem. Biol.* **7,** 709–18 (2000).
18. Schmid A, Dordick JS, Hauer B, Kiener A, Wubbolts M, Witholt B. Industrial biocatalysis today and tomorrow. *Nature* **409,** 258–268 (2001).
19. Cardenas F, de Castro MS, Sanchez-Montero JM, Sinisterra JV, Valmaseda M, Elson SW, Alvarez E. Novel microbial lipases: catalytic activity in reactions in organic media. *Enzyme Microb. Technol.* **28,** 145–154 (2001).
20. Kim HJ, Jeong YS, Jung WK, Kim SK, Lee HW, Kahng H-Y, Kim J, Kim H. Characterization of novel family IV esterase and family I.3 lipase from an oil-polluted mud flat

metagenome. *Mol. Biotechnol.* **57,** 781–792 (2015).
21. Sinclair JC, Sandy J, Delgoda R, Sim E, Noble MEM. Structure of arylamine N-acetyltransferase reveals a catalytic triad. *Nat. Struct. Biol.* **7,** 560–564 (2000).
22. Mei B, Zalkin H. A cysteine-histidine-aspartate catalytic triad is involved in glutamine amide transfer function in purF-type glutamine amidotransferases. *J. Biol. Chem.* **264,** 16613–9 (1989).
23. Kleiner B. Nutzung von hydrophilen „Green Solvents" zur biokatalytischen Estersynthese in zweiphasigen Reaktionssystemen. (Doctoral dissertation, Heinrich Heine University Düsseldorf, 2015).
24. Ogino H, Inoue S, Akagi R, Yasuda M, Doukyu N, Ishimi K. Refolding of a recombinant organic solvent-stable lipase, which is overexpressed and forms an inclusion body, and activation with lipase-specific foldase. *Biochem. Eng. J.* **40,** 507–511 (2008).
25. Lau RM, Van Rantwijk F, Seddon KR, Sheldon RA, De Diego T, Lozano P, Abad MA, Steffensky K, Vaultier M, Iborra JL. Lipase-catalyzed reactions in ionic liquids. *Org. Lett.* **2,** 4189–4191 (2000).
26. Andreoli PM, Cox MMJ, Farin F, Wohlfarth S. Molecular cloning and expression of genes encoding lipolytic enzymes. **EP0334462B,** (1988).
27. Nagarajan S. New tools for exploring 'old friends-microbial lipases'. *Appl. Biochem. Biotechnol.* **168,** 1163–96 (2012).
28. Villeneuve P, Muderhwa JM, Graille J, Haas MJ. Customizing lipases for biocatalysis: a survey of chemical, physical and molecular biological approaches. *J. Mol. Catal. - B Enzym.* **9,** 113–148 (2000).
29. Zaks A, Klibanov AM. Enzymatic catalysis in organic media at 100°C. *Science* **224,** 1249–1251 (1984).
30. Arpigny JL, Jaeger K-E. Bacterial lipolytic enzymes: classification and properties. *Biochem. J.* **343,** 177–83 (1999).
31. Martínez A, Soberón-Chávez G. Characterization of the *lipA* gene encoding the major lipase from *Pseudomonas aeruginosa* strain IGB83. *Appl. Microbiol. Biotechnol.* **56,** 731–735 (2001).
32. Javed S, Azeem F, Hussain S, Rasul I, Siddique MH, Riaz M, Afzal M, Kouser A, Nadeem H. Bacterial lipases: A review on purification and characterization. *Prog. Biophys. Mol. Biol.* **132,** 23–34 (2018).
33. Nardini M, Lang D a, Liebeton K, Jaeger K-E, Dijkstra BW. Crystal structure of *Pseudomonas aeruginosa* lipase in the open conformation. *J. Biol. Chem.* **275,** 31219–31225 (2000).
34. Stuer W, Jaeger K-E, Winkler UK. Purification of extracellular lipase from *Pseudomonas aeruginosa*. *J. Bacteriol.* **168,** 1070–4 (1986).
35. Singh M, Singh S, Singh RS, Chisti Y, Banerjee UC. Transesterification of primary and secondary alcohols using *Pseudomonas aeruginosa* lipase. *Bioresour. Technol.* **99,** 2116–2120 (2008).
36. Reetz MT, Carballeira JD, Peyralans J, Höbenreich H, Maichele A, Vogel A. Expanding the substrate scope of enzymes: Combining mutations obtained by CASTing. *Chem. Eur. J.* **12,** 6031–6038 (2006).
37. Ollis DL, Cheah E, Cygler M, Dijkstra B, Frolow F, Franken SM, Harel M, Remington SJ, Silman I, Schrag J. The α/β hydrolase fold. *Protein Eng.* **5,** 197–211 (1992).
38. El Khattabi M, Van Gelder P, Bitter W, Tommassen J. Role of the calcium ion and the disulfide bond in the *Burkholderia glumae* lipase. *J. Mol. Catal. B Enzym.* **22,** 329–338 (2003).

39. Liebeton K, Zacharias A, Jaeger K-E. Disulfide bond in *Pseudomonas aeruginosa* lipase stabilizes the structure but is not required for interaction with its foldase. *J. Bacteriol.* **183,** 597–603 (2001).
40. Douzi B, Ball G, Cambillau C, Tegoni M, Voulhoux R. Deciphering the Xcp *Pseudomonas aeruginosa* type II secretion machinery through multiple interactions with substrates. *J. Biol. Chem.* **286,** 40792–40801 (2011).
41. Rosenau F, Jaeger K-E. Bacterial lipases from *Pseudomonas*: regulation of gene expression and mechanisms of secretion. *Biochimie* **82,** 1023–32 (2000).
42. Watson MEE. Compilation of published signal sequences. *Nucleic Acids Res.* **12,** 5145–5164 (1984).
43. von Heijne G. The signal peptide. *J. Membrane Biol.* **115,** 195–201 (1990).
44. Saier HM. Protein secretion and membrane insertion systems in gram-negative bacteria. *J. Membrane Biol.* **214,** 75–90 (2006).
45. Rosenau F, Tommassen J, Jaeger K-E. Lipase-specific foldases. *ChemBioChem* **5,** 152–161 (2004).
46. Douzi B, Filloux A, Voulhoux R. On the path to uncover the bacterial type II secretion system. *Philos. Trans. R. Soc. B Biol. Sci.* **367,** 1059–1072 (2012).
47. Fröderberg L, Houben ENG, Baars L, Luirink J, de Gier J-W. Targeting and translocation of two lipoproteins in *Escherichia coli* via the SRP/Sec/YidC pathway. *J. Biol. Chem.* **279,** 31026–31032 (2004).
48. Halic M, Beckmann R. The signal recognition particle and its interactions during protein targeting. *Curr. Opin. Struct. Biol.* **15,** 116–125 (2005).
49. Tsirigotaki A, De Geyter J, Šoštaric´ N, Economou A, Karamanou S. Protein export through the bacterial Sec pathway. *Nat. Rev. Microbiol.* **15,** 21–36 (2017).
50. Ullers RS, Luirink J, Harms N, Schwager F, Georgopoulos C, Genevaux P. SecB is a bona fide generalized chaperone in *Escherichia coli*. *Proc. Natl. Acad. Sci.* **101,** 7583–7588 (2004).
51. Vrontou E, Economou A. Structure and function of SecA, the preprotein translocase nanomotor. *Biochim. Biophys. Acta - Mol. Cell Res.* **1694,** 67–80 (2004).
52. Sardis MF, Economou A. SecA: a tale of two protomers. *Mol. Microbiol.* **76,** 1070–1081 (2010).
53. Natale P, Brüser T, Driessen AJM. Sec- and Tat-mediated protein secretion across the bacterial cytoplasmic membrane—Distinct translocases and mechanisms. *Biochim. Biophys. Acta - Biomembr.* **1778,** 1735–1756 (2008).
54. du Plessis DJF, Berrelkamp G, Nouwen N, Driessen AJM. The lateral gate of SecYEG opens during protein translocation. *J. Biol. Chem.* **284,** 15805–15814 (2009).
55. Cranford-Smith T, Huber D. The way is the goal: how SecA transports proteins across the cytoplasmic membrane in bacteria. *FEMS Microbiol. Lett.* **365,** 15709–15713 (2018).
56. Tomkiewicz D, Nouwen N, van Leeuwen R, Tans S, Driessen AJM. SecA supports a constant rate of preprotein translocation. *J. Biol. Chem.* **281,** 15709–15713 (2006).
57. Urban A, Leipelt M, Eggert T, Jaeger K-E. DsbA and DsbC Affect Extracellular Enzyme Formation in *Pseudomonas aeruginosa*. **183,** 587–596 (2001).
58. D'Enfert C, Ryter A, Pugsley AP. Cloning and expression in *Escherichia coli* of the *Klebsiella pneumoniae* genes for production, surface localization and secretion of the lipoprotein pullulanase. *EMBO J.* **6,** 3531–8 (1987).
59. de Groot A, Koster M, Gérard-Vincent M, Gerritse G, Lazdunski A, Tommassen J, Filloux A. Exchange of Xcp (Gsp) secretion machineries between *Pseudomonas aeruginosa* and *Pseudomonas alcaligenes*: Species specificity unrelated to substrate recognition. *J.*

Bacteriol. **183,** 959–967 (2001).
60. Reichow SL, Korotkov K V., Hol WGJ, Gonen T. Structure of the cholera toxin secretion channel in its closed state. *Nat. Struct. Mol. Biol.* **17,** 1226–1232 (2010).
61. Campos M, Nilges M, Cisneros DA, Francetic O. Detailed structural and assembly model of the type II secretion pilus from sparse data. *Proc. Natl. Acad. Sci.* **107,** 13081–13086 (2010).
62. Senf F, Tommassen J, Koster M. Polar secretion of proteins via the Xcp type II secretion system in *Pseudomonas aeruginosa*. *Microbiology* **154,** 3025–3032 (2008).
63. Ball G, Durand É, Lazdunski A, Filloux A. A novel type II secretion system in *Pseudomonas aeruginosa*. **43,** 475–485 (2002).
64. Naganathan AN, Muñoz V. Scaling of folding times with protein size. *J. Am. Chem. Soc.* **127,** 480–481 (2005).
65. Ptitsyn OB. Secondary structure formation and stability. *Curr. Opin. Struct. Biol.* **2,** 13–20 (1992).
66. Berg JM, Tymoczko JL, Gatto GJ, Stryer L, Held A, Maxam G, Seidler L, Häcker B, Jarosch B. *Biochemie*. (Springer Spektrum, 2017).
67. Anfinsen CB, Haber E, Sela M, White FH. The kinetics of formation of native ribonuclease during oxidationof the reduced polypeptide chain. *Proc. Natl. Acad. Sci.* **47,** 1309–1314 (1961).
68. Anfinsen CB. Principles that govern the folding of protein chains. *Science* **181,** 223–230 (1973).
69. Strucksberg KH, Rosenkranz T, Fitter J. Reversible and irreversible unfolding of multi-domain proteins. *Biochim. Biophys. Acta* **1774,** 1591–1603 (2007).
70. Baker D, Agard DA. Kinetics versus thermodynamics in protein folding. *Biochemistry* **33,** 7505–7509 (1994).
71. Dobson CM, Šali A, Karplus M. Proteinfaltung aus theoretischer und experimenteller Sicht. *Angew. Chemie* **110,** 908–935 (1998).
72. Hartl FU, Bracher A, Hayer-Hartl M. Molecular chaperones in protein folding and proteostasis. *Nature* **475,** 324–332 (2011).
73. Hristozova N, Tompa P, Kovacs D. A novel method for assessing the chaperone activity of proteins. *PLoS One* **11,** e0161970 (2016).
74. Nagradova NK. *Foldases: Enzymes catalyzing protein folding*. *Nova Science Publishers Inc* (2008).
75. Ellis RJ. Steric chaperones. *Trends Biochem. Sci.* **23,** 43–45 (1998).
76. Jaswal SS, Sohl JL, Davis JH, Agard DA. Energetic landscape of α-lytic protease optimizes longevity through kinetic stability. *Nature* **415,** 343–346 (2002).
77. Sohl JL, Jaswal SS, Agard DA. Unfolded conformations of α-lytic protease are more stable than its native state. *Nature* **395,** 817–819 (1998).
78. Jaeger K-E, Ransac S, Dijkstra BW, Colson C, Heuvel M, Misset O. Bacterial lipases. *FEMS Microbiol. Rev.* **15,** 29–63 (1994).
79. Jørgensen S, Skov KW, Diderichsen B. Cloning, sequence, and expression of a lipase gene from *Pseudomonas cepacia*: Lipase production in heterologous hosts requires two *Pseudomonas* genes. *J. Bacteriol.* **173,** 559–567 (1991).
80. Rost B, Sander C. Prediction of protein secondary structure at better than 70% accuracy. *J. Mol. Biol.* **232,** 584–599 (1993).
81. Pauwels K, Lustig A, Wyns L, Tommassen J, Savvides SN, Van Gelder P. Structure of a membrane-based steric chaperone in complex with its lipase substrate. *Nat. Struct. Mol. Biol.* **13,** 374–375 (2006).

82. Frenken LGJ, Bos JW, Visser C, Müller W, Tommassen J, Verrips CT. An accessory gene, *lipB*, required for the production of active *Pseudomonas glumae* lipase. *Mol. Microbiol.* **9,** 579–589 (1993).
83. Shibata H, Kato H, Oda J. Molecular properties and activity of amino-terminal truncated forms of lipase activator protein. *Biosci. Biotechnol. Biochem.* **62,** 354–357 (1998).
84. Quyen DT, Schmidt-Dannert C, Schmid RD. High-level formation of active *Pseudomonas cepacia* lipase after heterologous expression of the encoding gene and its modified chaperone in *Escherichia coli* and rapid in vitro refolding. *Appl. Environ. Microbiol.* **65,** 787–94 (1999).
85. El Khattabi M, Van Gelders P, Bitter W, Tommassen J. Role of the lipase-specific foldase of *Burkholderia glumae* as a steric chaperone. *J. Biol. Chem.* **275,** 26885–91 (2000).
86. Aboubi R. Struktur und physiologische Funktion einer Lipase-spezifischen Foldase aus *Pseudomonas aeruginosa*. (Diploma thesis, Heinrich Heine University Düsseldorf, 2008).
87. Shibata H, Kato H, Oda J. Random mutagenesis on the *Pseudomonas* lipase activator protein, LipB: exploring amino acid residues required for its function. *Protein Eng.* **11,** 467–472 (1998).
88. Ihara F, Okamoto I, Akao K, Nihira T, Yamada Y. Lipase modulator protein (LimL) of *Pseudomonas* sp. strain 109. *J. Bacteriol.* **177,** 1254–8 (1995).
89. Shibata H, Kato H, Oda J. Calcium ion-dependent reactivation of a *Pseudomonas* lipase by its specific modulating protein, LipB. *J. Biochem.* **123,** 136–41 (1998).
90. Frenken LGJ, Groot A, Tommassen J, Verrips CT. Role of the lipB gene product in the folding of the secreted lipase of *Pseudomonas glumae*. *Mol. Microbiol.* **9,** 591–599 (1993).
91. El Khattabi M, Ockhuijsen C, Bitter W, Jaeger K-E, Tommassen J. Specificity of the lipase-specific foldases of gram-negative bacteria and the role of the membrane anchor. *Mol. Gen. Genet.* **261,** 770–776 (1999).
92. Hausmann S. Einfluss des Lipase-spezifischen Chaperons LipH auf die Faltung und Sekretion der Lipasen LipA und LipC aus *Pseudomonas aeruginosa*. (Doctoral dissertation, Heinrich Heine University Düsseldorf, 2008).
93. Hobson AH, Buckley CM, Jørgensen ST, Diderichsen B, McConnell DJ. Interaction of the *Pseudomonas cepacia* DSM3959 lipase with its chaperone, LimA. *J. Biochem.* **118,** 575–81 (1995).
94. Hanahan D. Studies on Transformation of *Escherichia coli* with plasmids. *J. Mol. Biol.* **166,** 557–580 (1983).
95. Studier FW, Moffatt BA. Use of bacteriophage T7 RNA polymerase to direct selective high-level expression of cloned genes. *J. Mol. Biol.* **189,** 113–30 (1986).
96. Wood WB. Host specificity of DNA produced by *Escherichia coli*: bacterial mutations affecting the restriction and modification of DNA. *J. Mol. Biol.* **16,** 118–33 (1966).
97. Holloway BW, Krishnapillai V, Morgan a F. Chromosomal genetics of *Pseudomonas*. *Microbiol. Rev.* **43,** 73–102 (1979).
98. Jaeger K-E, Schneidinger B, Rosenau F, Werner M, Lang D, Dijkstra BW, Schimossek K, Zonta A, Reetz MT. Bacterial lipases for biotechnological applications. *J. Mol. Catal. B Enzym.* **3,** 3–12 (1997).
99. Kovach M, Elzer P, Hill DS, Robertson GT, Farris MA, Roop RM, Perterson KM. Four new derivatives of the broad-host-range cloning vector pBBR1MCS, carrying different antibiotic-resistance cassettes. *Gene* **166,** 175–176 (1995).
100. Janosch D. Untersuchungen zur in vivo-Aktivierung bakterieller Lipasen durch

heterologe Foldasen. (Diploma thesis, University of Bochum, 2002).
101. Hausmann S, Wilhelm S, Jaeger K-E, Rosenau F. Mutations towards enantioselectivity adversely affect secretion of *Pseudomonas aeruginosa* lipase. *FEMS Microbiol. Lett.* **282,** 65–72 (2008).
102. Mariëlle Keijer. Preparation and fluorescence spectroscopic characterization of a lipase-specific foldase from *Pseudomonas aeruginosa*. (Bachelor thesis, Heinrich Heine University Düsseldorf, 2012).
103. NEB. Tm calculator. (2017). Available at: http://tmcalculator.neb.com/#!/.
104. IDT. Oligoanalyzer. (2017). Available at: https://eu.idtdna.com/calc/analyzer.
105. Owczarzy R, Tataurov A V., Wu Y, Manthey JA, McQuisten KA, Almabrazi HG, Pedersen KF, Lin Y, Garretson J, McEntaggart NO, Sailor CA, Dawson RB, Peek AS. IDT SciTools: a suite for analysis and design of nucleic acid oligomers. *Nucleic Acids Res.* **36,** W163–W169 (2008).
106. Sambrook J, Russel DW. *Molecular cloning - A laboratory manual*. (Cold Spring Harbor Laboratory Press, 2001).
107. Aslanidis C, de Jong PJ. Ligation-independent cloning of PCR products (LIC-PCR). *Nucleic Acids Res.* **18,** 6069–6074 (1990).
108. Aslanidis C, de Jong PJ, Schmitz G. Minimal length requirement of the single-stranded tails for ligation-independent cloning (LIC) of PCR products. *Genome Res.* **4,** 172–177 (1994).
109. Li MZ, Elledge SJ. Harnessing homologous recombination *in vitro* to generate recombinant DNA via SLIC. *Nat. Methods* **4,** 251–256 (2007).
110. Jeong J, Yim H, Ryu J, Lee HS, Lee J, Seen D-S, Kang SG. One-step sequence- and ligation-independent cloning as a rapid and versatile cloning method for functional genomics studies. *Appl. Environ. Microbiol.* **78,** 5440–5443 (2012).
111. Choi K-H, Kumar A, Schweizer HP. A 10-min method for preparation of highly electrocompetent *Pseudomonas aeruginosa* cells: Application for DNA fragment transfer between chromosomes and plasmid transformation. *J. Microbiol. Methods* **64,** 391–397 (2006).
112. Hendrickson WA, Ogata CM. Phase determination from multiwavelength anomalous diffraction measurements. in *Methods in Enzymology* **276,** 494–523 (1997).
113. EMBL. Expression - Seleno-methionine labelling of proteins in E. coli. (2017). Available at: https://www.embl.de/pepcore/pepcore_services/protein_expression/ecoli/seleno/.
114. Michael A. Ueber die Addition von Natriumacetessig- und Natriummalonsäureäthern zu den Aethern ungesättigter Säuren. *J. für Prakt. Chemie* **35,** 349–356 (1887).
115. Posner T. Beiträge zur Kenntniss der ungesättigten Verbindungen. II. Ueber die Addition von Mercaptanen an ungesättigte Kohlenwasserstoffe. *Berichte der Dtsch. Chem. Gesellschaft* **38,** 646–657 (1905).
116. Bradford MM. A rapid and sensitive method for the quantitation of microgram quantities of protein utilizing the principle of protein-dye binding. *Anal. Biochem.* **72,** 248–54 (1976).
117. Zor T, Selinger Z. Linearization of the Bradford protein assay increases its sensitivity: Theoretical and experimental studies. *Anal. Biochem.* **236,** 302–308 (1996).
118. Neuhoff V, Arold N, Taube D, Ehrhardt W. Improved staining of proteins in polyacrylamide gels including isoelectric focusing gels with clear background at nanogram sensitivity using Coomassie Brilliant Blue G-250 and R-250. *Electrophoresis* **9,** 255–262 (1988).

119. Renart J, Reiser J, Stark GR. Transfer of proteins from gels to diazobenzyloxymethyl-paper and detection with antisera: A method for studying antibody specificity and antigen structure. *Proc. Natl. Acad. Sci.* **76,** 3116–3120 (1979).
120. Burnette WN. "Western Blotting": Electrophoretic Transfer of Proteins from Sodium Dodecyl Sulfate-Polyacrylamide Gels to Unmodified Nitrocellulose and Radiographic Detection with Antibody and Radioiodinated Protein A. *Anal. Biochem.* **112,** 195–203 (1981).
121. Towbin H, Staehelin T, Gordon J. Electrophoretic transfer of proteins from polyacrylamide gels to nitrocellulose sheets: Procedure and some applications. *Proc. Natl. Acad. Sci. U. S. A.* **76,** 4350–4 (1979).
122. Whitehead TP, Thorpe GHG, Carter TJN, Groucutt C, Kricka LJ. Enhanced luminescence procedure for sensitive determination of peroxidase-labelled conjugates in immunoassay. *Nature* **305,** 158–159 (1983).
123. Thorpe GHG, Kricka LJ. Enhanced chemiluminescent reactions catalyzed by horseradish peroxidase. *Methods Enzymol.* **133,** 331–53 (1986).
124. Thorpe GH, Kricka LJ, Moseley SB, Whitehead TP. Phenols as enhancers of the chemiluminescent horseradish peroxidase-luminol-hydrogen peroxide reaction: Application in luminescence-monitored enzyme immunoassays. *Clin. Chem.* **31,** 1335–41 (1985).
125. Dunn SD. Effects of the modification of transfer buffer composition and the renaturation of proteins in gels on the recognition of proteins on western blots by monoclonal antibodies. *Anal. Biochem.* **157,** 144–153 (1986).
126. Mruk DD, Cheng CY. Enhanced chemiluminescence (ECL) for routine immunoblotting: An inexpensive alternative to commercially available kits. *Spermatogenesis* **1,** 121–122 (2011).
127. Goldberg JM, Wissner RF, Klein AM, Petersson EJ. Thioamide quenching of intrinsic protein fluorescence. *Chem. Commun.* **48,** 1550–1552 (2012).
128. Vivian JT, Callis PR. Mechanisms of tryptophan fluorescence shifts in proteins. *Biophys. J.* **80,** 2093–2109 (2001).
129. Albani JR. Fluorescence Spectroscopy Principles. in *Principles and Applications of Fluorescence Spectroscopy* 88–114 (Blackwell Publishing Ltd, 2008).
130. Weichel M, Bassarab S, Garidel P. Probing Thermal Stability of MAbs By Intrinsic Tryptophan Fluorescence. *Bioprocess Int.* (2008).
131. Teng T-Y. Mounting of crystals for macromolecular crystallography in a free-standing thin film. *J. Appl. Crystallogr.* **23,** 387–391 (1990).
132. Winn MD, Ballard CC, Cowtan KD, Dodson EJ, Emsley P, Evans PR, Keegan RM, Krissinel EB, Leslie AGW, McCoy A, McNicholas SJ, Murshudov GN, Pannu NS, Potterton EA, Powell HR, Read RJ, Vagin A, Wilson KS. Overview of the CCP 4 suite and current developments. *Acta Crystallogr. Sect. D Biol. Crystallogr.* **67,** 235–242 (2011).
133. Eggeling C, Berger S, Brand L, Fries JR, Schaffer J, Volkmer A, Seidel CAM. Data registration and selective single-molecule analysis using multi-parameter fluorescence detection. *J. Biotechnol.* **86,** 163–180 (2001).
134. Kühnemuth R, Seidel CAM. Principles of single molecule multiparameter fluorescence spectroscopy. *Single Mol.* **2,** 251–254 (2001).
135. Sisamakis E, Valeri A, Kalinin S, Rothwell PJ, Seidel CAM. Accurate single-molecule FRET studies using multiparameter fluorescence detection. in *Single Molecule Tools, Part B:Super-Resolution, Particle Tracking, Multiparameter, and Force Based Methods* **475,** 455–514 (Elsevier Inc., 2010).

136. Kudryavtsev V, Sikor M, Kalinin S, Mokranjac D, Seidel CAM, Lamb DC. Combining MFD and PIE for accurate single-pair Förster resonance energy transfer measurements. *ChemPhysChem* **13,** 1060–1078 (2012).
137. Antonik M, Felekyan S, Gaiduk A, Seidel CAM. Separating structural heterogeneities from stochastic variations in fluorescence resonance energy transfer distributions via photon distribution analysis. *J. Phys. Chem. B* **110,** 6970–8 (2006).
138. Kalinin S, Felekyan S, Antonik M, Seidel CAM. Probability distribution analysis of single-molecule fluorescence anisotropy and resonance energy transfer. *J. Phys. Chem. B* **111,** 10253–10262 (2007).
139. Sindbert S, Kalinin S, Nguyen H, Kienzler A, Clima L, Bannwarth W, Appel B, Müller S, Seidel CAM. Accurate Distance Determination of Nucleic Acids via Förster Resonance Energy Transfer: Implications of Dye Linker Length and Rigidity. *J. Am. Chem. Soc.* **133,** 2463–2480 (2011).
140. Kalinin S, Peulen T, Sindbert S, Rothwell PJ, Berger S, Restle T, Goody RS, Gohlke H, Seidel CAM. A toolkit and benchmark study for FRET-restrained high-precision structural modeling. *Nat. Methods* **9,** 1218–25 (2012).
141. Dimura M, Peulen TO, Hanke CA, Prakash A, Gohlke H, Seidel CA. Quantitative FRET studies and integrative modeling unravel the structure and dynamics of biomolecular systems. *Curr. Opin. Struct. Biol.* **40,** 163–185 (2016).
142. Wishart DS, Bigam CG, Holm A, Hodges RS, Sykes BD. ^{1}H, ^{13}C and ^{15}N random coil NMR chemical shifts of the common amino acids. I. Investigations of nearest-neighbor effects. *J. Biomol. NMR* **5,** 67–81 (1995).
143. Viegas A. Molecular determinants of ligand specificity in carbohydrate-binding module: an NMR and X-ray crystallography integrated study. (Doctoral dissertation, New University of Lisabon, 2012).
144. Güntert P. Automated NMR structure calculation with CYANA. in *Protein NMR Techniques* 353–378 (Humana Press).
145. Cornilescu G, Delaglio F, Bax A. Protein backbone angle restraints from searching a database for chemical shift and sequence homology. *J. Biomol. NMR* **13,** 289–302 (1999).
146. Kelley LA, Mezulis S, Yates CM, Wass MN, Sternberg MJE. The Phyre2 web portal for protein modeling, prediction and analysis. *Nat. Protoc.* **10,** 845–858 (2015).
147. Guex N, Peitsch MC. SWISS-MODEL and the Swiss-PdbViewer: An environment for comparative protein modeling. *Electrophoresis* **18,** 2714–2723 (1997).
148. Laskowski RA, MacArthur MW, Moss DS, Thornton JM. PROCHECK: a program to check the stereochemical quality of protein structures. *J. Appl. Crystallogr.* **26,** 283–291 (1993).
149. Benkert P, Tosatto SCE, Schomburg D. QMEAN: A comprehensive scoring function for model quality assessment. *Proteins Struct. Funct. Bioinforma.* **71,** 261–277 (2008).
150. Wiederstein M, Sippl MJ. ProSA-web: Interactive web service for the recognition of errors in three-dimensional structures of proteins. *Nucleic Acids Res.* **35,** 407–410 (2007).
151. Dolinsky TJ, Nielsen JE, McCammon JA, Baker NA. PDB2PQR: an automated pipeline for the setup of Poisson-Boltzmann electrostatics calculations. *Nucleic Acids Res.* **32,** W665-7 (2004).
152. Dolinsky TJ, Czodrowski P, Li H, Nielsen JE, Jensen JH, Klebe G, Baker NA. PDB2PQR: expanding and upgrading automated preparation of biomolecular structures for molecular simulations. *Nucleic Acids Res.* **35,** W522-5 (2007).

153. Sitkoff D, Sharp KA, Honig B. Accurate calculation of hydration free energies using macroscopic solvent models. *J. Phys. Chem.* **98,** 1978–1988 (1994).
154. Søndergaard CR, Olsson MHM, Rostkowski M, Jensen JH. Improved treatment of ligands and coupling effects in empirical calculation and rationalization of pKa values. *J. Chem. Theory Comput.* **7,** 2284–2295 (2011).
155. Olsson MHM, Søndergaard CR, Rostkowski M, Jensen JH. PROPKA3: Consistent treatment of internal and surface residues in empirical pKa predictions. *J. Chem. Theory Comput.* **7,** 525–537 (2011).
156. Baker NA, Sept D, Joseph S, Holst MJ, McCammon JA. Electrostatics of nanosystems: Application to microtubules and the ribosome. *Proc. Natl. Acad. Sci.* **98,** 10037–10041 (2001).
157. Gasteiger E, Hoogland C, Gattiker A, Duvaud S, Marc R W, Appel RD, Bairoch A. Protein identification and analysis tools on the ExPASy server. in *The Proteomics Protocols Handbook* 571–607 (Humana Press, 2005).
158. Altschul SF, Madden TL, Schäffer AA, Zhang J, Zhang Z, Miller W, Lipman DJ. Gapped BLAST and PSI-BLAST: A new generation of protein database search programs. *Nucleic Acids Res.* **25,** 3389–3402 (1997).
159. Huang Y, Niu B, Gao Y, Fu L, Li W. CD-HIT Suite: a web server for clustering and comparing biological sequences. *Bioinformatics* **26,** 680–682 (2010).
160. Wu S, Zhu Z, Fu L, Niu B, Li W. WebMGA: a customizable web server for fast metagenomic sequence analysis. *BMC Genomics* **12,** 444 (2011).
161. Larkin MA, Blackshields G, Brown NP, Chenna R, McGettigan PA, McWilliam H, Valentin F, Wallace IM, Wilm A, Lopez R, Thompson JD, Gibson TJ, Higgins DG. Clustal W and Clustal X version 2.0. *Bioinformatics* **23,** 2947–2948 (2007).
162. Goujon M, McWilliam H, Li W, Valentin F, Squizzato S, Paern J, Lopez R. A new bioinformatics analysis tools framework at EMBL-EBI. *Nucleic Acids Res.* **38,** W695–W699 (2010).
163. Winsor GL, Griffiths EJ, Lo R, Dhillon BK, Shay JA, Brinkman FSL. Enhanced annotations and features for comparing thousands of *Pseudomonas* genomes in the Pseudomonas genome database. *Nucleic Acids Res.* **44,** D646–D653 (2016).
164. Chihara-Siomi M, Yoshikawa K, Oshima-Hirayama N, Yamamoto K, Sogabe Y, Nakatani T, Nishioka T, Oda J. Purification, molecular cloning, and expression of lipase from *Pseudomonas aeruginosa*. *Arch. Biochem. Biophys.* **296,** 505–13 (1992).
165. Oshima-Hirayama N, Yoshikawa K, Nishioka T, Oda J. Lipase from *Pseudomonas aeruginosa* production in *Escherichia coli* and activation in vitro with a protein from the downstream gene. *Eur. J. Biochem.* **215,** 239–46 (1993).
166. Xiang Z. Advances in Homology Protein Structure Modeling. *Curr. Protein Pept. Sci.* **7,** 217–227 (2006).
167. Tramontano A. Homology modeling with low sequence identity. *Methods* **14,** 293–300 (1998).
168. Yaron A, Naider F, Scharpe S. Proline-dependent structural and biological properties of peptides and proteins. *Crit. Rev. Biochem. Mol. Biol.* **28,** 31–81 (1993).
169. Verma N, Kubiak J, Dollinger P, Kovacic F, Gohlke H, Seidel C, Jaeger K-E. Quantitative characterization of the conformational dynamics of the unbound lipase-specific foldase Lif by MD simulations and fluorescence spectroscopy. *Biophys. J.* **114,** 191a (2018).
170. Berman HM, Westbrook J, Feng Z, Gilliland G, Bhat TN, Weissig H, Shindyalov IN, Bourne PE. The Protein Data Bank. *Nucleic Acids Res.* **28,** 235–42 (2000).
171. Peulen TO, Opanasyuk O, Seidel CAM. Combining graphical and analytical methods with

molecular simulations to analyze time-resolved FRET measurements of labeled macromolecules accurately. *J. Phys. Chem. B* **121,** 8211–8241 (2017).
172. Pauwels K. Structure/function relationship of the lipase-foldase complex of *Burkholderia glumae*. (Doctoral dissertation, Free University of Brussels, 2008).
173. Rosenau F. Überexpression der Lipase aus *Pseudomonas aeruginosa* und physiologische Charakterisierung der Foldasefunktion. (Doctoral dissertation, Ruhr University of Bochum, 2001).
174. Tielen P, Kuhn H, Rosenau F, Jaeger K-E, Flemming H-C, Wingender J. Interaction between extracellular lipase LipA and the polysaccharide alginate of *Pseudomonas aeruginosa*. *BMC Microbiol.* **13,** 159 (2013).
175. Franklin MJ, Nivens DE, Weadge JT, Howell PL. Biosynthesis of the *Pseudomonas aeruginosa* extracellular polysaccharides, alginate, Pel, and Psl. *Front. Microbiol.* **2,** 1–16 (2011).
176. Diogo M., Silva S, Cabral JM., Queiroz J. Hydrophobic interaction chromatography of *Chromobacterium viscosum* lipase on polypropylene glycol immobilised on Sepharose. *J. Chromatogr. A* **849,** 413–419 (1999).
177. Snellman EA, Sullivan ER, Colwell RR. Purification and properties of the extracellular lipase, LipA, of *Acinetobacter* sp. RAG-1. *Eur. J. Biochem.* **269,** 5771–5779 (2002).
178. Gupta R, Gupta N, Rathi P. Bacterial lipases: an overview of production, purification and biochemical properties. *Appl. Microbiol. Biotechnol.* **64,** 763–781 (2004).
179. Jaeger K-E, Adrian F-J, Meyer HE, Hancock REW, Winkler UK. Extracellular lipase from *Pseudomonas aeruginosa* is an amphiphilic protein. **1120,** 315–321 (1992).
180. GE Healthcare. *Hydrophobic interaction and reversed phase chromatography - principles and methods*. (2006).
181. Tanaka J, Ihara F, Nihira T, Yamada Y. A low-M_r lipase activation factor cooperating with lipase modulator protein LimL in *Pseudomonas* sp. strain 109. *Microbiology* **145,** 2875–80 (1999).
182. Ogino H, Inoue S, Yasuda M, Doukyu N. Hyper-activation of foldase-dependent lipase with lipase-specific foldase. *J. Biotechnol.* **166,** 20–4 (2013).
183. Kantner T, Watts AG. Characterization of reactions between water-soluble trialkylphosphines and thiol alkylating reagents: Implications for protein-conjugation reactions. *Bioconjug. Chem.* **27,** 2400–2406 (2016).
184. Ahn JH, Lee YP, Rhee JS. Investigation of refolding condition for *Pseudomonas fluorescens* lipase by response surface methodology. *J. Biotechnol.* **54,** 151–60 (1997).
185. Novototskaya-Vlasova K, Petrovskaya L, Kryukova E, Rivkina E, Dolgikh D, Kirpichnikov M. Expression and chaperone-assisted refolding of a new cold-active lipase from *Psychrobacter cryohalolentis* K5T. *Protein Expr. Purif.* **91,** 96–103 (2013).
186. Akbari N, Khajeh K, Ghaemi N, Salemi Z. Efficient refolding of recombinant lipase from *Escherichia coli* inclusion bodies by response surface methodology. *Protein Expr. Purif.* **70,** 254–259 (2010).
187. Zheng X, Wu N, Fan Y. Characterization of a novel lipase and its specific foldase from *Acinetobacter* sp. XMZ-26. *Process Biochem.* **47,** 643–650 (2012).
188. Schneidinger B. Expression und traskriptionelle Regulation des Lipaseoperons von *Pseudomonas aeruginosa* und funktionelle Charakterisierung der Lipase-spezifischen Foldase LipH. (Doctoral dissertation, Ruhr-University of Bochum, 1997).
189. Hausmann S. Expression und Reinigung von Proteinen des lipolytischen Systems aus *Pseudomonas aeruginosa* für strukturaufklärende Verfahren und Interaktionsexperimente. (Diploma thesis, Ruhr University Bochum, 2004).

190. Seuter A. Molekulare Charakterisierung der Interaktion zwischen einer Lipase und deren Foldase aus *Pseudomonas aeruginosa*. (Diploma thesis, Ruhr University Bochum, 1998).
191. Voet D, Voet JG. *Biochemistry*. (Wiley VCH, 2010).
192. Atkins RC, Carey FA. *Organic chemistry: A brief course*. (McGraw-Hill Higher Education, 2001).
193. Noble MEM, Cleasby A, Johnson LN, Egmond MR, Frenken LGJ. The crystal structure of triacylglycerol lipase from *Pseudomonas glumae* reveals a partially redundant catalytic aspartate. *FEBS Lett.* **331,** 123–128 (1993).
194. Khan FI, Lan D, Durrani R, Huan W, Zhao Z, Wang Y. The lid domain in lipases: Structural and functional determinant of enzymatic properties. *Front. Bioeng. Biotechnol.* **5,** 1–13 (2017).
195. Verger R. 'Interfacial activation' of lipases: facts and artifacts. *Trends Biotechnol.* **15,** 32–38 (1997).
196. Jaeger K-E, Ransac S, Koch HB, Ferrato F, Dijkstra BW. Topological characterization and modeling of the 3D structure of lipase from *Pseudomonas aeruginosa*. *FEBS Lett.* **332,** 143–149 (1993).
197. Melander W, Horváth C. Salt effect on hydrophobic interactions in precipitation and chromatography of proteins: An interpretation of the lyotropic series. *Arch. Biochem. Biophys.* **183,** 200–15 (1977).
198. Simons JWFA, Kosters HA, Visschers RW, de Jongh HHJ. Role of calcium as trigger in thermal β-lactoglobulin aggregation. *Arch. Biochem. Biophys.* **406,** 143–152 (2002).
199. Platts L, Falconer RJ. Controlling protein stability: Mechanisms revealed using formulations of arginine, glycine and guanidinium HCl with three globular proteins. *Int. J. Pharm.* **486,** 131–135 (2015).
200. Wingender J, Volz S, Winkler UK. Interaction of extracellular *Pseudomonas* lipase with alginate and its potential use in biotechnology. *Appl. Microbiol. Biotechnol.* **27,** 139–145 (1987).
201. Wingender J, Jaeger K-E, Flemming H-C. Interaction between extracellular polysaccharides and enzymes. in *Microbial Extracellular Polymeric Substances* 231–251 (Springer Berlin Heidelberg, 1999).
202. Fang Y, Al-Assaf S, Phillips GO, Nishinari K, Funami T, Williams PA, Li L. Multiple steps and critical behaviors of the binding of calcium to alginate. *J. Phys. Chem. B* **111,** 2456–2462 (2007).
203. Heil S. Evolutive Optimierung mikrobieller Lipasen und Esterasen in Hinblick auf Substratspezifität und Enantioselektivität. (Doctoral dissertation, Technical University of Darmstadt, 2012).
204. Yang J, Kobayashi K, Iwasaki Y, Nakano H, Yamane T. In Vitro Analysis of Roles of a Disulfide Bridge and a Calcium Binding Site in Activation of *Pseudomonas* sp. Strain KWI-56 Lipase. *J. Bacteriol.* **182,** 295–302 (2000).
205. Simons J-WFA, van Kampen MD, Ubarretxena-Belandia I, Cox RC, Alves dos Santos CM, Egmond MR, Verheij HM. Identification of a calcium binding site in *Staphylococcus hyicus* Lipase: Generation of calcium-independent variants. *Biochemistry* **38,** 2–10 (1999).
206. Tiesinga JJW, van Pouderoyen G, Nardini M, Ransac S, Dijkstra BW. Structural basis of phospholipase activity of *Staphylococcus hyicus* lipase. *J. Mol. Biol.* **371,** 447–456 (2007).
207. Hagedoorn P-L. Microbial Metalloproteomics. *Proteomes* **3,** 424–439 (2015).

208. Barber-Zucker S, Shaanan B, Zarivach R. Transition metal binding selectivity in proteins and its correlation with the phylogenomic classification of the cation diffusion facilitator protein family. *Sci. Rep.* **7,** 16381 (2017).
209. Glogauer A, Martini VP, Faoro H, Couto GH, Müller-Santos M, Monteiro R a, Mitchell D a, de Souza EM, Pedrosa FO, Krieger N. Identification and characterization of a new true lipase isolated through metagenomic approach. *Microb. Cell Fact.* **10,** 54 (2011).
210. Rashid N, Shimada Y, Ezaki S, Atomi H, Imanaka T. Low-temperature lipase from psychrotrophic *Pseudomonas* sp. strain KB700A. *Appl. enviromental Microbiol.* **67,** 4064–4069 (2001).
211. Pearson RG. Hard and soft acids and bases, HSAB, part I: Fundamental principles. *J. Chem. Educ.* **45,** 581 (1968).
212. Pearson RG. Hard and soft acids and bases, HSAB, part II: Underlying theories. *J. Chem. Educ.* **45,** 643 (1968).
213. Permyakov EA. *Metalloproteomics*. (John Wiley & Sons, Inc., 2009).
214. Pauwels K, Sanchez del Pino MM, Feller G, Van Gelder P. Decoding the folding of *Burkholderia glumae* lipase: Folding intermediates en route to kinetic stability. *PLoS One* **7,** e36999 (2012).
215. Gasymov OK, Glasgow BJ. ANS fluorescence: Potential to augment the identification of the external binding sites of proteins. *Biochim. Biophys. Acta - Proteins Proteomics* **1774,** 403–411 (2007).
216. Kelly S, Price N. The use of circular dichroism in the investigation of protein structure and function. *Curr. Protein Pept. Sci.* **1,** 349–384 (2000).
217. Invernizzi G, Casiraghi L, Grandori R, Lotti M. Deactivation and unfolding are uncoupled in a bacterial lipase exposed to heat, low pH and organic solvents. *J. Biotechnol.* **141,** 42–46 (2009).
218. Wilhelm S, Rosenau F, Becker S, Buest S, Hausmann S, Kolmar H, Jaeger K-E. Functional cell-surface display of a lipase-specific chaperone. *ChemBioChem* **8,** 55–60 (2007).
219. Kalusche SM. Rolle der Foldase auf den Mechanismus der Sekretion von Lipase A aus *Pseudomonas aeruginosa*. (Bachelor thesis Institute of Applied Sciene of Aachen, 2016).
220. Pauwels K, Van Molle I, Tommassen J, Van Gelder P. Chaperoning Anfinsen: the steric foldases. *Mol. Microbiol.* **64,** 917–922 (2007).
221. Hobson AH, Buckley CM, Aamand JL, Jørgensen ST, Diderichsen B, McConnell DJ. Activation of a bacterial lipase by its chaperone. *Proc. Natl. Acad. Sci. U. S. A.* **90,** 5682–6 (1993).
222. Sauter NK, Mau T, Rader SD, Agard DA. Structure of α-lytic protease complexed with its pro region. *Nat. Struct. Biol.* **5,** 945–950 (1998).
223. Antonoaea R, Fürst M, Nishiyama K, Müller M. The periplasmic chaperone PpiD interacts with secretory proteins exiting from the SecYEG translocon. *Biochemistry* **47,** 5649–5656 (2008).
224. Eder J, Rheinnecker M, Fersht AR. Folding of subtilisin BPN': Role of the pro-sequence. *J. Mol. Biol.* **233,** 293–304 (1993).
225. Eder J, Rheinnecker M, Fersht AR. Folding of subtilisin BPN': characterization of a folding intermediate. *Biochemistry* **32,** 18–26 (1993).
226. Yang L, Haagensen JAJ, Jelsbak L, Johansen HK, Sternberg C, Hoiby N, Molin S. In situ growth rates and biofilm development of *Pseudomonas aeruginosa* populations in chronic lung infections. *J. Bacteriol.* **190,** 2767–2776 (2008).
227. Chen Y, Inouye M. The intramolecular chaperone-mediated protein folding. *Curr. Opin. Struct. Biol.* **18,** 765–770 (2008).

228. Kang Y, Zarzycki-Siek J, Walton CB, Norris MH, Hoang TT. Multiple FadD acyl-coA synthetases contribute to differential fatty acid degradation and virulence in *Pseudomonas aeruginosa*. *PLoS One* **5,** e13557 (2010).
229. Tsirigotaki A, Chatzi KE, Koukaki M, De Geyter J, Portaliou AG, Orfanoudaki G, Sardis MF, Trelle MB, Jørgensen TJD, Karamanou S, Economou A. Long-lived folding intermediates predominate the targeting-competent secretome. *Structure* **26,** 695–707.e5 (2018).

8. Appendix

8.1. DNA sequence of *lipAH* operon

LipAH operon (pseudomonas.com, gene number:PA2862-PA2863*)
(* PA2863 wrongly annotated: +156 bp upstream)

Upstream Sequence:

CGGTTCTCCCGGAAGGATTCGGGCGATGGCTGGCAGGACGCGCCCCTCGGCCCCATCAACCTGAGATGAGAACAA
C

LipA:

Signal sequence:
ATGAAGAAGAAGTCTCTGCTCCCCCTCGGCCTGGCCATCGGTCTCGCCTCTCTCGCTGCCAGCCCTCTGATCCAG
GCC

Sequence for mature LipA:
AGCACCTACACCCAGACCAAATACCCCATCGTGCTGGCCCACGGCATGCTCGGCTTCGACAACATCCTCGGGGTC
GACTACTGGTTCGGCATTCCCAGCGCCTTGCGCCGTGACGGTGCCCAGGTCTACGTCACCGAAGTCAGCCAGTTG
GACACCTCGGAAGTCCGCGGCGAGCAGTTGCTGCAACAGGTGGAGGAAATCGTCGCCCTCAGCGGCCAGCCCAAG
GTCAACCTGATCGGCCACAGCCACGGCGGGCCGACCATCCGCTACGTCGCCGCCGTACGTCCCGACCTGATCGCT
TCCGCCACCAGCGTCGGCGCCCCGCACAAGGGTTCGGACACCGCCGACTTCCTGCGCCAGATCCCACCGGGTTCG
GCCGGCGAGGCAGTCCTCTCCGGGCTGGTCAACAGCCTCGGCGCGCTGATCAGCTTCCTTTCCAGCGGCAGCACC
GGTACGCAGAATTCACTGGGCTCGCTGGAGTCGCTGAACAGCGAGGGTGCCGCGCGCTTCAACGCCAAGTACCCG
CAGGGCATCCCCACCTCGGCCTGCGGCGAAGGCGCCTACAAGGTCAACGGCGTGAGCTATTACTCCTGGAGCGGT
TCCTCGCCGCTGACCAACTTCCTCGATCCGAGCGACGCCTTCCTCGGCGCCTCGTCGCTGACCTTCAAGAACGGC
ACCGCCAACGACGGCCTGGTCGGCACCTGCAGTTCGCACCTGGGCATGGTGATCCGCGACAACTACCGGATGAAC
CACCTGGACGAGGTGAACCAGGTCTTCGGCCTCACCAGCCTGTTCGAGACCAGCCCGGTCAGCGTCTACCGCCAG
CACGCCAACCGCCTGAAGAACGCCAGCCTGTAG

non-coding spacer region:

GACCCCGGCCGGGGCCTCGGCCCCGGCCCTTTCCCGGAAGCCCCCTCGC

LipH:

TMD
GTGAAGAAAATCCTCCTGCTGATTCCACTGGCGTTCGCCGCCAGCCTGGCCTGGTTCGTCTGGCTGGAACCT
VD:
TCCCCCGCACCCGAGACGGCGCCCCCGGCCAGCCCGCAGGCGGGCGCAGTCCACGCCCCGCCAGCAGCCTCCGCG
GGAGAAGCGGTGCCGGCCCCTCAGGTCATGCCGGCCAAGGTCGCGCCG
MD1:
CTGCCAACCTCCTTCAGGGGCACCAGCGTCGATGGCAGTTTCAGTGTCGACGCCAGCGGCAACCTGCTGATCACC
CGCGACATCCGCAACCTGTTCGACTACTTCCTCAGCGCCGTCGGCGAAGAGCCCCTGCAGCAAAGCCTGGACCGC
CTGCGCGCCTACATCGCCGCCGAACTCCAGGAGCCGGCGCGCGGCCAGGCGTTGGCGCTGATGCAGCAATACATC
GACTACAAGAAGGAACTG
EHD:
GTGCTGCTCGAACGCGACCTGCCGCGCCTGGCCGACCTCGACGCCCTGCGCCAGCGGGAAGCCGCGGTGAAAGCC
CTGCGCGCGCGGATCTTCAGCAACGAAGCGCACGTGGCGTTCTTCGCCGACGAGGAAACCTACAACCAGTTCACC
CTGGAGCGCCTGGCGATCCGCCAGGACGGCAAGCTCAGCGCCGAGGAAAAGGCCGCCGCCATCGACCGCCTGCGC
GCCAGCCTGCCGGAAGACCAGCAGGAAAGCGTGCTGCCGCAACTGCAAAGCGAACTGCAGCAGCAGACCGCCGCC
CTCCAGGCCGCTGGCGCCGGCCCGGAAGCCATCCGCCAGATGCGTCAGCAACTGGTGGGC
MD2:
GCCGAAGCCACCACCCGCCTGGAGCAACTCGATCGGCAACGCTCGGCCTGGAAGGGCCGGCTGGACGACTATTTC
GCCGAGAAGAGCCGGATCGAAGGCAATACCGGGCTGAGCGAAGCCGACCGCCGCGCGGCGGTCGAACGCCTGGCC
GAGGAGCGCTTCAGCGAACAGGAACGCTTGCGCCTGGGCGCGCTGGAACAGATGCGCCAGGCCGAGCAGCGCTGA

Downstream sequence:

CCGGCACGGAAACGCCGAGAACGCGGCG

8.2. Detailed DNA sequence description of used parental plasmids

Sequential organization of given parental plasmids determined by sequencing. Sequential differences compared to empty vectors are printed in bold. Sequential changes compared to WT genes of PAO1 (see Appendix 8.1) are given in brackets.

pEHTHis19:

pET-19b(+)(Novagen, Merck): Soluble His_{10} Tag - NdeI **- LipH(Δaa1-20) – downstream sequence(28 bp)** - BamHI

pLipA-SS:

pET-22b(+) (Novagen, Merck): NdeI **- ΔLipA signal sequence – LipA(ΔSer1) – non coding spacer region - LipH(GTGAAGA)-** BamHI

pBBR1MCS/PA *lipAH:*

pBBR1MCS1[99]: XbaI **– unknown sequence(ACTAGTGGATCGATCCCC) - 76 bp upstream sequence - LipA – mutated(*)non coding spacer region – LipH(Val1Met [GTG->ATG] ΔLeu6, Ala31Thr [GCG->ACG], Glu145Ala [GAA->GCA]) - unknown sequence (CTCGAGCGGAAACGGG) -** Bsp120I

(*):

```
PAO1:                 GACCCCGGCCGGGGCCTCGGCCCCGGCCCTTTCCCGGA----AGCCCCCT
                      ||||||||||||||||||||||||||||||||||#|#|    |##|||#|
pBBR1MCS/PA lipAH:    gaccccggccggggcctcggccccggcccttccggaaggagatacccat
```

8.3. Protein sequence alignment of LipH_PA and LipB_BG

```
#=======================================
# Aligned_sequences: 2
# 1: LipH_PA
# 2: LipB_BG
# Matrix: EBLOSUM62
# Gap_penalty: 12
# Extend_penalty: 2
#
# Length: 364
# Identity:     117/364 (32.1%)
# Similarity:   166/364 (45.6%)
# Gaps:          35/364 ( 9.6%)
# Score: 258
#=======================================

LipH_PA         1 VKKI-------LLLIPL-----------AFAASLAWFVWLEPSPAPETAP     32
                  :.:.       |...|:           |.||..|..:||.|: ||..||
LipB_BG         1 MAQADRPARGGLAARPMRGASFALAGLVACAACAAVVLWLRPA-APSPAP     49

LipH_PA        33 PASPQAGAVHAPPAASAGEAVPAPQVMPAKVAPLPTSFRGTSVDGSFSVD     82
                  ..:...|.....|||::|.|..|   ||...| ||.:..|:... ...:.
LipB_BG        50 AGAVAGGPAAGVPAAASGAAEAA---MPLPAA-LPGALAGSHAP-RLPLA     94

LipH_PA        83 ASGNLLITRDIRNLFDYFLSAVGEEPLQQSLDRL-RAYIAAELQ-EPARG    130
                  |.|.|..||.:|..|||.|:|.||.. ..:||.| |..|||:|. .||:.
LipB_BG        95 AGGRLARTRAVREFFDYCLTAQGELT-PAALDALVRREIAAQLDGSPAQA    143

LipH_PA       131 QALALMQQYIDYKKELVLLERDLPRLAD-LD-ALRQREAAVKALRARIFS    178
                  :||.:.::|..|...|..|..|...|.| || |..|.....:|..|....
LipB_BG       144 EALGVWRRYRAYFDALAQLPGDGAVLGDKLDPAAMQLALDQRAALADRTL    193

LipH_PA       179 NEAHVAFFADEETYNQFTLERLAIRQDGKLSAEEKAAAIDRLRASL-PED    227
                  .|....||.||:...:..|||:.|..|..||.|:|||.:..|.|.| |::
LipB_BG       194 GEWAEPFFGDEQRRQRHDLERIRIANDTTLSPEQKAARLAALDAQLTPDE    243

LipH_PA       228 QQESVLPQLQSELQQQTAALQAAGAGPEAIRQMRQQLVGAEATTRLEQLD    277
                  :.:......|.:...:.|.||.|||.|:.:|....|.:|.||..|..|:.
LipB_BG       244 RAQQAALHAQQDAVTKIADLQKAGATPDQMRAQIAQTLGPEAAARAAQMQ    293

LipH_PA       278 RQRSAWKGRLDDYFAEKSRIEGNTGLSEADRRAAVERLAEERFSEQ-ERL    326
                  :...||:.|...|.||:.||... ||:..||.|.:.:|.::.|:.. |.:
LipB_BG       294 QDDEAWQTRYQAYAAERDRIAAQ-GLAPQDRDARIAQLRQQTFTAPGEAI    342

LipH_PA       327 RLGALEQMRQAEQR    340
                  |..:|::   ....
LipB_BG       343 RAASLDR---GAGG    353
```

8.4. Protein sequence alignment of LipA_PA and LipA_BG

```
#=======================================
# Aligned_sequences: 2
# 1: LipA_PA
# 2: LipA_BG
# Matrix: EBLOSUM62
# Gap_penalty: 12
# Extend_penalty: 2
#
# Length: 361
# Identity:     134/361 (37.1%)
# Similarity:   186/361 (51.5%)
# Gaps:          53/361 (14.7%)
# Score: 480
#=======================================

LipA_PA         1 MKKK--------------SLLPLGLAIGLASLAASPLIQASTYTQTKYPI     36
                  |.:.              :::||..|.||...|:...:.|.||..|:||:
LipA_BG         1 MVRSMRSRVAARAVAWALAVMPLAGAAGLTMAASPAAVAADTYAATRYPV     50

LipA_PA        37 VLAHGMLGFDNILGV-DYWFGIPSALRRDGAQVYVTEVSQLDTSEV---R     82
                  :|.||:.|.|....| |||:||.|.|:..||:|||..:|...:.:.   |
LipA_BG        51 ILVHGLAGTDKFANVVDYWYGIQSDLQSHGAKVYVANLSGFQSDDGPNGR    100

LipA_PA        83 GEQLLQQVEEIVALSGQPKVNLIGHSHGGPTIRYVAAVRPDLIASATSVG    132
                  |||||..|::::|.:|..||||||||.||.|.||||||.|.|:||.|::|
LipA_BG       101 GEQLLAYVKQVLAATGATKVNLIGHSQGGLTSRYVAAVAPQLVASVTTIG    150

LipA_PA       133 APHKGSDTADFLRQI---PPGSAGEAVLSGLVNSLGALISFLSSGSTGTQ    179
                  .||:||:.|||::.:   .|......|::..||..|.|:|  ||.:|. |
LipA_BG       151 TPHRGSEFADFVQDVLKTDPTGLSSTVIAAFVNVFGTLVS--SSHNTD-Q    197

LipA_PA       180 NSLGSLESLNSEGAARFNAKYPQ---GIPTSA-CGEGAYKVNGVSY--YS    223
                  ::|.:|.:|.:...|.:|..:|.   |.|.|. .|.....|.|..:  ||
LipA_BG       198 DALAALRTLTTAQTATYNRNFPSAGLGAPGSCQTGAATETVGGSQHLLYS    247

LipA_PA       224 WSGSS---------------------PLTNFLDPSDAFLGASSLTFKNGT    252
                  |.|::                     .:.|..|||...|.|:.....|..
LipA_BG       248 WGGTAIQPTSTVLGVTGATDTSTGTLDVANVTDPSTLALLATGAVMINRA    297

LipA_PA       253 A--NDGLVGTCSSHLGMVIRDNYRMNHLDEVNQVFGLTSLFETSPVSVYR    300
                  :  |||||..|||..|.||..:|..|||||:||:.|:.......||:|.|
LipA_BG       298 SGQNDGLVSRCSSLFGQVISTSYHWNHLDEINQLLGVRGANAEDPVAVIR    347

LipA_PA       301 QHANRLKNASL    311
                  .|.||||...:
LipA_BG       348 THVNRLKLQGV    358
```

8.5. Association numbers of used foldase genes

Table 8.1: Association numbers of used sequences for proline comparison.

Burkholderia genus		*Pseudomonas* genus		
AAY82369.2	WP_069256344.1	ACP20255.1	WP_058068831.1	WP_090503080.1
ABS57472.1	WP_071334273.1	AGL91257.1	WP_059391650.1	WP_090538885.1
OJD04525.1	WP_074287673.1	CDM40738.1	WP_061237992.1	WP_092286368.1
OXH94649.1	WP_075304758.1	CEA04230.1	WP_061341268.1	WP_092375582.1
WP_006756710.1	WP_081922968.1	KFF32079.1	WP_068825867.1	WP_092388534.1
WP_009895779.1	WP_082742263.1	KXG18585.1	WP_068827243.1	WP_093396633.1
WP_016355456.1	WP_085037186.1	OCX98101.1	WP_069083432.1	WP_093473006.1
WP_027782586.1	WP_085039924.1	OYT96151.1	WP_069519049.1	WP_093986853.1
WP_031400651.1	WP_089427973.1	OYT96408.1	WP_069562019.1	WP_095625486.1
WP_034184350.1	WP_096470569.1	SFA50479.1	WP_073299541.1	WP_095626597.1
WP_035556815.1	WP_097396792.1	WP_003239805.1	WP_074678191.1	WP_095648768.1
WP_035973681.1	WP_098552546.1	WP_003244571.1	WP_074779522.1	WP_095938774.1
WP_036055904.1	WP_100556357.1	WP_003300115.1	WP_074864942.1	WP_095940786.1
WP_038743470.1	WP_102648084.1	WP_003454118.1	WP_074867661.1	WP_096004530.1
WP_039224811.1		WP_009316209.1	WP_074968748.1	WP_096219435.1
WP_040139398.1		WP_011913156.1	WP_076428741.1	WP_096346330.1
WP_042628288.1		WP_015277129.1	WP_076578618.1	WP_096717682.1
WP_043293726.1		WP_016493186.1	WP_077523009.1	WP_096723583.1
WP_044848400.1		WP_017362891.1	WP_077526174.1	WP_096725729.1
WP_048244298.1		WP_019339448.1	WP_079202308.1	WP_101192785.1
WP_048803873.1		WP_021220359.1	WP_079387700.1	WP_102819690.1
WP_049106134.1		WP_021445590.1	WP_079453093.1	WP_102825801.1
WP_051376787.1		WP_021446295.1	WP_081262937.1	WP_102829288.1
WP_057923961.1		WP_022963877.1	WP_082629018.1	WP_102836296.1
WP_059494571.1		WP_024308421.1	WP_083251856.1	WP_102850773.1
WP_059513136.1		WP_025167235.1	WP_083491768.1	WP_102894110.1
WP_059514986.1		WP_028627304.1	WP_083728149.1	WP_103454692.1
WP_059524688.1		WP_037001142.1	WP_084333760.1	pir||JS0571
WP_059561053.1		WP_037047769.1	WP_085063280.1	
WP_059597651.1		WP_037053538.1	WP_086245331.1	
WP_059700627.1		WP_038660461.1	WP_088276245.1	
WP_059809367.1		WP_041978923.1	WP_090241872.1	
WP_059855647.1		WP_043307396.1	WP_090242202.1	
WP_059955911.1		WP_044874278.1	WP_090253127.1	
WP_059966912.1		WP_045161561.1	WP_090253446.1	
WP_060028000.1		WP_048910073.1	WP_090274712.1	
WP_060085300.1		WP_052080941.1	WP_090386911.1	
WP_060126537.1		WP_052237583.1	WP_090425727.1	
WP_060228093.1		WP_054093205.1	WP_090438272.1	
WP_069247680.1		WP_057384475.1	WP_090448213.1	

8.6. Determination of extinction coefficient of *para*-nitrophenol

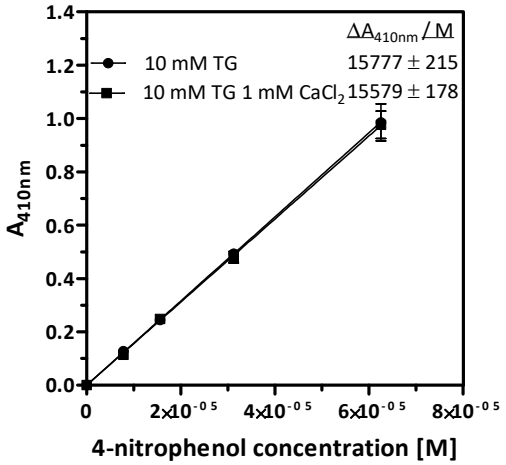

Figure 8.1: Determination of extinction coefficient of *para*-nitrophenol.
4-nitrophenol (purchased from Sigma Aldrich in ReagentPlus®, (≥99%) quality) was weight in independently three times for 1 M stocks in isopropanol. Stocks were used for the preparation of dilution serien in TG puffer with and without 1 mM $CaCl_2$. Absorption at 410 nm was determined in 1 cm cuvettes at GENESYS™ 10S UV-Vis Spectrophotometer (Thermo Fisher Scientific) and 200 µl in microtiter plates using Spectramax 250 plate reader (Molecular Devices). The adsorption was normalized to path length of 1 cm. The slope gives the molecular extinction coefficient.

8.7. Influence of pH and $CaCl_2$ on thermal stability of native LipA

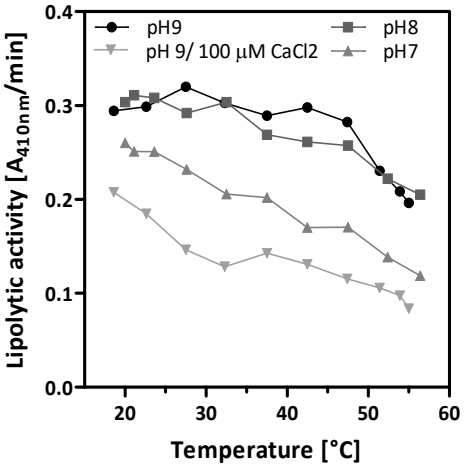

Figure 8.2: Influence of pH and CaCl2 on thermal stability of native LipA.
2 nM native purified LipA in different TG buffers was divided into aliquots and incubated in temperature gradient for 1 h. Afterwards, remaining lipolytic activity was determined.

8.8. Determination of EC_{50} constant for calcium in LipAH complex

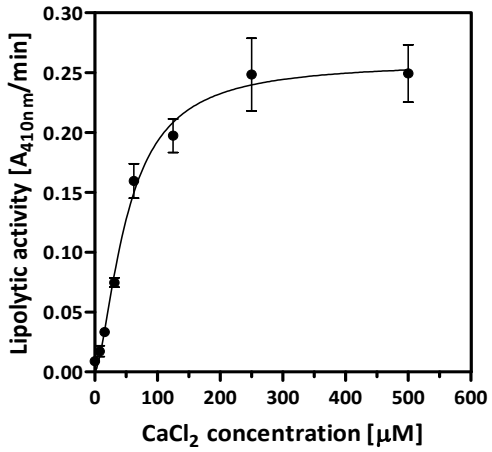

Figure 8.3: Determination of EC_{50} constant for calcium in LipAH complex.
Calcium dependent increasing activity of LipAH complex. EC 50 was determined by One site- Specific binding with Hill slope equation as 51 µM from 3 independent measurements. Therefore, 200 µM LipAH complex refolded in TG buffer over night was mixed 1:1 with a dilution series of calcium chloride in TG buffer in a glass coated deep well plate. After 15 min incubation, activity was measured using substrate solutions with the same calcium chloride concentrations.

8.9. Thermal inactivation of LipH

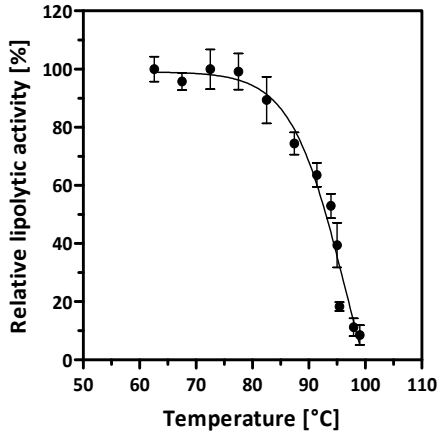

Figure 8.4: Thermal inactivation of LipH.
100 nM LipH were divided into aliquots and incubated in temperature gradient for 1 h. Renatured LipA was added in an equal molar ratio compared to LipH. After incubation at 4 °C overnight, activities were measured.

8.10. Complex melting of preactive LipA and LipH at high concentrations

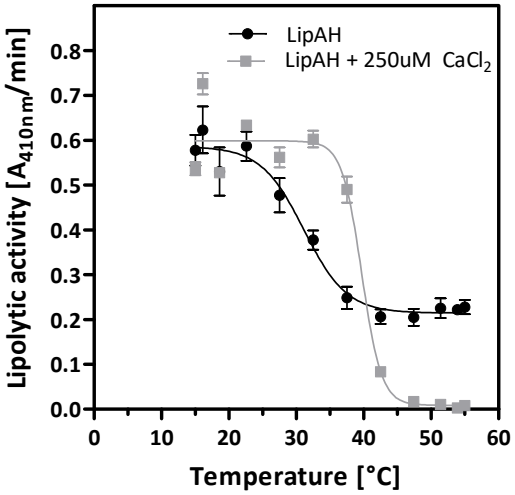

Figure 8.5: Complex melting of preactive LipA and LipH at high concentrations.
2 µM freshly prepared LipAH complex was incubated in TG buffer with and without calcium for 1 h in temperature gradient in low-binding PCR plates. After thermal treatment, samples were diluted just before activity measurement.

Selbständigkeitserklärung

Hiermit versichere ich an Eides statt, dass die vorgelegte Dissertation “Lipase-specific foldase-aided folding of Lipase A from *Pseudomonas aeruginosa*“ von mir selbstständig verfasst und unter ausschließlicher Verwendung der angegebenen Literatur und Hilfsmittel gemäß der „Grundsätze zur Sicherung guter wissenschaftlicher Praxis an der Heinrich-Heine-Universität Düsseldorf“ erstellt wurde. Bisher habe ich keine erfolglosen Promotionsversuche unternommen.

_____ _____

Ort, Datum Peter Dollinger